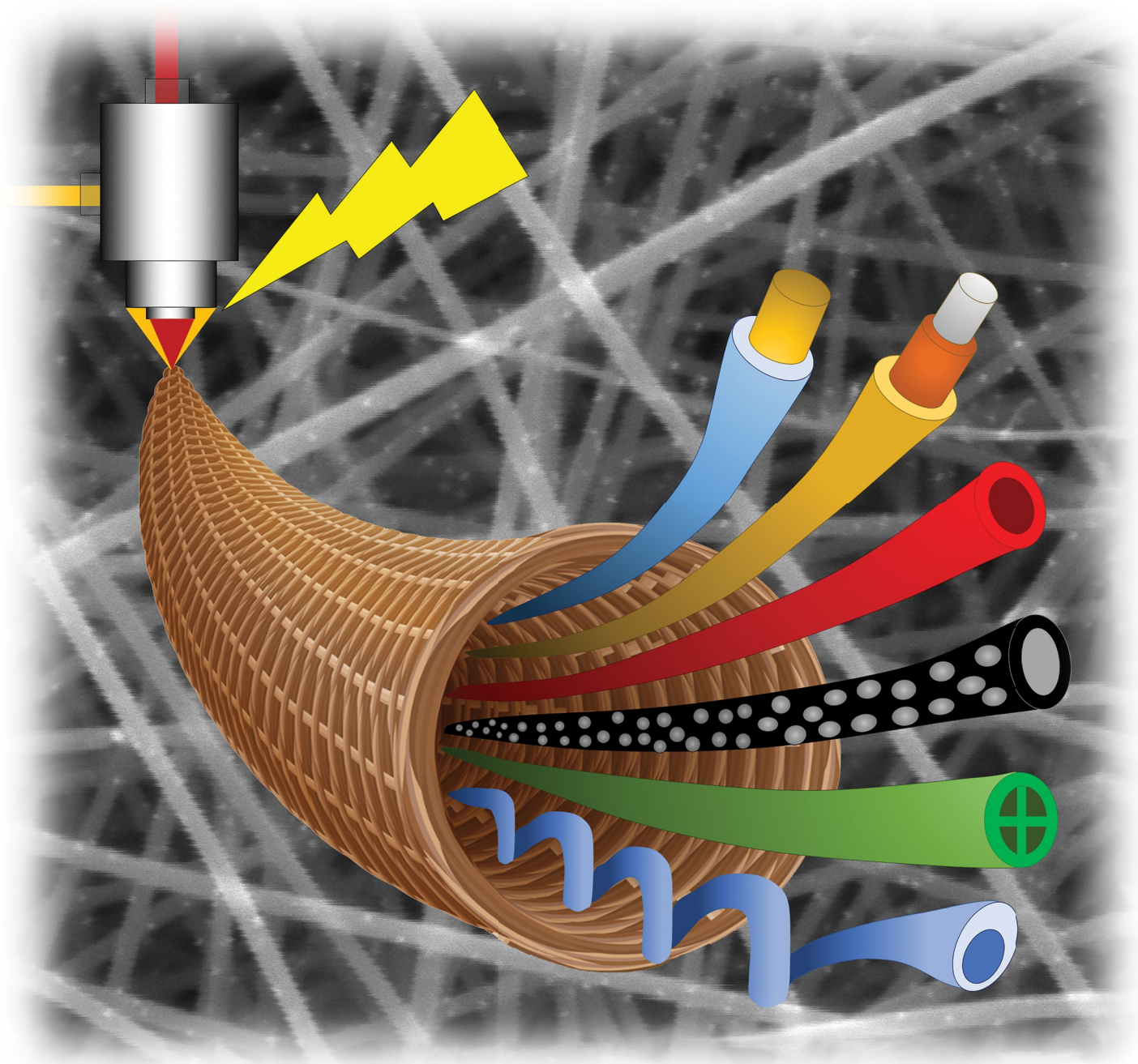


A GENUINELY MULTIDISCIPLINARY JOURNAL

CHEMPLUSCHEM

CENTERING ON CHEMISTRY



10/2019

Cover Feature:

D. Han and A. Steckl

Coaxial Electrospinning Formation of Complex Polymer Fibers
and their Applications

A Journal of

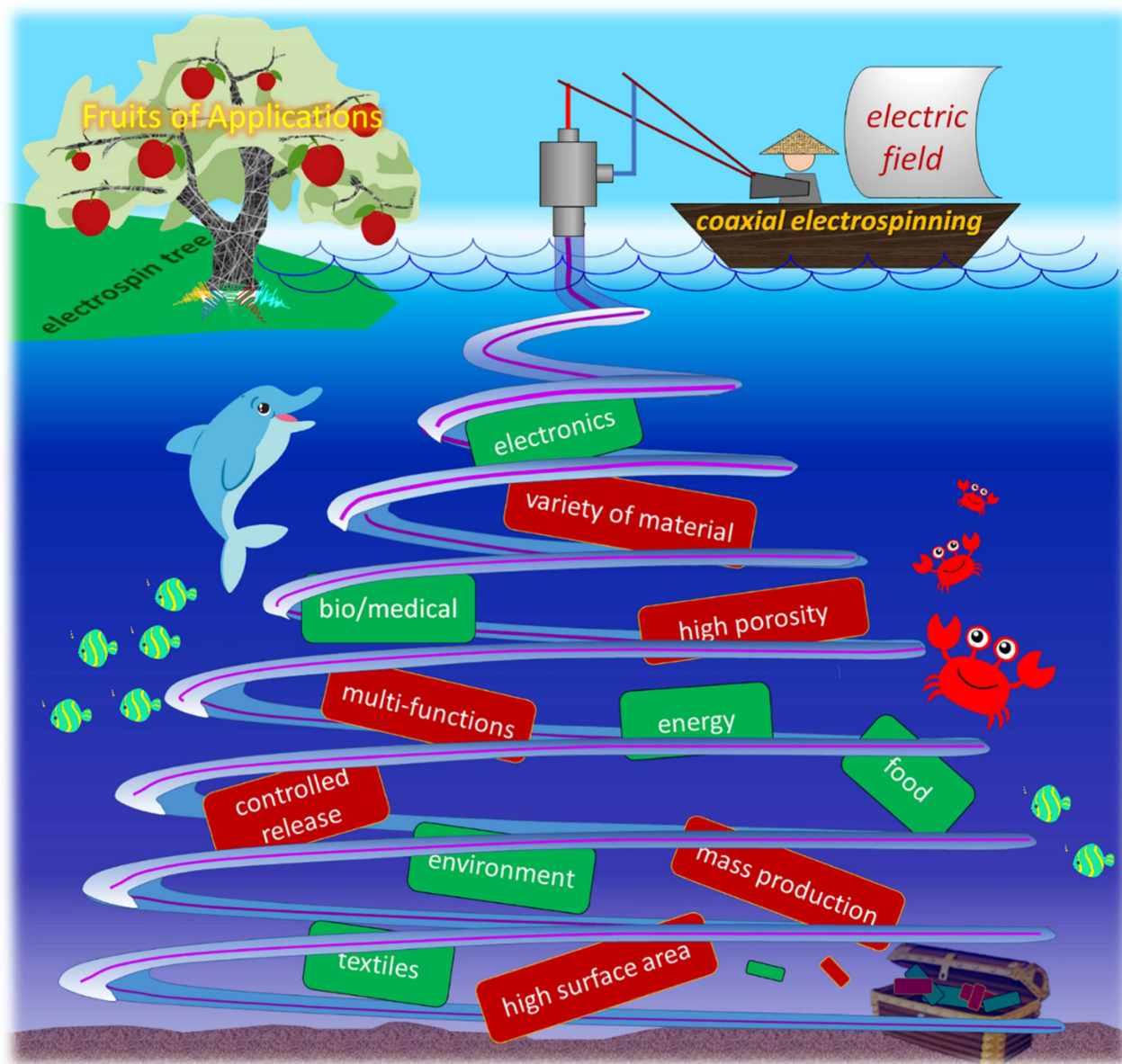


WILEY-VCH

www.chempluschem.org

Very Important Paper

Coaxial Electrospinning Formation of Complex Polymer Fibers and their Applications

Daewoo Han and Andrew J. Steckl^{*[a]}

The formation of fibers by electrospinning has experienced explosive growth in the past decade, recently reaching 4,000 publications and 1,500 patents per year. This impressive growth of interest is due to the ability to form fibers with a variety of materials, which lend themselves to a large and rapidly expanding set of applications. In particular, coaxial electrospinning, which forms fibers with multiple core–sheath layers from different materials in a single step, enables the combina-

tion of properties in a single fiber that are not found in nature in a single material. This article is a detailed review of coaxial electrospinning: basic mechanisms, early history and current status, and an in-depth discussion of various applications (biomedical, environmental, sensors, energy, catalysis, textiles). We aim to provide readers who are currently involved in certain aspects of coaxial electrospinning research an appreciation of other applications and of current results.

Introduction

Fibers are a form of string-like material that is distinguished by a large ratio of length to width. Fibers are ubiquitous in nature and are widely developed in synthetic forms. Natural fibers present in hair, fur of animals and in bird feathers consisting mainly of proteins provide essential functionality, such as protection, sensing, regulation, etc. Silk, produced by spiders, worms and other species, is also a protein-based fiber with an extremely high strength-to-weight ratio. Fiber-like cellulose filaments, with diameters ranging from micrometers to nanometers, present in the cellular walls of plants serve as the base component of paper and cardboard. Plant fibers in various forms are also used in textiles and for nutrition. Man-made fibers are produced with higher uniformity and reproducibility in order to enable a more predictable manufacturing process. In particular, membranes containing fibers with nanometer diameters provide an extremely high surface area and high porosity material, presenting extraordinary properties in terms of mechanical strength, breathability, sensitivity to external stimuli, and biomimetic environment.

Various methods have been developed to produce different types of micro- and nano-fibers. The simplest approach is a drawing method. A microtip is dipped into the viscous polymer droplet, where it moves to pull the thin liquid string from the droplet towards the desired location. Relatively long single fibers can be formed with good control of fiber orientation. However, this process requires the placement of a polymer droplet that is continuously evaporating its solvent and thus changing its viscoelastic properties, leading to inconsistent fiber diameter values. Since the fiber production rate is limited, this technique is primarily useful when investigating single nanofiber properties.^[1] Self-assembly is also a well-known method to synthesize nanofibers made of biomaterials, such as peptides and proteins. Without the presence of external factors, organized structures including nanofibers can be formed from

macromolecules through localized interactions, such as hydrogen and ionic bonds, and hydrophobic interactions. Although the diameter of nanofibers formed in this manner is typically well below 100 nm, the length can be only up to a few microns and the formation process is relatively complex.^[2]

Template-based synthesis utilizes a nanoporous membrane as a template to synthesize or extrude nanofibers or nanorods. This technique exhibits very good control of the nanofiber diameter down to a few nanometers with monodispersed distribution. However, the length of these fibers is limited to the micrometer range and they cannot form a porous membrane.^[3] The melt-blowing method is a traditional method for non-woven fiber membrane production. A polymer melt is fed into a nozzle and a high-pressure gas blows the melt into nanofibers. Using small microfabricated nozzles and high-speed heated gas blowing, nanofibers ranging from 100 to 1000 nm have been reported. However, it is still challenging to obtain fibers with diameter less than ~100 nm and the source material has to be a thermoplastic polymer.^[4] Solution blow spinning is also a simple and interesting technique, which uses compressed air to blow the concentration polymer solution into nanofibers using a painting airbrush. Fibers can be deposited in any location, which can be useful as a wound dressing and in textile applications.^[5] CO₂ laser supersonic drawing (CLSD) uses a CO₂ laser to melt thermoplastic microfibers and draw the melt into nanofibers using supersonic airflow in a vacuum chamber. The main advantage of this technique is the absence of any chemical solvents, which is beneficial to the environment and for health aspects.^[6] Centrifugal jet spinning was inspired by the cotton candy machine. Centrifugal force is used to extract fibers from viscoelastic polymer solutions. This results in a highly efficient and low-cost method with a high fiber production rate. Some issues, such as fiber quality consistency, fiber alignment and morphology control, remain to be improved. However, unlike electrospinning, highly conductive polymer solution can be spun conveniently, because no electrical potential is applied.^[7] Other methods such as sonochemical synthesis,^[8] plasma-induced synthesis^[9] have also been utilized recently.

An important direction in fiber manufacturing is the formation of complex fibers with desired properties brought about by the use of composite materials and novel structure and morphology. Compared to other nanofiber production methods, complex fiber formation using the electrospinning method is a surprisingly versatile method that has enabled the production of a large variety of materials with extremely high surface-to-volume ratio.

[a] Dr. D. Han, Prof. A. J. Steckl
Department of Electrical Engineering and Computer Science
University of Cincinnati
Nanoelectronics Laboratory
Cincinnati, OH 45221-0030 (USA)
E-mail: a.steckl@uc.edu

© 2019 The Authors. Published by Wiley-VCH Verlag GmbH & Co. KGaA. This is an open access article under the terms of the Creative Commons Attribution Non-Commercial NoDerivs License, which permits use and distribution in any medium, provided the original work is properly cited, the use is non-commercial and no modifications or adaptations are made.

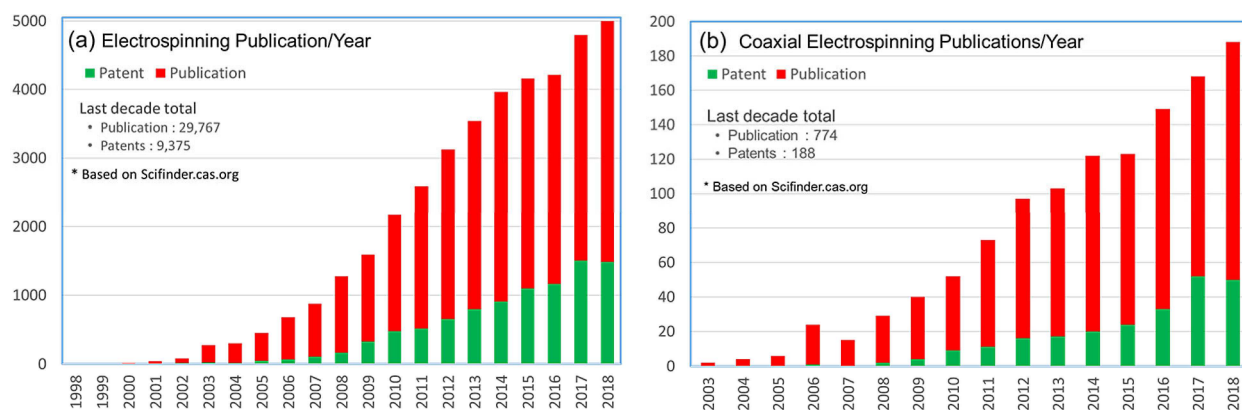


Figure 1. Publications and patents per year dealing with (a) overall electrospinning and (b) coaxial electrospinning. Data were updated as of June 3, 2019. From search results, duplicates were removed, and all languages were considered.

The first electrospinning patent was granted to J. F. Cooley in 1902, but a commercially valuable patent for the fabrication of textile yarns was published by A. Formhals in 1934.^[10] In the 1960s, important research on electrofluidics was accomplished by G. Taylor. He studied and modeled the effect of electric fields on polymer droplets^[11] and associated liquid jet ejection.^[12] The distorted conical shape of a polymer droplet under high electric field (such that present during the electrospinning process) is known as a Taylor cone. In the middle of the 1990s, the versatile nanofiber production technique called *electrospinning* was revived by the Reneker group at the University of Akron by realizing poly(ethylene oxide) (PEO) nanofibers.^[13]

Demonstrating an ability to use a broad range of materials clearly indicated the potential of fiber electrospinning for many applications. In conjunction with the exploding interests in nanotechnology, this timely revival of the electrospinning technique attracted the attention of researchers and industries worldwide. Since the revival of electrospinning, related research has made rapid in multiple directions. The unique and attractive features of electrospun nanofiber membranes provide many versatile elements that can be excellent resources for many applications, especially in bio/medical, energy, textiles, environments, food and electronics, and also provide great potential and impetus for nascent areas under early development. As expected from its versatility and popularity, the number of publications and patents has been increasing rapidly every year, as shown in Figure 1a. An extension of the electrospinning

technique has been developed to produce the multi-layered core-sheath structured nanofibers (*aka* coaxial fibers) using *coaxial electrospinning*.

The versatility of electrospinning has been greatly expanded by enabling core-sheath or hollow nanofiber production, providing multi-functional properties from a single fiber. By forming a fiber that consists of complementary materials in the core and the sheath, one can design complex materials with a combination of ("mix-and-match") properties (Figure 2) that are not available in homogeneous nanofibers from single-nozzle electrospinning. Compared to alternative methods, such as TUFT (tubes by fiber templates) process,^[14] self-assembly^[15] and template synthesis^[16] for core-sheath fiber production, coaxial electrospinning provides unsurpassed benefits – a simple one step, highly efficient process (without the need of vacuum, elevated temperature treatment, plasma exposure, and/or sophisticated chemistry); large variety of material combinations; easily adjustable core-sheath dimensional ratio; controllable stack thickness of core-sheath fibers. This provides novel, multi-functional properties combining mechanical reinforcement, electrical/magnetic properties, biocompatibilities, antimicrobials/anticancer properties, photovoltaic properties, fire resistance, etc. Interestingly, functional materials, such as nanoparticles/nanotubes, drugs, proteins and living cells, can be easily incorporated into core-sheath fibers by dispersing or dissolving them in electrospinning solutions. Due to its uniqueness and versatility, the number of publications involving



Daewoo Han is Senior Research Associate at the University of Cincinnati. His current research activities are mainly focused on the development of multi-axially electrospun nanofiber applications such as (1) "on-demand" drug delivery systems for wound dressing and localized cancer therapy, (2) carbon-nanofiber-based electrochemical sensors, (3) protective textiles with antimicrobial and anti-warfare agents, and (4) membrane-based microfluidic devices for point-of-care diagnostics.



Andrew Steckl is Distinguished Research Professor, Gieringer Chair Professor, and Ohio Eminent Scholar at the University of Cincinnati. Current research activities in his NanoLab group include bio/organic sensors, microfluidic devices for Lab-on-Chip and Point-of-Care diagnostic applications, and nanofiber formation by electrospinning for chem/bio/med applications. He is a Fellow of AAAS and Life Fellow of IEEE. In 2006 he received the Rieveschl Award for Distinguished Scientific Research at the University of Cincinnati.

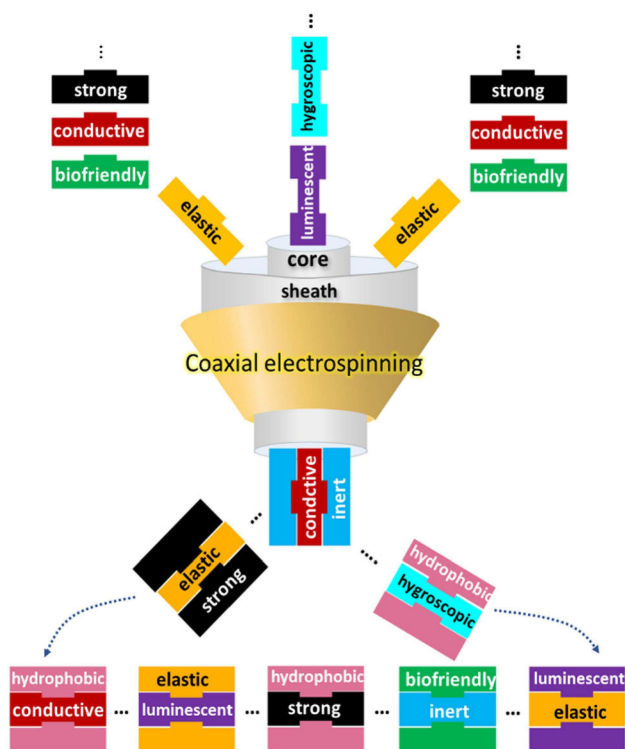


Figure 2. Mix-and-match: multiple properties and functions of coaxial electrospinning.

coaxial electrospinning has also dramatically increased, as shown in Figure 1b.

In the earlier stage of coaxial electrospinning research, a comprehensive review paper covering theories, parameters, and applications was published by Moghe and Gupta.^[17] As the field is growing rapidly and extensively, recent reviews have focused on current advances^[18] and/or specific application areas.^[19] This review provides a thorough outline of coaxial electrospinning covering wide ranging applications by critically selecting important earlier findings, recent achievements, and theoretical considerations for successful coaxial electrospinning.

Trends of coaxial electrospinning research in various applications are presented to provide a milestone for researchers either initiating or continuing research using coaxial electrospinning technique.

The article first briefly reviews the basic operation of conventional electrospinning for the formation of homogenous fibers and then describes coaxial electrospinning and process parameters for the formation of complex core-sheath fibers. Early breakthroughs in coaxial electrospinning are then introduced. Next, recent results are reviewed in some detail regarding the formation and properties of coaxial fibers for several key application areas: biomedical, sensors, textiles, energy and catalysis. The following section covers novel approaches to coaxial electrospinning, such as triaxial electrospinning, multi-inlet sheath approach, near field electrospinning. A discussion of high throughput fiber membrane production and related aspects important for commercialization are also discussed. Finally, a summary for the review provides a look ahead at the future prospects of electrospinning.

Electrospinning

To introduce the formation of nanofibers by electrospinning, the basic electrospinning setup is illustrated in Figure 3a. It consists of four main parts: a syringe pump connected to the various type of nozzles determining fiber structure, a separated conducting collector and a high voltage power supply that is connected to both. For coaxial electrospinning, an additional set of syringe pump and a coaxial nozzle are used (Figure 3b). A high electric field (\sim kV/cm) is used to eject the liquid jet from the polymer solution at the nozzle. When high voltage is applied, the polymer liquid droplet becomes highly electrified, and its naturally hemispherical shaped droplet takes on a distorted conical shape, the so-called Taylor cone. Forces operating on the liquid jet during electrospinning were investigated by Reneker et al.^[20] When the electric field overcomes the surface tension of the droplet, a very thin liquid jet is ejected from the droplet. Viscoelastic and charge repulsion

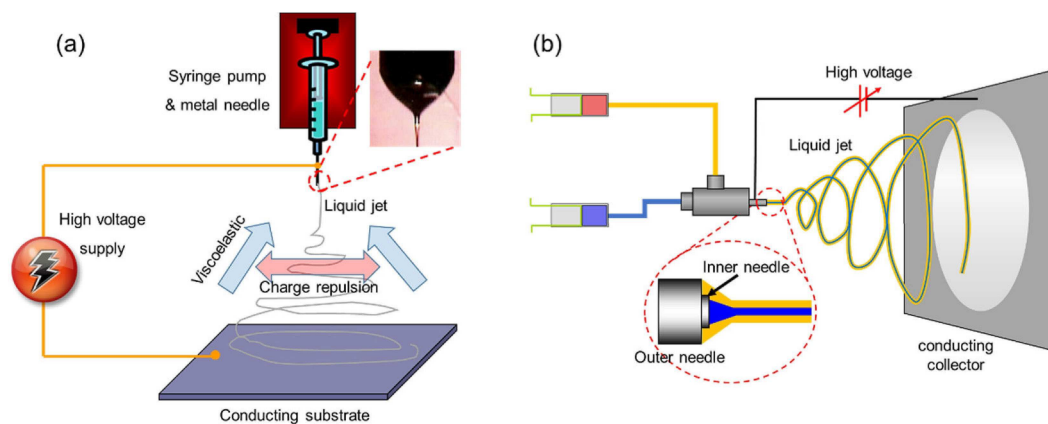


Figure 3. Basic fiber electrospinning concept diagrams: (a) conventional method for homogenous fibers; (b) coaxial electrospinning for core-sheath fibers. Reprinted (adapted) with permission from Ref [113]. Copyright 2017 American Chemical Society.

forces compete to control the jet behavior. Initially, because the diameter of the liquid jet is relatively thicker, the viscoelastic force dominates and the liquid jet travels in a straight path. As the liquid jet stretches during transport, beyond a certain distance the charge repulsion force dominates over the viscoelastic force. At that point, the liquid jet experiences very vigorous bending and whipping actions, leading to progressively thinning jet diameter and thorough evaporation of the jet solvent. Consequently, solidified polymeric nanofibers are deposited on the collector, forming a non-woven porous membrane. Essentially the same fundamental mechanisms also apply to coaxial electrospinning (Figure 3b). Interactions between the two solutions in this case can be quite complex and are discussed in a later section.

Electrospinning Parameters

Although electrospinning is fundamentally a simple and straightforward method, many parameters have to be manipulated to obtain desired properties from resultant nanofiber membranes including fiber surface morphology, dimensions and orientations. The main considerations are: (a) solute properties including molecular weight and its concentration; (b) solvent properties including vapor pressure, surface/interfacial tension, conductivity, dielectric constant, and viscosity; (c) processing parameters including electric potential, gap distance, flow rate of solution, needle/nozzle dimensions; (d) environmental conditions, including temperature,^[21] humidity,^[22] ambient gas and pressure. Evaluating polymer chain entanglement is an effective gauge to leverage the fiber forming capability during electrospinning.^[23] Polymer molecular weight and its concentration in solution are the two main factors in determining chain entanglement. In solution, polymer molecules occupy a certain effective volume with an average radius of gyration (R_g). At low concentrations (dilute solutions) polymer chains of the molecules in solution do not overlap (Figure 4a), and the viscoelasticity of solution is governed by the individual polymer chains. With increasing polymer concentration, the chains start to overlap and become entangled (Figure 4b). The critical concentration (c^*), at which entanglement initially occurs is generally accepted to be proportional to the ratio of the polymer molecular weight (M_w) and the effective volume [Eq. (1)]:

$$c^* = \frac{3M_w}{4\pi R_g^3 N_A}, \quad (1)$$

where N_A is the Avogadro's constant.^[24]

At concentrations higher than the critical concentration, the chain entanglement increases rapidly (Figure 4c). This results in an abrupt increase in the viscoelasticity of the solution. The dependence of the solution viscosity on polymer concentration is illustrated in Figure 4d. The slope above c^* is ~ 3.4 compared with ~ 1.4 below c^* , because its rheological behavior is governed by interactions between multiple polymer chains rather than by the individual polymer molecules. When the

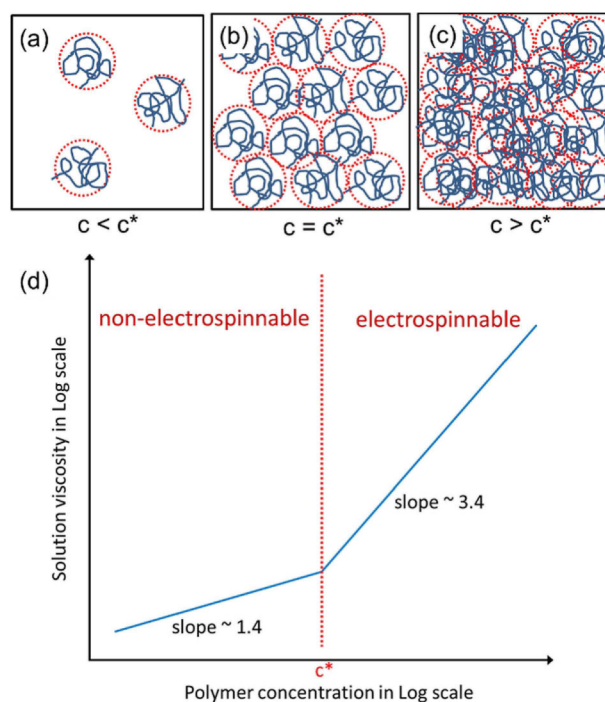


Figure 4. Effect on solution viscosity and related electrospinning feasibility: (a) polymer chains in dilute solution; (b) chain entanglement at polymer critical concentration; (c) chain entanglement in concentrated solutions; (d) solution viscosity vs. polymer concentration.

polymer concentration is relatively low ($c < c^*$), insufficient chain entanglement results in the elongated liquid jet breaking up or forming beaded fibers due to liquid surface tension ("Rayleigh instability"). Stable electrospinning requires a polymer concentration in solution higher than the critical concentration c^* . The critical concentration can be estimated from the slopes in Figure 4d when two data points are obtained in each region. The effect of polymer molecular weight has a very similar trend to the polymer concentration in solution because it is directly related with the radius of gyration.

Polymer solution conductivity is another important parameter for stable and smooth fiber formation. More conductive solutions have higher charge densities, leading to stronger overall repulsion forces between charges in the liquid. As the jet stretching effect becomes stronger the result is thinner fiber diameter and reduced bead formation.

For *coaxial electrospinning*, because two solutions are used for each core and sheath layer, additional considerations of viscosity, miscibility, conductivities, vapor pressures and feeding rate ratio between core and sheath solutions are critical for successful operation. In the case where a combination of electrospinnable and non-electrospinnable solutions are used, the polymer concentration of the electrospinnable solution needs to be high enough to produce uniform core-sheath fibers.

An early review by Moghe and Gupta^[17] indicated general conditions for successful coaxial electrospinning, namely the use of a sheath solution with higher viscosity, conductivity and flow rate than those of the core solution is desirable, along with low interfacial tension between core and sheath solutions and

the use of relatively less volatile sheath solvents for stable Taylor cone formation.^[17] In addition to these conditions, many exceptions producing uniform core-sheath fibers have also been reported, such as superhydrophobic fibers using non-electrospinnable sheath solution^[26] and drug encapsulated fibers using very volatile sheath solution.^[27]

The selection of solvents for the selected polymers is an important and complex consideration to obtain successful coaxial electrospinning of core-sheath fibers. The effects of solvent inter-miscibility during coaxial electrospinning are outlined in Figure 5. Completely immiscible (Figure 5a) or miscible

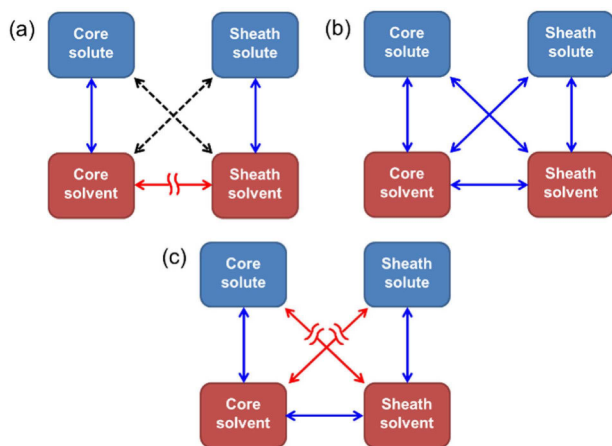


Figure 5. Miscibility of core and sheath solutions used in coaxial electrospinning: (a) totally immiscible solutions (solute and solvent); (b) totally miscible solutions (solute and solvent); (c) partially miscible solutions (solvent-only miscible). Reprinted with permission from Ref [107]. Copyright 2013 American Chemical Society.

(Figure 5b) solutions cause the least issue during coaxial electrospinning because there is no negative interaction between the solvent and the solute in the two solutions. However, when solvents are miscible but their solutes are not soluble in the solvent of the other layer (Figure 5c), core/sheath solutes can precipitate out of solution at the nozzle tip, resulting in an unstable coaxial electrospinning process. The use of two *immiscible* solutions can provide better core-sheath separation by preventing or minimizing interdiffusion between layers, but such possible combinations are limited. Coaxial electrospinning with two *miscible* solutions can produce fibers with distinct core-sheath structure if the jet travel time is shorter than the solution diffusion time constant and the evaporation rate of the polymer solvents is sufficiently fast. In this condition, however, it is challenging to obtain good hollow fiber structure because even minor diffusion between core and sheath can result in damage to the sheath layer during the removal of the core material. Therefore, to obtain robust hollow fibers using miscible solvents the two solutes in the core and sheath solutions need to be immiscible in the same solution.

Kurban et al. suggested the interesting solution selection model for coaxial electrospinning using Hansen solubility parameters (HSPs).^[25] The solubility of a given solute can be predicted considering dispersion (δ_d), polar (δ_p), and hydrogen

bonding (δ_h) interaction energies between molecules of solutes and solvents, with units of (MPa)^{1/2}. These parameters can be treated in 3-D coordinates. The solute's solubility sphere with a radius of interaction (R_0) is calculated empirically. Solvents within this sphere can be a potential solvent for the solute. The length from the origin of the solute solubility sphere for a specific solvent (R_a) can be obtained using Equation (2):

$$R_a^2 = 4(\delta_d^p - \delta_d^s)^2 + (\delta_p^p - \delta_p^s)^2 + (\delta_h^p - \delta_h^s)^2, \quad (2)$$

where δ_d^p , δ_p^p , δ_h^p are HSPs for the solute and δ_d^s , δ_p^s , δ_h^s are HSPs for the solvent. Smaller R_a values indicate better solvents. The 3-D model is simplified to a 2-D model by defining a new parameter (δ_v) that combines the dispersive and polar parameters [Eq. (3)]:

$$\delta_v = (\delta_d^2 - \delta_p^2)^{1/2}. \quad (3)$$

One example of solvent selection using Hansen parameters is shown in Figure 6a for polystyrene (PS) as the polymer and various solvents. PS's radius of interaction (R_0) is shown in the graph and solvents inside the solubility circle can be good solvents for PS. Solvents outside the circle do not dissolve PS, hence they can be used for polymers selected for the other layer of coaxial electrospinning. For porous fibers, either thermally induced phase separation (TIPS)^[29] or vapor induced phase separation (VIPS)^[30] is mainly responsible for pore formation on the fiber surface during electrospinning. It is also suggested that the electrical charge instability between core and sheath solutions within the liquid jet is responsible for pore formation on the fiber surface in semi-miscible solutions. When the core conductivity is higher than that of sheath solution, charge will accumulate at the core-sheath interface. When the interfacial surface tension is minimal, the electric charge driven instability at the interface can produce porous fibers. Figure 6b illustrates pore formation on the fiber surface caused by the growing instability at the core-sheath interface, leading to the intrusion of core into the fiber surface. SEM and TEM images of porous fibers produced when using a core solution with three orders of magnitude higher conductivity ($\sim 5.0 \times 10^{-8}$ S/cm) than that of the sheath solution ($\sim 1.0 \times 10^{-5}$ S/cm) are shown in Figure 6c and d, respectively. Less miscible or more viscous solutions for core and sheath can suppress this pore formation.

Polymeric microtubes were demonstrated (Figure 7a, b) by combining fast evaporating sheath and less volatile immiscible core solutions. As illustrated in Figure 7c, the sheath layer (region I) solidified quickly at first, then the core solvent evaporated gradually through the sheath layer. Evaporation from the core meniscus is negligible in very long electrospun fibers. Although the diffusion coefficient is very low $\sim 10^{-13}$ m²s⁻¹, extremely large surface area enables significant mass transport for quick core solidification.

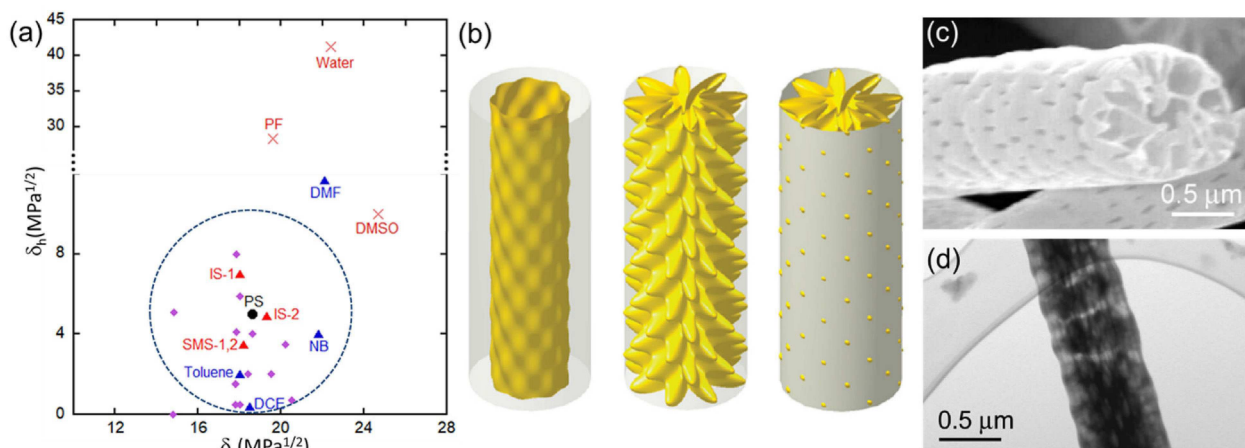


Figure 6. Solvent selection model using Hansen solubility parameters (HSPs): (a) two-dimensional diagram showing the extent of solubility of PS in selected solvents; (b) illustration of pore formation on the fiber surface due to the core-sheath instability; (c, d) related SEM and TEM images of porous fibers produced by using a core solution that 3 order of magnitude more conductive than the sheath solution. Adapted with permission from Ref [25]. Copyright 2010 American Chemical Society.

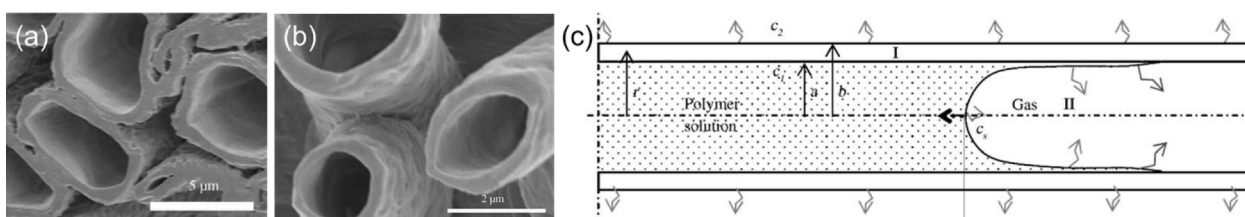


Figure 7. Polymeric microtubes production by coaxial electrospinning: cross-sectional SEM images of coaxially electrospun microtubes using volatile PCL sheath solution (in chloroform solvent) and either immiscible PEO (a) or PVA (b) core solution (in water/ethanol solvent mixture); (c) schematic illustration of microtube formation from the initial quick sheath solidification followed by core film deposition on the inner sheath wall. Reprinted with permission from Ref [28]. Copyright 2007 Wiley-VCH.

Nozzle Design

Nozzle design is another critical consideration in coaxial electrospinning. Preferably, the entire nozzle unit is electrically conductive and resistive to harsh chemicals. Interestingly, the use of electrically insulating material for the sheath nozzle can be beneficial to produce core-sheath fibers when non-electrospinnable material was used for the sheath layer.^[31] The core nozzle diameter and the gap width between its outer wall and the inner wall of the sheath nozzle need to be selected carefully considering solution flow rates in order to obtain stable core-sheath or hollow fibers. Concentricity of the core component in the combined nozzle is an important aspect to produce the stable compound Taylor cone that is necessary for the formation of uniform core-sheath structured fibers. In general, coaxial electrospinning has utilized mechanically aligned concentric coaxial nozzle in which the nozzle ends of both core and sheath components are either level or the core nozzle tip slightly protrudes. Reznik et al. experimentally and theoretically demonstrated that successful entrainment of the core liquid by the sheath solution was obtained when the core nozzle protrudes outside the sheath nozzle a distance of approximately one half of the sheath nozzle radius.^[33] Other interesting coaxial nozzle configurations include eccentric core nozzle

location and a shortened core nozzle. The latter configuration (known as core-cut) uses a core nozzle length that is shorter than the outer sheath nozzle. As reported by Lee et al., while the normal coaxial nozzle induces the physical transition and abrupt electric potential change on the compound droplet simultaneously, the core-cut coaxial nozzle enables microfluidic focusing of the core solution enveloped by the sheath solution before it reaches the exit of the sheath nozzle where the electric charges are accumulated. While the noticeable charge accumulation is shown on the core fluid (light blue color) and near the interface between core and sheath liquid stream (yellow color) at the end of normal coaxial nozzle (Figure 8a), no charge accumulation is observed using the core-cut coaxial nozzle (Figure 8b). Due to no charge accumulation using core-cut coaxial nozzle, a more stable operation is achieved which minimizes intermixing between the core and sheath fluids. Experimentally, core-cut coaxial nozzle electrospinning was able to produce more consistent hollow carbon fibers than that using normal coaxial nozzle. Both normal and core-cut coaxial nozzles produced hollow fibers when the sheath layer is thick enough (lower flow rate of core solution) as shown in Figure 8c and d, respectively. However, when a higher flow rate was used for the core solution, only core-cut nozzle produced stable

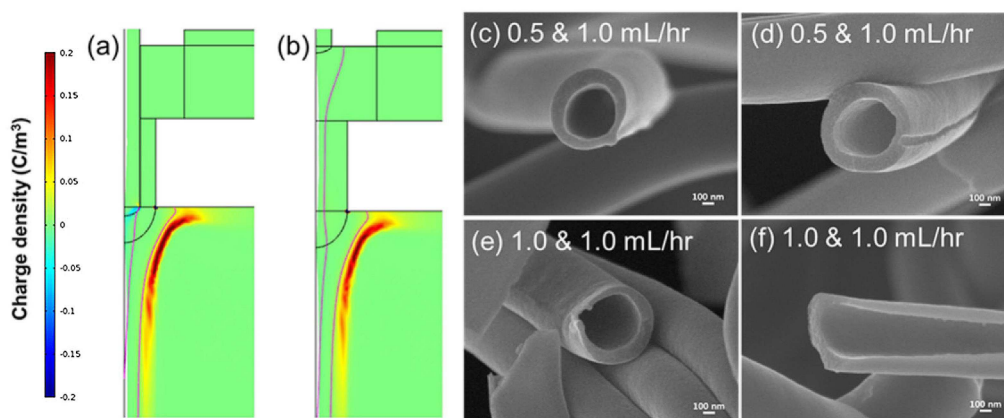


Figure 8. Space charge distribution on normal coaxial nozzle (a) and core-cut coaxial nozzle (b); (c)–(f) SEM images of hollow carbon nanofibers electrospun using normal coaxial nozzle (c) and (e) and core-cut coaxial nozzle (d) and (f). Flow rates of SAN core and PAN sheath are shown in each SEM image. Reprinted with permission from Ref [32]. Copyright 2014 Springer Nature.

hollow carbon fibers (Figure 8e) while normal coaxial nozzle produced C-shaped fibers as shown in Figure 8f.

Electrospinning Advantages

Electrospinning provides a simple, straightforward, and cost-effective method for producing continuous nanofibers from a wide range of natural and/or synthetic materials. Materials that can be either dissolved or dispersed in a solution or melt can be electrospun into nanofibers. Manipulating solution properties, such as viscosity and conductivity, can control the fiber diameter and pore size from micrometers to tens of nanometers. When necessary, fibers can be oriented in certain directions either by manipulating the electric field or using a rotating collector. Resulting electrospun nanofiber membranes provide unique and attractive features, including exceptionally high surface area, high porosity with large pore size, and self-supporting structure. Specific fiber morphologies can be obtained under excellent control. This combination of process and materials properties provide an enormous potential for developing various applications.

Further advantages and unique features of electrospinning can be realized using the coaxial concept: (a) combining properties from two different materials into a single core-sheath fiber; (b) producing hollow fibers or very thin fibers after removing either core or sheath layer; (c) encapsulating/protecting sensitive materials from outer environment; (d) providing programmable release kinetics of functional macromolecules from core minimizing initial burst problem; (e) enabling normally non-electrospinnable materials to be electrospun by being entrained by adjacent electrospinnable material.

Mass Production of Nanofibers

However, to commercialize the electrospinning products, the very low production rate was initially a big hurdle to be solved.

Although multiple nozzles can be a simple solution to increase the production rate, the production rate and fiber quality are not good enough to enable the mass production of electrospun membranes. When the nozzles are densely packed, there are repulsive interactions between multiple jets. Moreover, a nozzle cleaning system has to be integrated to deal with nozzle blockage. More recently, due to the substantial interest in electrospinning, many dedicated companies are providing lab-scale electrospinning equipment, apparatus and accessories. In addition, many companies have started to provide industrial level mass production units for electrospinning. Elmarco first introduced a mass production unit by moving from lab-scale equipment to industrial level (Figure 9a). To be relevant for mass production, various needle-less electrospinning techniques have been developed to enable industrial level production by electrospinning equipment companies, such as Elmarco, SPUR, Revolution Fibres, etc. These techniques include free surface electrospinning with 1st generation rotary spinneret (Figure 9b), recent wire spinneret (Figure 9c), rotary spikes spinneret (Figure 9d), bubble electrospinning^[39] and corona-alternating current electrospinning.^[40] Figure 9f shows a very large electrospun membrane produced by the Revolution Fibres pilot-unit (Figure 9e). Recent advances in needless electrospinning is thoroughly reviewed by Yu et al.^[41] As the mass production of electrospun fiber material is becoming increasingly feasible, the number of companies developing commercial products using electrospinning has steadily increased, as listed in Table 1.

Early Breakthroughs

While this article reviews primarily recent achievements in coaxial electrospinning, it is worthwhile to glimpse at early breakthroughs. In 2002, the first scientific article utilizing coaxial electrospinning (Figure 10a) was published in by Loscertales et al.^[38] Using two immiscible solutions, a compound Taylor cone and a liquid jet were clearly observed, as seen in

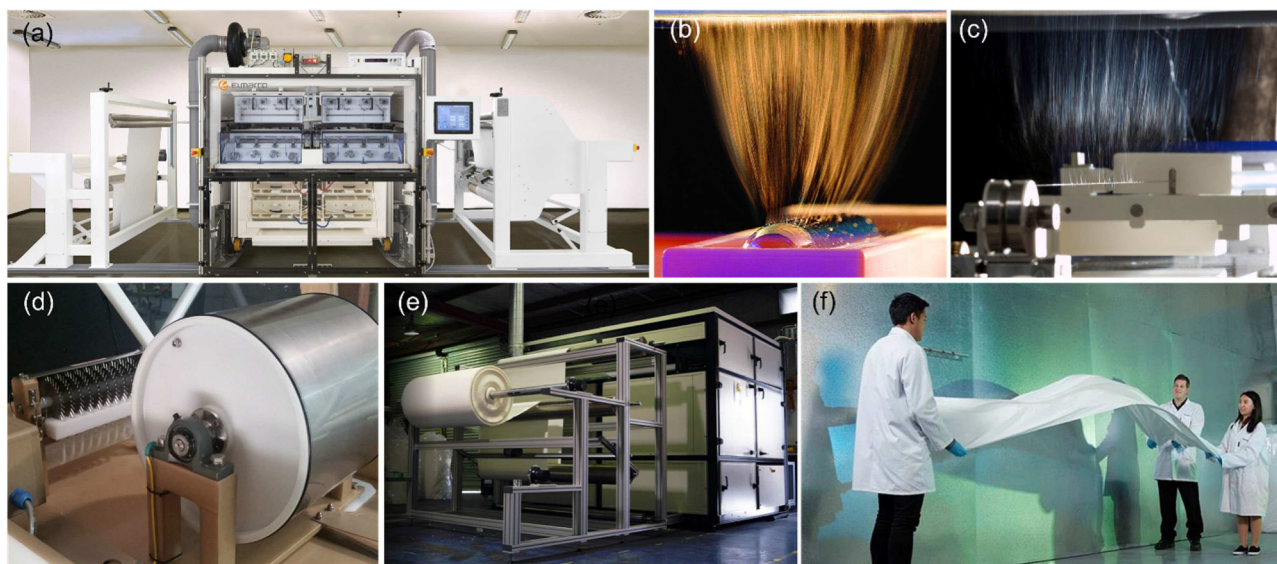


Figure 9. Industrial mass production units for electrospinning of fiber membranes: (a) Elmarco Nanospider™ Industrial level production unit (NS Production Line NS 8S1600U); ejection of numerous liquid jets using first-generation rotary cylinder (b)^[34] and recent generation wire electrode (c)^[35] reprinted with permission, courtesy of Elmarco s.r.o.; (d) lab-scale AGL electrospinning platform with rotating spikes and (e) pilot-scale Komodo platform, (f) large area nanofiber membrane produced with Revolution Fibres pilot-unit,^[36] reprinted with permission, courtesy of Revolution Fibres LLC.

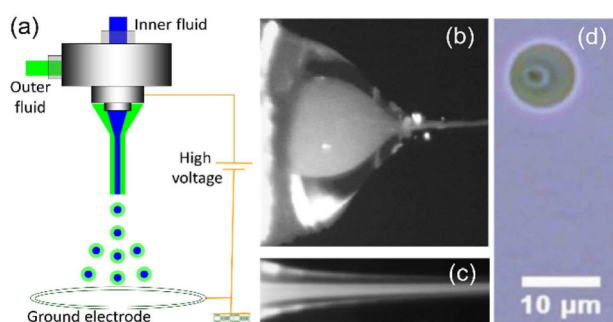


Figure 10. First coaxial electrospay report: (a) coaxial electrospay setup; (b) coaxial Taylor cone; (c) downstream detail of the two coaxial jets emitted from the vertexes of the two menisci. Reprinted with permission from Ref [38a]. Copyright 2006 John Wiley and Sons; (d) microscopic image of collected coaxial capsules. Reprinted with permission from Ref [38c]. Copyright 2007 American Physical Society.^[38]

Figure 10b and c, respectively. Monodispersed compound liquid (water core and olive oil shell) or capsules (ethylene glycol core and DuPont photopolymer Somos 6120 shell) were successfully produced with diameters varying between 10 and 0.15 μm , depending on the operational parameters. Collected coaxial capsules with different diameters (10 μm and 8 μm) are obtained. The hardening process of the sheath can also be thermally or chemically initiated under the use of appropriate reagents.^[38b]

Subsequent to the report of coaxial electrospaying, the first core-sheath fibers were demonstrated by Sun et al.^[42] from the Marburg (Greiner/Wendorff) and Technion groups (Yarin/Zussman) in the following year, 2003. Core-sheath fibers made of PDT core – PEO sheath (Figure 11a) and PSU core – PEO sheath (Figure 11b) were demonstrated using coaxial electrospinning. They also reported that normally non-electrospinnable materi-

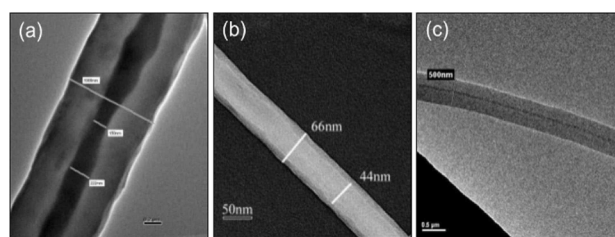


Figure 11. First core-sheath fibers by coaxial electrospinning. TEM images: (a) coaxially electrospun PDT core and PEO sheath fiber; (b) PSU core and PEO sheath fiber; (c) non-electrospinnable Pd(OAc)₂ core and electrospinnable PLA sheath fiber. Reprinted with permission from Ref [42]. Copyright 2003 Wiley-VCH.

als, such as palladium acetate (Pd(OAc)₂), could be electrospun as the core component under the influence of electrospinnable PLA sheath material, (Figure 11c). Interestingly, even when the same material (PEO) was used for both core and sheath, a core-sheath structure with a sharp boundary was observed because the electrospinning process is fast enough to prevent noticeable diffusion between core and sheath layers.

Highly diluted polymer solutions have very low viscosity and cannot be electrospun or at best produce extremely beaded fibers. The Rutledge group at MIT addressed this issue using the electrospinnable sheath polymer as a sacrificial layer.^[43] Using this approach, extremely thin nanofibers < 100 nm can be obtained after removing sacrificial layer. Electrospinnable copolymer or PEO was used for sheath and very diluted PAN or silk solutions were used for core. Although single nozzle electrospinning of PAN 8 wt% solution generates beaded fibers, as shown in the inset of Figure 12a, coaxial electrospinning with PAN 8 wt% as a core produced very thin and uniform fiber diameter (Figure 12a). Even much lower

Table 1. Companies that produce electrospun fiber-based products and/or electrospinning equipment. ^[37]					
Company	Country	Product	Company	Country	Product
Clarcor	USA	ProTura® Nanofiber, air filter cartridge	Electrospinning Company	UK	96-well plate, 12-well and 6-well plate w. random nanofibers
Sigma Aldrich	USA	Nanofiber culture plates	Neotherix	UK	Manufactures nanofiber scaffold for tissue regeneration
Zeus	USA	Bioweb™ medical; filtration membrane	Cella Energy	UK	Low-cost hydrogen storage
PolyRemedy	USA	HealSmart™ Personalized Antimicrobial Dressings	Nicast	Israel	AVflo™ Vascular Access Graft
PolyElements	USA	6-well, 12-well plate w. random & aligned nanofibers	NanoSpun Technologies	Israel	Developer of nanofibers for commercial application
3D Biotek	USA	Cell culture inserts	Finetex EnE, Inc	South Korea	Nanofiber-based air filters, water filters, oil filters and textiles
Donaldson	USA	Fineweb™; Ultra-Web® Electrospun Nanofiber	Hirose Paper Mfg Co., Ltd	Japan	Nanofiber coated paper
Nanofiber Solutions	USA	NanoECM, NanoAligned, NanoHep cell culture plates	Koken	Japan	FERENA filtering unit used in KOACH (Clean zone)
SNS Nanofiber Technol.	USA	Nanosan®, material	Ortho ReBirth	Japan	Rebossis, synthetic bone
eSpin Technologies	USA	Exceed™, residential, commercial building filters	MANN + HUMMEL	Germany	Micrograde NF filter, air cleaners for vehicles
Liquidity Corporation	USA	Naked Filter for water	BIOTRONIX	Germany	Papyrus, Coronary Balloon-Expandable Stent Systems
Coway	USA	Nanotrap	PolyNanoTec	Germany	Formulation of electrospinning material
Arsenal Medical	USA	Hemorrhage treatment	ske Advanced Therapies	Italy	Silk Fibroin tubular scaffold, flat sheet scaffold, disc
Biomimetic Electrospinning Technologies	USA	Customized scaffold for biomedical application	Soft Materials and Technologies S.r.l.	Italy	Customized nanofiber products
BioSurfaces Inc.	USA	Drug loaded electrospun fibers for medical applications	IQ Commercial	New Zealand	Return focus pod, office partitions
fiber Trap	USA	Pest control	RevolutionFibres	New Zealand	Nanodream, nanofibre pillow lining; Xantu-Layr composite; Phonix sound barrier
Nanofiber Separations LLC	USA	Separation media composed of functionalized nanofibers	HRV	New Zealand	SETA™, Home Filtration Technology
Axium Nano	USA	Battery material	Kilwell	New Zealand	Kilwell NZ Xantu, advance fishing rod
SPUR Nanotechnologies	Czech	Liquid and air filtration membrane	Esfil Techno	Estonia	Filtering materials, half-masks, analytical tapes
Pardam nanotechnology	Czech	NnF MBRANE®; NnF CERAM®	NASK	Hong Kong	Smart Mask
Astrapool	Australia	Filtration system for residential pools	Sorbent	Russia	Petryanov's filtering cloth, air filters and mask
Stellenbosch Nanofiber Company	South Africa	Develop, manufacture nanofiber materials for med. applications	Zurich Biomaterials AG	Switzerland	Bonewool®, implant material for bone regeneration
Nano109 Co., Ltd	Turkey	Air Filter Media			

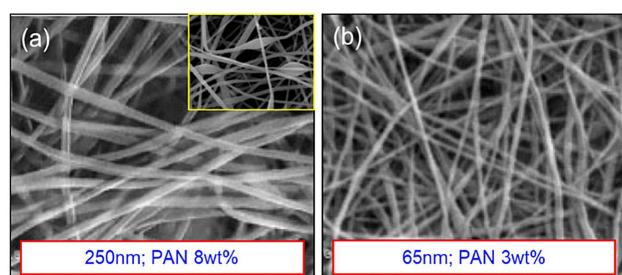


Figure 12. Thin nanofibers after removing sacrificial sheath. SEM of coaxially electrospun PAN fibers after removing PAN-co-PS sheath layer. Different concentrations were used for the PAN core solution: (a) 8 wt%; (b) 3 wt%. Reprinted with permission from Ref [43]. Copyright 2004 Wiley-VCH.

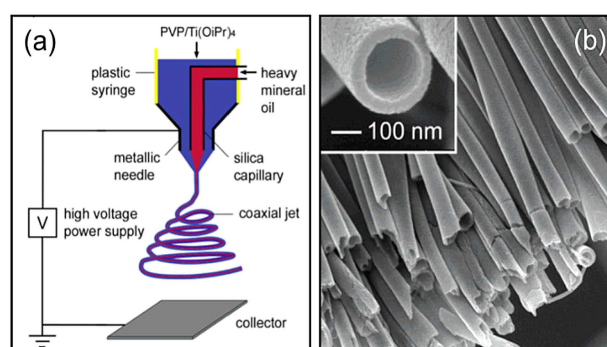


Figure 13. Nanotube formation using coaxial electrospinning: (a) setup; (b) SEM image of a uniaxially aligned array of TiO₂ hollow fibers. Reprinted with permission from Ref [44]. Copyright 2004 American Chemical Society.

concentration of 3 wt% could produce uniform PAN nanofibers with ~65 nm diameter, as shown in Figure 12b.

In 2004, Li and Xia demonstrated titania hollow nanotubes using coaxial electrospinning. Non-electrospinnable heavy min-

eral oil core and electrospinnable PVP/Ti(OiPr)₄ composite sheath solution were used, as illustrated in Figure 13a. Heavy mineral oil is not evaporated during electrospinning and is

entrapped by the sheath polymer, leading to hollow fibers (Figure 13b) after selective core removal (dipping into octane). Upon calcination, hollow structured titania nanotubes were obtained. Fluid flow rates can control the fiber diameter and wall thickness.^[44]

Coaxial electrospinning has been used to resolve the premature solidification issue that occasionally may occur at the nozzle tip during the electrospinning process, especially when highly volatile solvents are used. Solvent-saturated nitrogen gas was flown into the outer nozzle, while the volatile solution was fed into the inner nozzle. The same solvent with the core solvent was selected to generate vapor for the outer nozzle. Due to the presence of an effective gas jacket, the Taylor cone solidification is much reduced. In this case, a very stable Taylor cone and liquid jet ejection were maintained (Figure 14a), while the solution at the nozzle without the gas

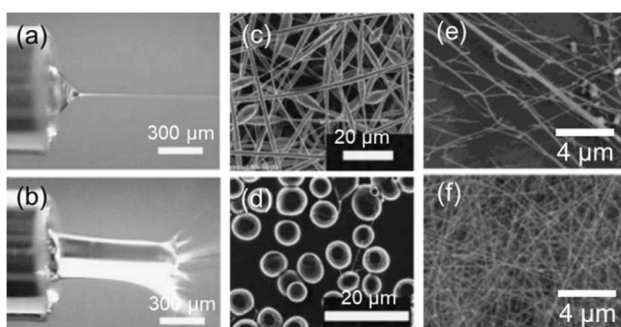


Figure 14. Gas jacket using coaxial spinneret – Larsen^[45] & Chu:^[46] (a) stable core Taylor cone and liquid jet ejection with solvent-saturated N₂ gas jacket; (b) solidified core solution when no gas jacket present. SEM images of beaded fibers (c) at 8 cm³/min and electrospayed particles (d) at 80 cm³/min. Reprinted with permission from Ref [45]. Copyright 2004 Wiley-VCH; high molecular weight (3.5 MDa) hyaluronic acid fibers produced with heated air jacket at 39 °C (e) and 57 °C (f). Reprinted with permission from Ref [46]. Copyright 2004 American Chemical Society.

jacket experienced solidification/clogging issues (Figure 14b). Interestingly, increasing the gas flow rate can change the fiber morphology from fibers (Figure 14c) to microparticles (Figure 14d) without changing solution properties.^[45]

Heated air as a gas jacket was used to improve uniform fiber production.^[46] While very irregularly sized fibers were obtained at 39 °C (Figure 14e), highly uniform thin fibers were obtained at the higher temperature of 57 °C (Figure 14f).

The Ramakrishna group at the National University of Singapore first reported the use of coaxial tissue scaffold, consisting of collagen sheath and PCL core (Figure 15a). As shown in Figure 15b, coaxially electrospun fibers made of PCL core and collagen sheath (red line) show similar cell culture efficiency to the pure collagen fibers (green line) due to the excellent biocompatibility of collagen sheath surface, and provide better human dermal fibroblasts (HDF) cell density increase (~32%) after 6 day culture than that of dip-coated collagen-PCL fibers (~21%).^[47] The enhancement of mechanical tensile properties from the PCL core was also demonstrated by other groups.^[48]

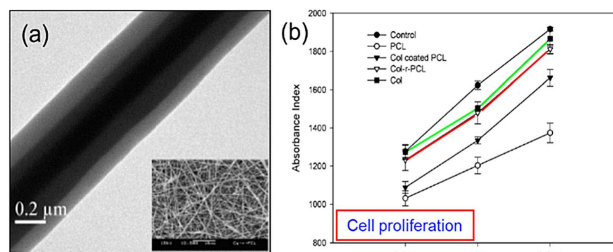


Figure 15. Tissue engineered scaffold: (a) TEM image of coaxial fibers with PCL core and collagen sheath; (b) cell proliferation of human dermal fibroblasts on fibers of different compositions. Reprinted with permission from Ref [47]. Copyright 2005 American Chemical Society.

One of great benefits from coaxial electrospinning is the ability to encapsulate functional macromolecules, such as proteins and drugs, in a simple one-step process. Jiang et al. first demonstrated^[49] this capability of coaxial fibers for the controlled release of encapsulated proteins. Bovine serum albumin (BSA) and lysozyme were loaded as a model protein in polyethylene glycol (PEG) core, and PCL sheath was used for encapsulating the core proteins. The release kinetics can be controlled by adjusting core flow rate (Figure 16a), since as the

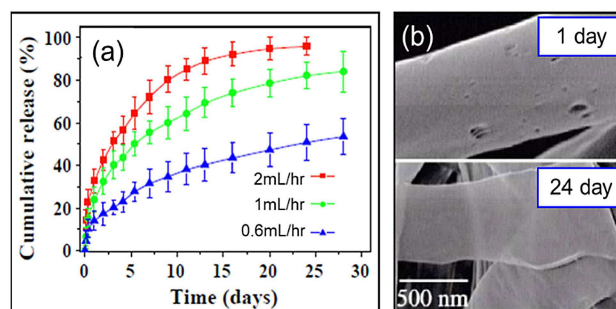


Figure 16. Sustained molecule delivery – Jiang et al. using structured nanofibers composed of PCL as shell and BSA-loaded PEG as core: (a) BSA release profiles for several feed rates of the inner component; (b) fiber morphologies after incubation in release media for 1 day (top) and 24 days (bottom). Reprinted with permission from Ref [49]. Copyright 2005 Elsevier.

core flow rate increases the sheath becomes thinner. SEM images in Figure 16b shows the change of fiber morphology before (upper) and after (lower) releasing most of core materials. Electrospinning had no apparent negative effect on either structure or stability of lysozyme based on both electrophoresis and CD spectra analysis.^[49]

In 2006, the melt coaxial electrospinning developed^[50] by Xia group provides a simple method for the encapsulation of phase change materials (PCMs), such as octadecane and eicosane, with melting points near room and body temperatures, respectively. As illustrated in Figure 17a, the PCM core material is heated to reach a liquid state and injected into the inner channel of the coaxial nozzle. The electrospinning process is governed by the electrospinnable sheath solution. After the liquid is ejected from the nozzle, cooling due to sheath solvent evaporation solidifies the PCM material and encapsulates it into

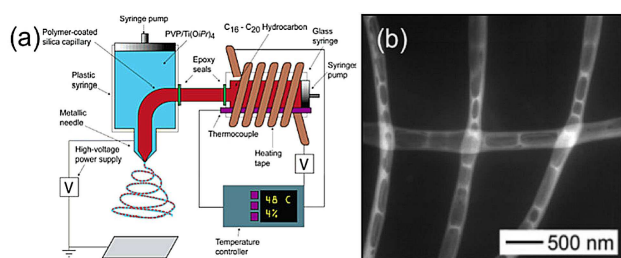


Figure 17. Melt coaxial electrospinning by McCann et al.: (a) schematic of the melt coaxial electrospinning setup; (b) TEM image of segmented hollow fibers after the octadecane core removal. Reprinted with permission from Ref [50]. Copyright 2006 American Chemical Society.

the fiber. Due to the low viscosity of the PCM core melt, a segmented core morphology was obtained (Figure 17b). Melt coaxially electrospun fibers show excellent thermal insulation and stabilization properties.^[50] This technique can possibly be applied to other thermoplastics and their combinations, such as PCL,^[51] PLGA,^[52] and PP,^[53] which were demonstrated using single nozzle melt electrospinning.^[54] Because little or no solvent is used, this technique is environmentally friendly and cost-effective.^[55] While melt electrospinning using single nozzle electrospinning generally covers a smaller fiber deposition area because of weak whipping action, coaxial melt electrospinning provides good whipping and bend actions because of the electrospinnable sheath solution, resulting in much thinner nanofiber diameters.

In 2006, Townsend-Nicholson and Jayasinghe of University College London directly electrospun living cells suspensions using coaxial electrospinning. Normally, stable electrospinning process cannot be formed with biosuspensions containing live organisms because they require a high ion concentration and have a relatively low viscosity. However, by utilizing a PDMS electrospinnable sheath solution, a stable electrospinning process was established that produced fibers encapsulating living cells with no negative effect on cell viability (~70%). These results successfully demonstrated the feasibility of active biological scaffolds with a living organism using coaxial electrospinning. Figure 18a shows the successful cell encapsulation

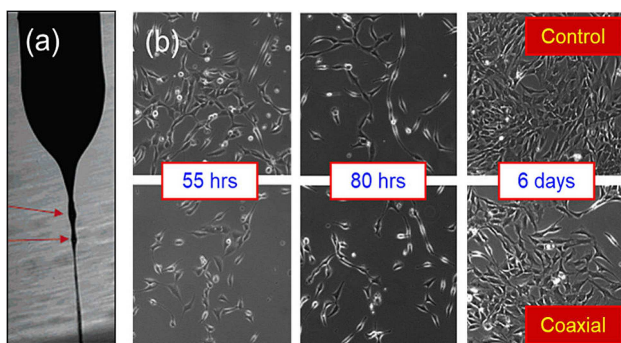


Figure 18. Cell electrospinning by Townsend-Nicholson et al.: (a) stable Taylor cone formation and liquid jet ejection with cells; (b) photomicrographs of collected cells cultured over 6 days. Reprinted with permission from Ref [56]. Copyright 2006 American Chemical Society.

during electrospinning process and comparable cell viability and morphology compared to no electric field control case (Figure 18b).^[56]

Also in 2006, Ma et al. from the Rutledge group at MIT and Kalra from the Joo group at Cornell demonstrated various stable periodic structures formed by confining block copolymers in the core using coaxial electrospinning. Block copolymers, such as poly(styrene-*b*-isoprene-*b*-styrene) (SIS) and poly(styrene-*b*-isoprene) (SI), were encapsulated into a polymer shell, such as P(MMA-*ran*-MAA) and sol-gel precursors (Figure 19a). After annealing the fibers above the glass transition

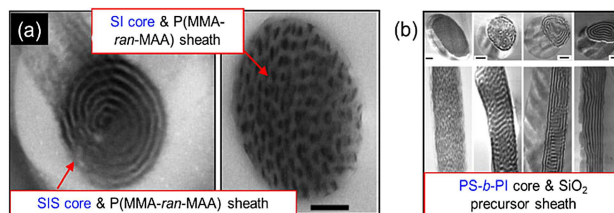


Figure 19. Internal Periodic Structure^[57] & Confined Assembly^[58] Structures with different periodicities depending on: (a) block copolymer core material (Reprinted with permission from Ref [57]. Copyright 2006 American Chemical Society); (b) annealing conditions (Reprinted with permission from Ref [58]. Copyright 2006 Wiley-VCH).

temperature of the block copolymer, well-defined periodic structures were formed in the block copolymer core. The glass transition temperature of the sheath polymer needs to be higher than the annealing temperature in order to retain the integrity of the fiber structure. After removing the sheath polymer, a pure block copolymer fiber mat having various well-defined periodic structures is obtained by adjusting annealing conditions, as illustrated in Figure 19b.

Recent Results & Applications

Biomedical Applications

Electrospinning for biomedical applications has rapidly emerged because of its ability to produce highly porous nanofiber membranes/scaffolds that are very similar to the natural extracellular matrix (ECM) and because it has at its disposal a very wide material selection of synthetic (PCL,^[59] PLLA,^[60] PLGA,^[61] PVA^[62]) and natural (cellulosic derivatives,^[63] chitosan,^[64] collagen,^[65] gelatin,^[66] zein^[67]) polymers. In addition to these attractive characteristics of conventional electrospinning, coaxial electrospinning provides additional important and unique features relevant to biomedical applications, including (a) combination of two or more materials in a single fiber; (b) design of controlled release kinetics of incorporated drugs; (c) protection of incorporated drugs from the outer environment. Biomedical applications frequently using coaxial electrospinning of core/sheath fiber membranes are tissue engineered scaffolds, wound dressings and drug delivery devices. The controlled release of incorporated drugs is a very important feature,

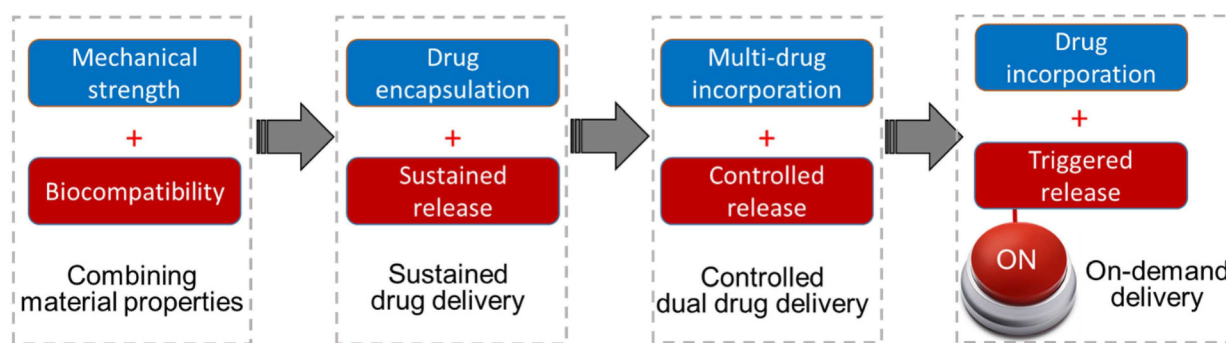


Figure 20. Evolving trend of drug delivery approaches using coaxial electrospinning.

especially for toxic drugs (such as doxorubicin^[68]) in order to minimize negative side effects for patients.

In the early stage of coaxial electrospinning development, as indicated in Figure 20, core-sheath fibers enabled the incorporation of two different polymers into a single fiber. This provided, among other possibilities, the ability to combine good mechanical properties from synthetic polymers and cell biocompatibility from biomaterials.^[47–48,69] Since the first demonstration of controlled release of encapsulated molecules from coaxial fibers as described earlier, coaxial electrospinning has become one of most popular techniques for developing novel drug delivery vehicles. In most cases, drug molecules are incorporated into the core and encased by the sheath layer, enabling the sustained release of the drug from the core. At later stages of development, two or more drugs were incorporated either into the core or in both layers, enabling a synergistic effect from multiple drugs.^[70] An emerging development in controlled release from coaxial fibers is the incorporation of release “triggered” by external stimuli. Key details of selected research works will be described in the following sections.

Combination of Biocompatibility and Mechanical Strength

The combination of complementary properties from two different materials can provide unique features. This is very attractive for many applications, starting with tissue engineering. Biomaterials, such as gelatin, collagen, and chitosan, possess excellent biocompatibility but often suffer from weak mechanical properties especially in wet condition. On the other hand, synthetic polymers, such as PCL, PLA, and PLGA provide good mechanical strength, while their biocompatibility is not comparable to that of natural biomaterials. Since the early demonstration of combined PCL core and gelatin or collagen sheath, core-sheath fibers with medical grade polyurethane (PU) core and collagen sheath demonstrated both improved mechanical properties (vs. collagen fibers) and higher cell proliferation results than both collagen-only and PU-only fibers.^[69c] Another important example of core-sheath fibers for biomedical application was demonstrated with PLLA core and chitosan sheath. Cytocompatibility and proliferation of human

bone marrow-derived UE7T-13 cells, blood compatibility considering blood coagulation and hemolysis of RBCs, and mechanical (tensile) properties are shown to be superior to those of PLA fibers.^[69d] Coaxial fibers using two natural biomaterials were demonstrated using electrospinnable gelatin as a core and non-electrospinnable chitosan as a sheath. Generally, mechanical properties of core-sheath membranes were enhanced by incorporating a synthetic polymer in one of the layers. Another option for the same purpose is to use naturally derived cross-linking agents, such as dextran aldehyde and sucrose aldehyde. These were utilized with gelatin-chitosan core-sheath fibers to enhance the mechanical integrity in wet environment without inducing cytotoxicity (as is the case with conventional cross-linking agents). Human osteoblast-like MG-63 cells were grown much better on membranes crosslinked by naturally derived crosslinking agents than on membranes crosslinked by chemically synthesized glutaraldehyde agent.^[71]

The incorporation and controlled release of drug molecules from core-sheath fibers is being widely investigated for various tissue engineering areas, including bone,^[72] muscle,^[73] skin,^[74] cardiac,^[75] blood vessels,^[76] and nerve regeneration.^[77] Many different growth factors such as basic fibroblast growth factor (bFGF),^[78] vascular endothelial growth factor (VEGF),^[76a] bone morphogenetic protein 2 (BMP 2) and dexamethasone (DEX),^[72] and nerve growth factor (NGF)^[77b] were incorporated into the core layer to provide better cell culture performance. The use of coaxial electrospinning of fiber membranes for drug delivery was expanded to other biomedical applications, such as suture,^[79] gene therapy through either viral gene delivery^[80] or non-viral gene delivery,^[81] probiotics medication delivering living bacteria^[82] and bioremediation for water treatment,^[83] sustained drug delivery using liposomes in core,^[84] anti-bacterial phase therapy delivering T4-bacteriophage.^[85] Selected examples are listed in Table 2.

Nerve Tissue Engineering

Every year more than 200,000 procedures are being carried out for peripheral nerve injuries in the United States alone.^[86] Unlike the central nervous system (such as the brain and spinal cord), damaged peripheral nerve system can be regenerated and

Table 2. Summary of selected coaxial fibers as controlled drug delivery vehicles.					
Core Composition	Purpose	Sheath Composition	Purpose	Features	Ref.
Epidermal growth factor, retinoic acid, insulin, hydrocortisone + BSA	Multiple epidermal induction factors delivery	PLLCL + gelatin (4:6)	Encapsulation & fiber formation	Deliver multiple factors with no burst release. Compared to blended fibers, 44% higher cell proliferation and higher cell differentiation (62 vs 43%) to epidermal lineages.	[74]
Tetracycline hydrochloride	Model drug	PLLA	Drug encapsulation & fiber formation	Sustained release and braided coaxial nanofibers also demonstrated for sutures.	[79]
Adenovirus + BSA	Virus delivering gene	PCL	Encapsulating core material.	Demonstrating sustained and localized cell transduction via viral gene delivery.	[80]
Plasmid DNA + PEG	gene for delivery	poly(ethyleneimine)-hyaluronic acid (PEI-HA) + PCL	Delivering non-viral gene delivery vector	Significantly improved transfection efficiency by subsequent release of non-viral gene delivery vector	[81]
<i>B. animalis</i> Bb12 bacteria	Bacteria for delivery	PVOH	Encapsulating bacteria	Encapsulated bacteria remain viable much longer than non-encapsulated.	[82]
Bacteria + PEO	Bacteria for bioremediation	PCL + PEG	Microtube formation encapsulating bacteria	Encapsulated bacteria in microtubes maintain enzymatic activities.	[83]
bFGF	Growth factor	PLGA	Fiber formation encapsulating growth factor	bFGF loaded scaffold shows better cell culture and sustained release of bFGF.	[78]
vascular endothelial growth factor (VEGF) + Dextran	Growth factor	PLGA	Fiber formation encapsulating growth factor	Sustained release > 28 days promoting cell proliferation.	[76a]
DEX + BMP2	Growth factor + Drug	PLLACL + collagen	Fiber formation and hMSC cell compatibility	Controlled release of two growth factors inducing hMSC to differentiate into osteogenic cell.	[72]
PVA + horseradish peroxidase (HRP) encapsulated liposomes.	Combining liposomes into nanofibers	PCL	Encapsulating liposome carriers	Sustained efficacy of encapsulated liposomes in core-sheath fibers.	[84]
B-NGF + PEG	Nerve growth factor	PLGA	Fiber formation encapsulating NGF	Coaxial fibers delivering NGF better nerve regeneration than that of PLGA fiber-only, yet comparable to nerve autograft.	[77b]

recovered. The current method using autografts has many limitations, including neuroma formation, limited supply of donor sites, and dimensional differences. Nerve repair using tissue engineering is an alternative approach with potential significance for treatment of nerve damaged patients. For this purpose, nerve guide conduits (NGCs) have been developed to guide the nerve regeneration between disconnected nerves. Coaxial electrospinning has been used to develop novel nerve guide conduits made of core-sheath fibers incorporating nerve growth factor (NGF).^[77a] Biodegradable P(LLA-CL) was used for the fiber sheath material to encapsulate NGF in the core of nanofibers. Coaxially electrospun fibers collected on a thin rotating rod have been used to form the tubular structured

membrane shown in Figure 21a. NGC bridging 10 mm long were prepared to form sciatic nerves in rats (Figure 21b). Nerve regeneration (Figure 21c) comparable to the autograft approach was obtained. Aligned coaxial fibers have been reported to promote peripheral nerve regeneration.^[77b]

In nerve regeneration, laminin stimulates neurite outgrowth and influences the growth of Schwann cells, which provide guidance to the axon re-growth. Kijeńska et al. demonstrated core-sheath fibers made of laminin core and PLCL sheath to promote nerve regeneration.^[87] Although its mechanical elongation properties (42%) were slightly lower than PLCL-only fibers (69%), significant increase of ~78% of Schwann cell (SC) growth was obtained when compared to blended fibers, because of the controlled release of bioactive laminin from the core. Higher SC proliferation and maturation were also observed using coaxial fibers. Air plasma treated coaxial fibers with NGF/silk fibroin (SF) core and PLA sheath were also demonstrated for peripheral nerve tissue regeneration.^[88] Air plasma treatment improved the surface hydrophilicity of the membrane. Although plasma treated membrane does not provide higher cell proliferation, it enables elongated neurites with length of up to 95 μm .

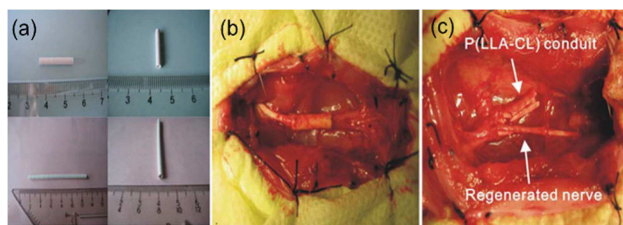


Figure 21. Peripheral nerve regeneration using aligned coaxial fibers: (a) composite nerve conduit tube fabricated using coaxial electrospinning on thin rotating rod; (b) composite nerve conduit implanted by epineurium suturing across the 10-mm gap in the sciatic nerve; (c) regenerated nerve and degraded conduit after 12-week post-implantation. Reprinted with permission from Ref [77a]. Copyright 2010 John Wiley and Sons.

Bone Tissue Engineering

Bone tissue engineering is also an important research topic because current autograft and allograft methods suffer from limited available supply and possible disease transfer, respectively. Tissue engineered scaffolds have been developed using various methods including coaxial electrospinning. Coaxial fibers incorporating osteo-inductive bone morphogenetic protein-2 (BMP-2) growth factor in the core and an osteoconductive silk fibroin/chitosan/nanohydroxyapatite (SF/CS/nHAP) composite material in the sheath were demonstrated. Chitosan shows good differentiation of bone marrow mesenchymal stem cells (MSC), while its poor mechanical strength was enhanced by adding biocompatible SF and osteoconductive nHAP, synergistically promoting bone regeneration. Mineralization of human-bone-marrow-derived MSCs (hMSCs) on various substrate surfaces were evaluated using von Kossa staining (Figure 22).

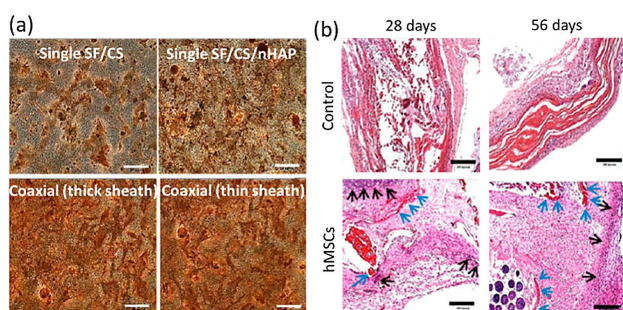


Figure 22. Evaluation of bone regeneration on various fiber membranes: (a) hMSCs mineralization comparison after 28 days on different types of fiber scaffolds by von Kossa staining; (b) histological staining of acellular control and hMSC-seeded coaxial fiber scaffold after 4 and 8 weeks of subcutaneous implantation in nude mice. Black arrows denote osteoblasts in the bone matrix, while blue arrows denote osteoids. Bar = 200 μm . Reprinted with permission from Ref [89]. Copyright 2015 American Chemical Society.

Coaxial samples show much higher mineralization of hMSCs as shown in Figure 22a, indicating that controlled release of BMP-2 promoted osteogenic differentiation of hMSCs. Figure 22b shows osteoblasts and unmineralized osteoids as a dark-violet region (black arrows) and a purple color region (blue arrows), respectively, for samples with hMSCs after 28 and 56 days. No osteoblasts and osteoids are shown in acellular controls having only reddish color because of cell ingrowth into the scaffold. Results from *in vivo* rat implantation of prepared coaxial fibers with hMSCs demonstrated the ectopic bone formation and osteogenesis of hMSCs from synergistic effect of osteoconductive nHAP and osteo-inductive BMP-2.^[89]

Coaxial fibers with a structure similar to the architecture of native bone were also demonstrated using a core of nanoparticle composite of hydroxyapatite and tussah silk fibroin encased in a sheath of tussah silk fibroin. Compared to the single tussah silk nanofibers, the coaxial fiber provides better mechanical strength, with 90 \times and 2 \times higher Young's modulus and breaking stress, respectively. Osteoblast-like MG-6 cells adhered and proliferated well. Coaxial fiber promoted alkaline

phosphatase and mineral deposition with better biocompatibility than pure tussah silk fibroin.^[90] Due to the higher growth rate of fibroblast in soft tissue than bone cells, bone regeneration can be disturbed by fibroblast growth into the bone defect area. To avoid this issue, guided tissue regeneration membranes were prepared by configuring PLGA/HA core and collagen/amoxicillin shell fibers. While the sheath material promotes wound healing, the core blocks the fibroblast growth into bone defect, as well as promoting bone growth.^[91]

Periodontal Regeneration

Coaxial fibers have been also utilized for periodontal regeneration. Gum tragacanth with tetracycline hydrochloride (TCH) was encapsulated by PLGA sheath. Gum tragacanth, an anionic polysaccharide, provides a more sustained release of hydrophilic drug TCH, which is important to treat the periodontal disease. Using the coaxial structure, TCH can be released up to 75 days with a small initial burst release of $\sim 19\%$ within 2 hr.^[92] Another combination with PEI (polyethylenimine)/pBMP2 (bone morphogenetic protein-2 plasmid) core and PLGA sheath was demonstrated for periodontal regeneration, delivering pBMP2 to human periodontal ligament stem cells (hPDLSCs). Although PEI polymer is useful for its high transfection efficiency, it is toxic under *in vivo* condition. However, in the coaxial structure, any cytotoxicity was prevented by the PLGA sheath, while still providing high transfection efficiency of PEI core. Coaxial fiber showed BMP2 expression over 28 days, which is much longer than for single PLGA nanofibers.^[93]

Other Tissue Engineering

The sustained release of hydrophilic therapeutic molecules is a challenging issue because hydrophilic molecules are easily soluble in aqueous media resulting in a quick release. To minimize the initial burst release of hydrophilic drug from the core, blended core (hydrophobic PMMA/hydrophilic PVA) incorporated with ciprofloxacin hydrochloride (CIP) drug was used with PMMA shell. Compared to monolithic PVP core, it achieved long sustained release of more than 14 days with no initial burst release. Its release rate can be controlled by adjusting the ratio of hydrophobic and hydrophilic polymers.^[94]

Heparin encapsulated P(LLA-CL) coaxial fiber (heparin core & P(LLA-CL) sheath) has been reported for to promote graft patency rate, releasing heparin over a period of 12 weeks. In conjunction with autologous endothelial cell (EC) pre-endothelialization in the canine femoral artery replacement model, it promoted a 24-week patency rate of P(LLA-CL) scaffolds up to 88.9% versus 12.5% in the control group. Heparin-loaded P(LLA-CL) scaffolds with autologous EC pre-endothelialization have the potential to be substitutes for natural small-diameter vessels in planned vascular bypass surgery.^[95]

Metronidazole (MNA)-loaded PCL/zein core/sheath nanofibers have been demonstrated as a potential guided tissue regeneration (GTR) membrane. Because GTR failure is mostly

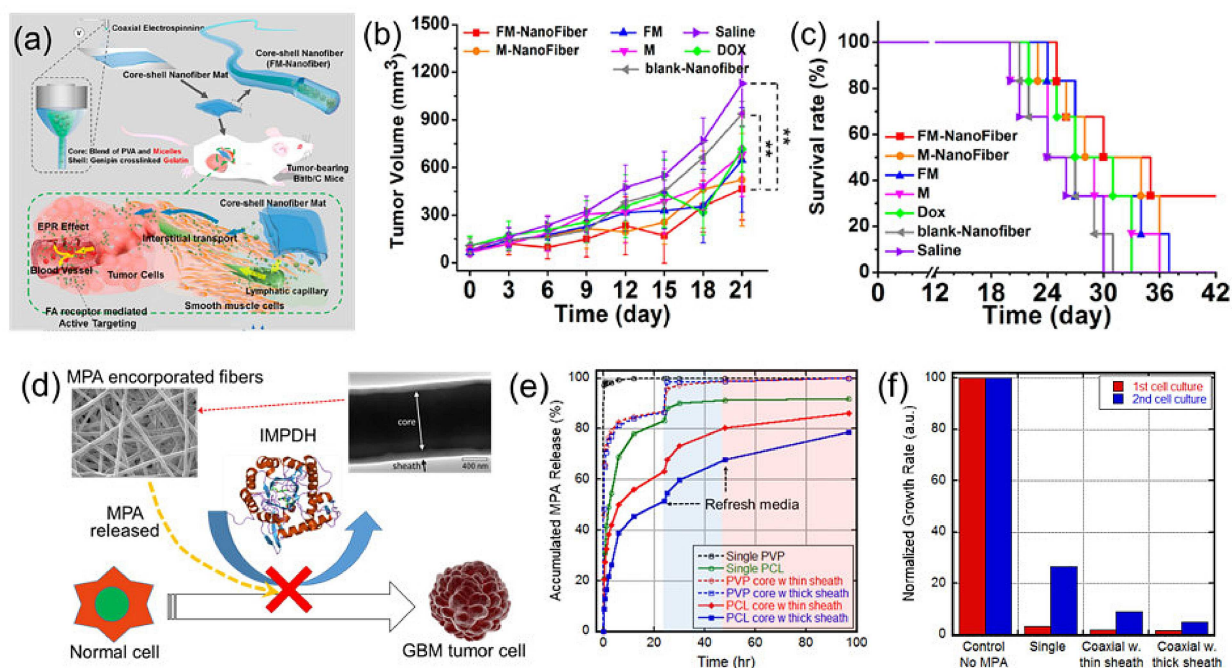


Figure 23. Coaxial fibers for the targeted localized cancer therapy using PVA with DOX-encapsulated micelles core and gelatin sheath fibers: (a) illustrations of the implantable active-targeting micelle-in-nanofiber device (FM-Nanofiber) delivering DOX-loaded micelles (FM) from nanofibers to tumor sites; (b) *in vivo* tumor volume changes over time; (c) survival rate of tumor-bearing Balb/C mice implanted with different membranes. Reprinted with permission from Ref [96]. Copyright 2015 American Chemical Society. PCL/MPA core and PCL sheath fibers: (d) basic concept schematic; (e) accumulated MPA release from various MPA incorporated fibers; (f) relative growth rate of tumor cell cultures exposed to MPA-loaded fiber membranes. Reprinted with permission from Ref [97]. Copyright 2017 Elsevier.

due to infection, the antibiotic drug MNA was incorporated into the PCL core. The PCL core provides good mechanical properties, while the zein sheath provides good biocompatibility and a hydrophobic barrier for prolonged drug release from the core. MNA was found to provide antibacterial activities against anaerobic bacteria over 4 days, as well as enhanced cell proliferation and adhesion with no cytotoxicity.^[98]

Local Cancer Therapy

Nanoparticle-based targeted delivery to the specific cancer cells has been and continues to be investigated widely. Nanoparticle surfaces are treated with various ligands (such as antibody, peptide, nucleic acid) to selectively bind to the targeted cancer cells.^[99] Because the nanoparticles are circulating in the blood stream, they are susceptible to changes in stability, solubility, and efficacy of the attached therapeutic molecules. The shelf life, aggregation, leakage, and toxicity of materials used to make nanoparticles also need to be considered.^[100] First coaxial fibers for cancer treatment were demonstrated using polyvinyl alcohol (PVA) with doxorubicin (DOX) anticancer drug core and chitosan sheath by Yan et al. in 2014. Coaxial fiber membranes delivering DOX inhibit the cell viability of human ovary cancer cells *in vitro*.^[101] A more detailed investigation, including *in vivo* experiments, has been reported by the Zhou group in 2015. Tumor targeted DOX-encapsulated micelles are incorporated into the PVA core and released locally through the crosslinked

gelatin sheath near targeted sites (Figure 23a). This delivery method provides a safe option for local cancer therapy due to a lower drug dose and reduced frequency of administration. *In vitro* antitumor activity was evaluated on 4T1 tumor cells. After 1 day of culture, free DOX and micelle groups not embedded into fibers show higher cytotoxicity because they have higher initial burst release compared to micelle-in-fiber groups: ~60% and 40% within 12 hr, respectively. At day 7, however, micelle-in-fiber samples display higher cell inhibition than other cases. *In vivo* mice tests show that DOX accumulation from coaxial fibers was significantly higher than the free DOX group. 21 days after implantation into 4T1 tumor-bearing Balb/c mice, the mean tumor volume of nanofiber groups (<500 mm³) was significantly smaller than that of intravenously delivered DOX groups (>1000 mm³), as shown in Figure 23b. A single local implant shows comparable effect with 4 times intravenous injections of DOX formulation *in vivo*. Micelle-in-fiber group also shows longer survival rate than other cases in Figure 23c.^[96] Another interesting report for targeted local delivery was published by Han et al.^[97] FDA-approved immunosuppressant mycophenolic acid (MPA) was incorporated into the PCL core of fibers encased by a PCL sheath. As shown in Figure 23d, the released MPA is targeted to IMPDH (inosine monophosphate dehydrogenase) enzyme. This is one of the key enzymes for GTP biosynthesis, especially for cancer cell metabolism. Core-sheath PCL fibers show much more sustained release compared to single PCL fibers (Figure 23e). MPA release kinetics are highly dependent on the core material selection and the thickness of

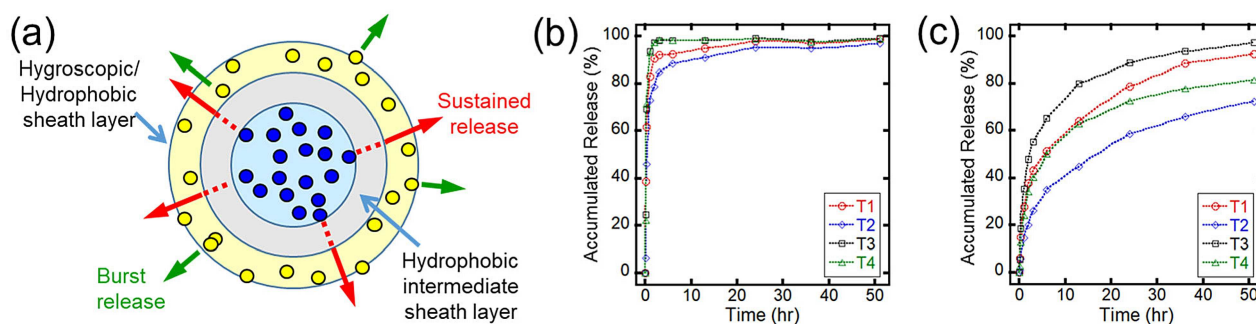


Figure 24. Dual drug delivery using triaxial fibers: (a) schematic of fiber cross-sectional structure and the release process of incorporated drugs; (b) release from the Drug 1 incorporated in sheath; (c) release from the Drug 2 incorporated in core. T1 and T3 has lower intermediate flow rate than T2 and T4, while T1 and T2 has smaller core nozzle diameter and wider intermediate nozzle width than T3 and T4. Reprinted with permission from Ref [107]. Copyright 2013 American Chemical Society.

sheath layers. MPA encapsulated core-sheath PCL fibers provide excellent *in vitro* cytotoxicity to U-87MG glioblastoma cells for two consecutive cell culture tests using the same membranes, as shown in Figure 23f. All MPA incorporated fiber samples show excellent cancer cell inhibition during a 1st cell culture period. In the following 2nd cell culture, coaxial fibers provide better cancer cell inhibition than that of single fibers since the latter release most of their encapsulated MPA in the 1st cell culture.^[97]

Wound Dressing

Wound dressing is another important biomedical application of coaxial electrospinning. Traditionally, the role of wound dressing is to protect the wound from the outer environment. The modern dressing has evolved into a multi-functional item, which also can provide anti-microbial, healing-promoting and pain-relieving functionalities. Chitosan has inherent antimicrobial properties, but it is hard to be electrospun due to its high viscosity and polycationic nature. Cationic polymers have polyelectrolytic effects because of CH molecules in aqueous solution and denaturation in toxic organic solvents. Significant expansion of polymer coils by charged groups results in viscosity values that are too high for electrospinning even at very low concentration.^[102] To combat these issues, coaxial electrospinning was utilized with electrospinnable PLA core to produce non-woven fibrous membranes. Chitosan coated PLA fiber membranes prepared in this manner presented antimicrobial properties against *Escherichia coli*.^[64b] Another approach to produce membranes with antimicrobial properties is releasing antimicrobial agents incorporated into the core and/or sheath of coaxial fibers. Antimicrobial ampicillin sodium salt incorporated into core-sheath fibers with PMMA core and nylon 6 sheath were successfully produced, presenting antimicrobial activities against Gram-positive *Listeria innocua*.^[103] Unlike small wounds, full-thickness wounds require special care, with additional treatments, especially in diabetes due to the excess level of glucose in blood (hyperglycemia). Hyaluronic acid (HA) core-PLGA/EGCG sheath fiber membrane was demonstrated for diabetic wound healing. Released HA and EGCG synergistically

promoted the healing process of diabetic full thickness wound and provided significantly higher wound healing rate than that of control, PLGA fiber, HA core-PLA sheath fiber and the commercially available Rapiderm (Dalim Tissen Medical Co., Seoul, Korea) case in a rat animal study.^[104] Multi-functional core-sheath fiber membranes with both antimicrobial and healing promoting properties was demonstrated. PCL core and collagen sheath were combined to provide both good mechanical properties and biocompatibility, respectively. While silver nanoparticles (Ag-NPs) embedded in the sheath provide antimicrobial properties, palmitate was incorporated into core to act as a healing agent.^[105]

Dual Drug Delivery

A very important aspect of coaxial electrospinning is that drug molecules can be easily incorporated into the desired layer of either core or sheath. Therefore, two different drugs can be conveniently incorporated individually into selected layers. Su et al. incorporated Rhodamine B and BSA into core-sheath fibers and found that drug release profiles can be affected by the location where the compound was loaded.^[106] However, when a hygroscopic polymer is used for the fiber sheath, it is challenging to obtain a sustained release rate from the drug incorporated in the fiber core because of water infiltration. Han et al. reported tri-layered coaxial fiber (so-called "triaxial fiber") to address this issue. With different drugs encapsulated in the core and sheath layers, an intermediate hydrophobic layer was added to provide a barrier between hygroscopic sheath and the core, as shown in Figure 24a. While the release from the sheath shows abrupt burst release of Drug 1 (Figure 24b), Drug 2 from the core shows a gradual release even though a hygroscopic nylon sheath was present (Figure 24c). Core-sheath fibers with hygroscopic sheath layer showed much faster release than triaxial fibers with intermediate barrier layer between core and sheath. The sustained release rate can be adjusted by varying the sheath thickness and coaxial nozzle dimensions.^[107]

Another synergistic co-delivery of two active components was shown for cartilage tissue engineering. Coaxial fibers made of PVP/BSA/rhTGF- β 1 core and PCL sheath were prepared and

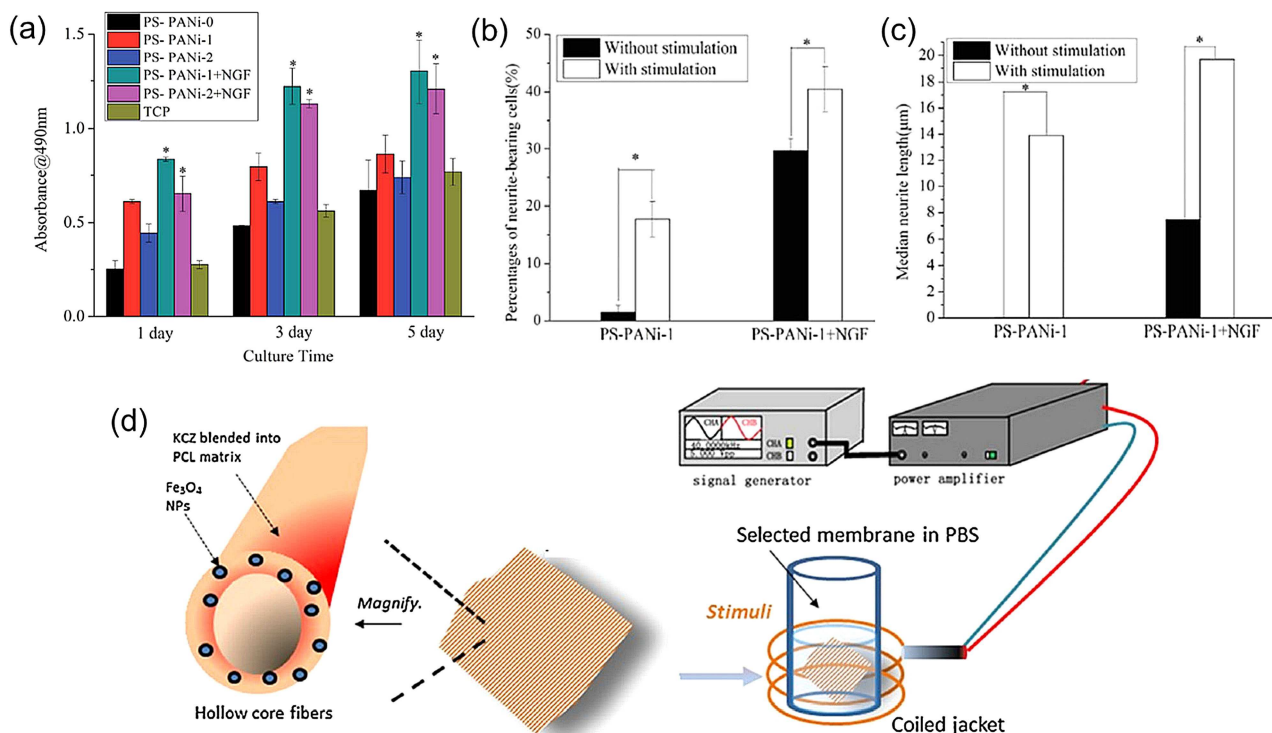


Figure 25. Synergistic effect of electrical stimulation and NGF delivery for nerve tissue engineering: (a) MTT assay of Schwann cell proliferation on various fiber substrates. Tissue culture plate (TCP) is used as control; (b) median neurite length; (c) percentage of neurite-bearing PC12 cells on the PS-PANI-1 nanofibers with or without electric stimulations. Reprinted with permission from Ref [108]. Copyright 2014 Royal Society of Chemistry. (d) Magnetic particles incorporated into hollow fibers loaded with KCZ drug provide stimulated release using mechanical agitation by applying alternating magnetic fields. Reprinted with permission from Ref [109]. Copyright 2016 Elsevier.

then conjugated with bone marrow derived stem cells (BMSC)-specific affinity peptide E7 on the fiber surface, providing the most favorable conditions for BMSC survival. Peptide E7 on the fiber surface promotes adhesion of BMSCs and the released rhTGF- β 1 growth factor promotes chondrogenic differentiation of BMSCs.^[110] Since this coaxial fiber ultimately has a tri-layered structure, triaxial electrospinning can be utilized in principle to prepare it in a single process step.

Externally Controlled Release

The combined effect of electrical stimulation and nerve growth factor (NGF) on neuron growth has been reported.^[108] Highly aligned NGF-encapsulated conductive PANi/P(LLA-CL)/silk fibroin (SF) core-sheath fiber was prepared for this purpose. *In vitro* cytotoxicity of membranes was evaluated, as shown in Figure 25a. Although addition of PANi in the sheath layer (PS-PANI-1) improved cell proliferation, increasing the content of PANi (PS-PANI-2) to a higher mass percentage can result in decreasing cell proliferation. As shown in Figures 25b and 25c, further significant improvement in cell proliferation is obtained with the addition of NGF. Rat pheochromocytoma cells (PC12) exhibited longer neurites (Figure 25b) and higher percentage of cells (Figure 25c) under electrical stimulation. Clearly, synergistic effect of NGF release and electrical stimulation was exerted in

both cases. Interestingly, electrical stimulation also increased the amount of released NGF.

Magnetically triggered drug release has been demonstrated^[109] by using hollow PCL fibers containing ketoconazole (KCZ), a broad spectrum antifungal drug, and Fe₃O₄ magnetic nanoparticles, as shown in Figure 25d. Dimethyl silicone oil was used for the core, which later perfused out forming hollow structures. An external auxiliary magnetic field enhanced the drug release from the membranes due to the mechanical actuation of embedded Fe₃O₄ nanoparticles.

On-Demand Release

Sonication triggered release from core-sheath fibers decorated with nanoparticles was demonstrated.^[111] Core-sheath fibers were prepared by coaxial electrospinning, while nanoparticles were simultaneously deposited onto the fibers by electro-spraying (Figure 26a), and then annealed by solvent vapor (Figure 26b), forming clusters on the fiber surface. External sonication detached nanoparticles from the fiber surface, forming openings in the fiber surface that can release drugs from the fiber core, illustrated in Figure 26c. This method for on-demand release was evaluated with encapsulated rhodamine dye molecules, where the dye was abruptly released after triggering by 30 min sonication, while no significant release observed without sonication (Figure 26d). Another on-

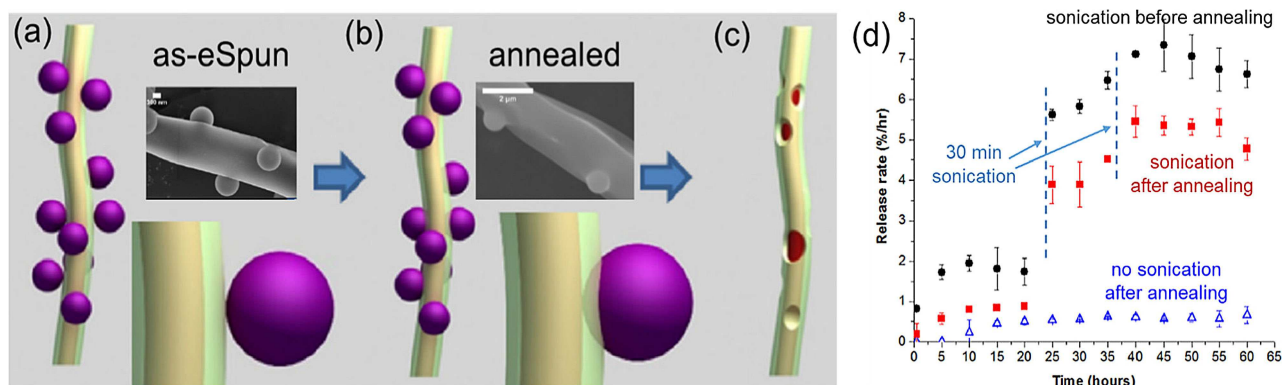


Figure 26. Sonication triggered release: (a) as-spun nanoparticles attached core-sheath fibers; (b) nanoparticles embedded onto core-sheath fibers after solvent-vapor annealing; (c) nanoparticles detached core-sheath fiber after sonication; (d) sonication-triggered rhodamine dye release profiles from core-sheath fibers. Reprinted with permission from Ref [111]. Copyright 2016 Elsevier.

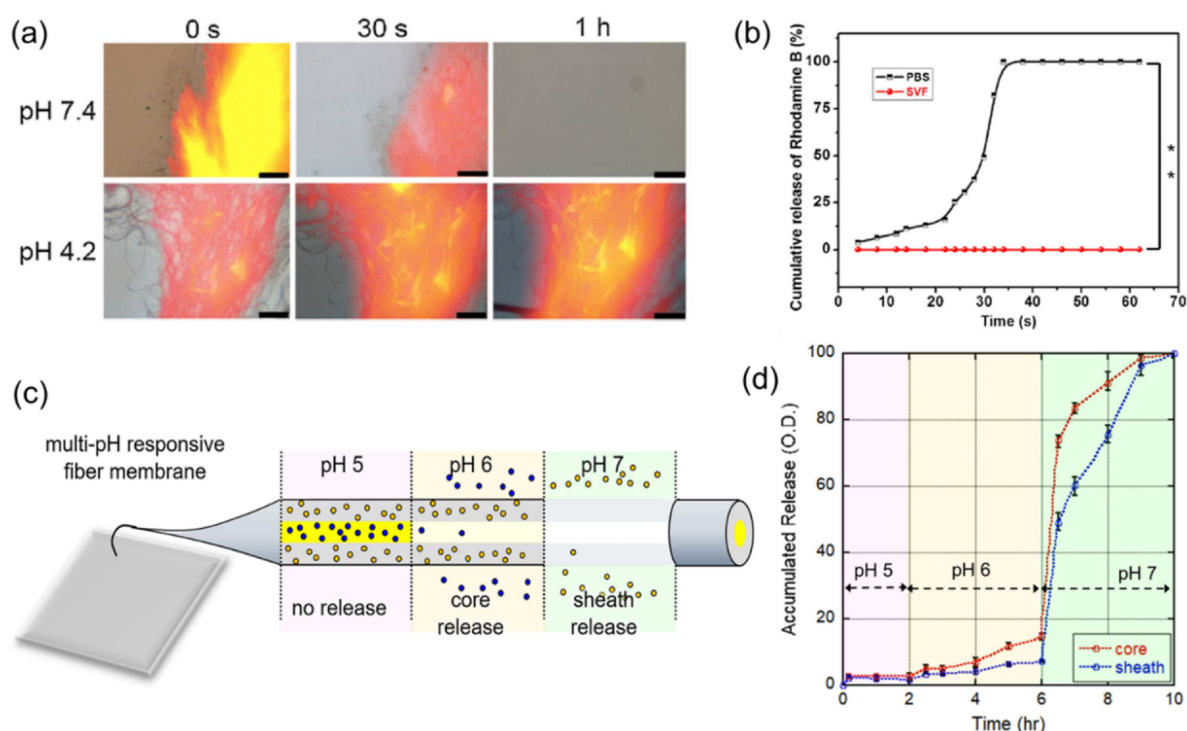


Figure 27. pH responsive drug delivery. Polyurethane core and cellulose acetate phthalate sheath – (a) images of pH responsive rhodamine release; (b) accumulated release of rhodamine dye at different pH condition. Reprinted with permission from Ref [112]. Copyright 2016 Elsevier. Eudragit EL100/KAB core and Eudragit ES100/KAU sheath – (c) schematic of tri-phasic pH responses on core-sheath fibers; (d) core and sheath release profiles at consecutively changing pH conditions. Reprinted with permission from Ref [113]. Copyright 2017 American Chemical Society.

demand release method involves pH responsive core-sheath fibers. An example involves fibers using polyurethane in the core and cellulose acetate phthalate (CAP) in the sheath. Because the solubility of CAP is pH-dependent, rhodamine dyes incorporated into the coaxial fibers were released in PBS solution with a pH of 7.4, while they remained incorporated into fibers in simulated vaginal solution with a pH 4.2, as shown in Figure 27a-b. This membrane can potentially be used as a semen triggered drug delivery vehicle.^[112]

Another pH-controlled response used core-sheath fibers incorporating two separate pH responsive Eudragit polymers.

Due to different pH dissolving range of core (pH 6 or higher) and sheath (pH 7 or higher), it shows tri-phasic pH response: (a) no release at pH 5, (b) sustained release of core in pH 6, and quick release of core and sheath in pH 7 or higher, as illustrated in Figure 27c. Selective pH responsive release is shown in Figure 27d.^[113]

Triaxial electrospinning was also utilized to produce the pH-sensitive core-sheath fibers. High quality core-sheath fibers can be obtained with non-electrospinnable lecithin-diclofenac sodium core solution using electrospinnable Eudragit S 100 and pure solvent for middle and outer layers, respectively.^[114]

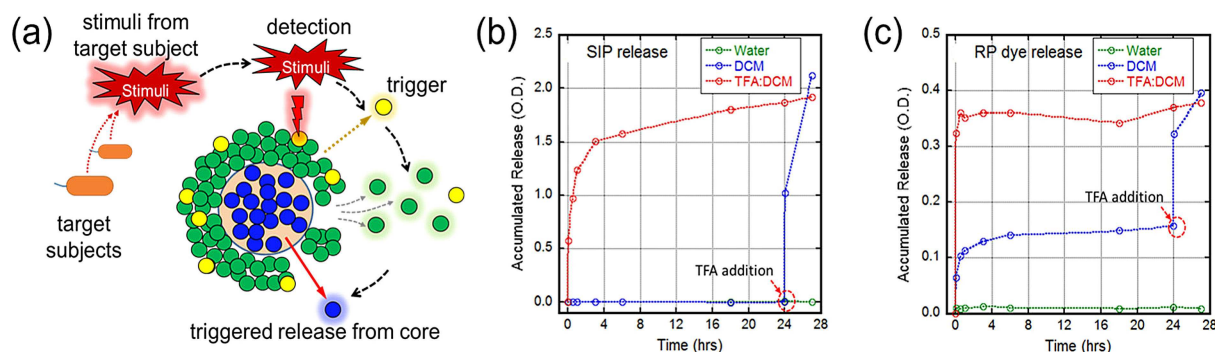


Figure 28. Stimuli-triggered self-immolative coaxial fibers: (a) basic concept diagram: cross section of coaxial fiber with self-immolative sheath and encapsulated core material (yellow dot, head molecules of SIP; green dot, SIP monomers, blue dot, encapsulated molecules); release profiles: (b) depolymerized SIP from sheath; (c) RP dye from the core in either water, DCM-only solvent, or TFA:DCM (1:20 vol. ratio) solvent. Reprinted with permission from Ref [115]. Copyright 2017 American Chemical Society.

Stimuli-triggered release from the core was demonstrated by using self-immolative polymer (SIP) as a sheath layer. Once triggered by target stimuli, the SIP sheath polymer is depolymerized leading to the physical opening of the fiber surface, which initiates the release from the core material as shown in Figure 28a. Triggered depolymerization of SIP sheath and

ingly, injectable short nanofibers for tissue engineering were reported by Ravichandran et al. in 2012 for the regeneration of infarcted myocardium. Very short poly(glycerol sebacate) (PGS) fibers (Figure 29) obtained after PLLA sheath removal from PGS-PLLA core-sheath fibers. PGS is a biocompatible and inexpensive elastomer, which can be degraded into non-toxic by-products. Injected PGS short nanofibers along with cells provide the environment that cells can adhere minimizing cell loss and providing more site-directed cardiac repair mechanism.^[75]

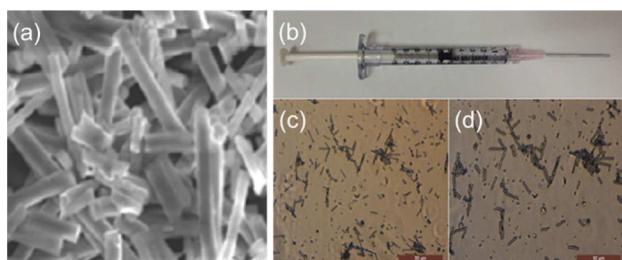


Figure 29. Locally injectable short fibers for site-directed cardiac repair: (a) SEM of short PGS fibers after removing PLGA sheath; (b) PBS short fiber loaded syringe with 18 G needle; microscopic images of ejected PBS short fibers from syringe at (c) 40X and (d) 60X magnification. Reprinted with permission from Ref [75]. Copyright 2012 IOP Publishing.

encapsulated KAB release from the core after triggered SIP depolymerization are shown in Figure 28b and Figure 28c, respectively. Upon adding TFA, encapsulated dye was released swiftly and reached 100% within a few hours. Depolymerized SIP was also abruptly released indicating a quick sheath depolymerization.^[115] Since this report demonstrated the concept of SIP core-sheath nanofibers, possibly other SIP materials triggered by UV light,^[116] enzyme,^[117] or specific ions^[118] can be adopted for novel application developments.

Injectable Short Fibers

Most tissue engineered scaffolds need to be implanted into the site of interest. However, surgical implantation of the large scaffold into very sensitive area can be a challenging issue to treat certain diseases such as myocardial infarction. Interest-

Zero-Order Linear Release

Zero-order linear release of encapsulated drug over the long-term period, during which the release rate is constant and not dependent on time, is one of most desired properties for drug delivery systems. Although the zero-order linear release can be very closely related with the material & drug properties and interactions, some interesting results have been reported to provide the consistent release rate over time. Emulsion electrospinning using single nozzle has been utilized to produce core-sheath fibers using water-in-oil emulsions. While it is a relatively simple method, emulsion electrospinning cannot provide the precise control of location and continuity of core part, leading to less consistent drug release behaviors from the core. Viry et al. present a novel technique combining coaxial and emulsion electrospinning for the better drug release control over a sustained period. Emulsified solution was used for core solution (Figure 30a) and a nearly constant linear release of the model drug was obtained over 20 days as shown in Figure 30b.^[119] Another approach using tri-layered coaxial (aka "triaxial") fibers is reported by Yu et al. in 2015. By incorporating gradually decreasing the ketoprofen (KET) concentration from the outer to the inner layer (Figure 30c), zero-order linear release of KET over 20 h was obtained (Figure 30d) due to smaller surface area and longer diffusion distance of inner layers. However, this approach may not applicable to long-term release over several days.^[120]

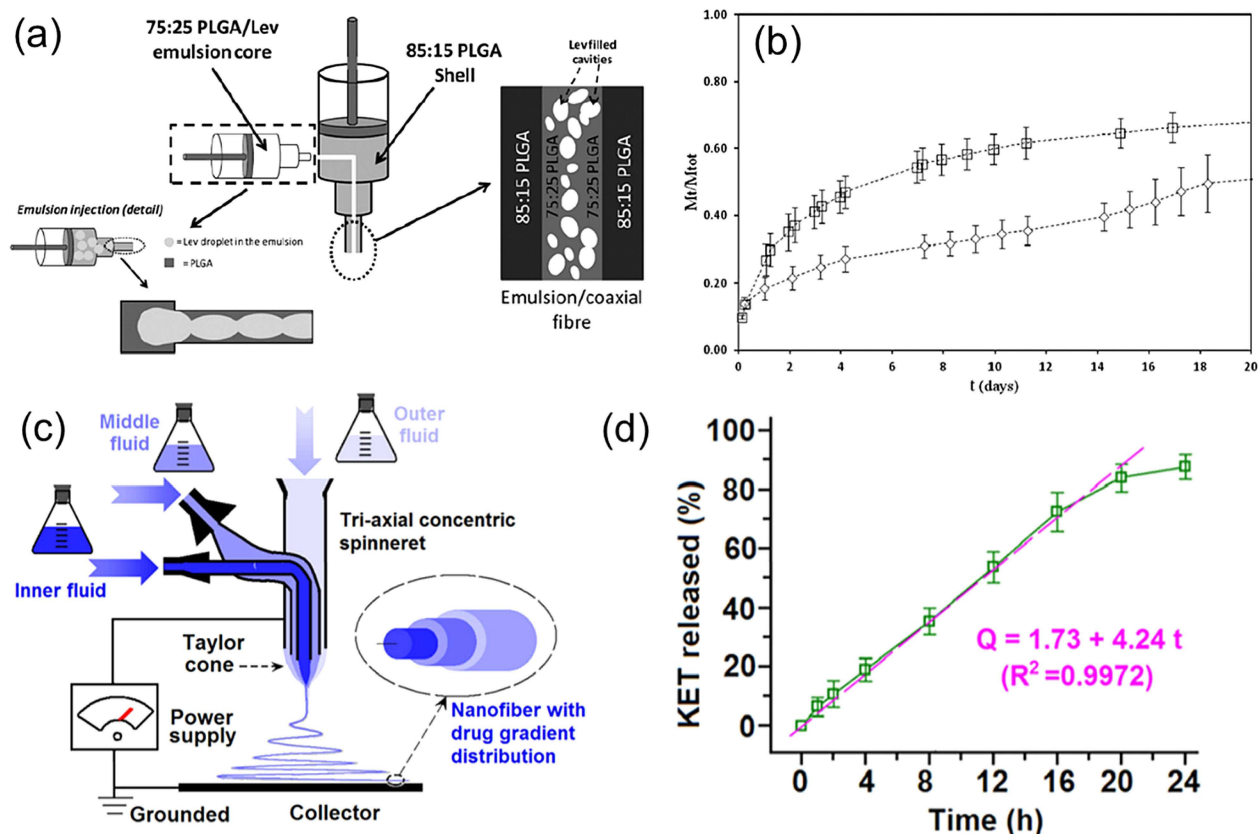


Figure 30. Zero-order drug delivery: (a) schematic of emulsion coaxial electrospinning; (b) release profile comparison between coaxial electrospinning (\square) and emulsion coaxial electrospinning (\diamond) Reprinted with permission from Ref [119]. Copyright 2012 Royal Society of Chemistry; (c) schematic of triaxial electrospinning with higher drug concentrations in inner layers; (d) the linear release profile of KET up to 20 h. Reprinted with permission from Ref [120]. Copyright 2015 American Chemical Society.

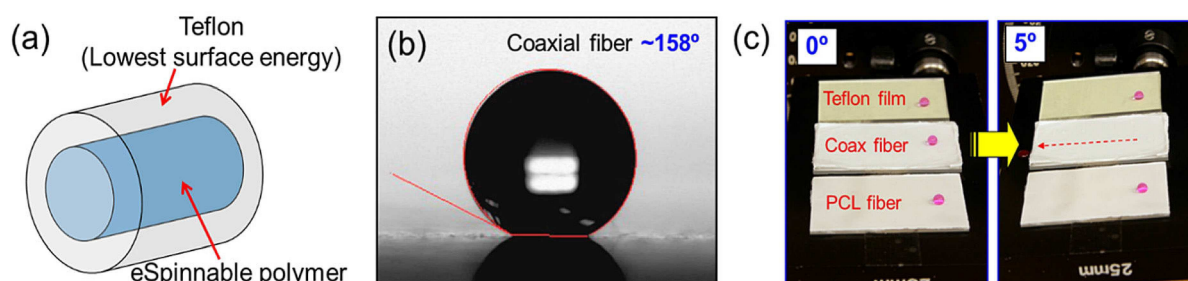


Figure 31. Superhydrophobic and oleophobic coaxial Teflon™ fibers: (a) core-sheath fiber composition; (b) water contact angle on coaxially electrospun Teflon™ coated PCL fibers; (c) water rolling-off angle comparison between a Teflon™ film, Teflon™ coated PCL fiber membrane, and a PCL fiber membrane. Reprinted with permission from Ref [26]. Copyright 2009 American Chemical Society.

Textile/Environmental Applications

Having a large surface-to-volume ratio, a porous network with small pore size, light weight and availability of a large materials selection, electrospun fiber membranes are very attractive for a variety of textile applications, especially for functional textiles such as protective clothing and sportswear. Additional functionality can be incorporated, such as enhanced mechanical properties, water-repellence and self-cleaning. Weather proof properties with good breathability can be obtained from micro-/nanoporous electrospun membranes. In addition, coaxial electro-

spinning can provide fibers with unique combinations of multiple functions that cannot be obtained from conventional electrospun membranes.

Han and Steckl have reported^[26] Teflon™ coated PCL core-sheath fibers that provide superhydrophobic and oleophobic properties. Teflon™ is known as the most hydrophobic and chemically resistive polymeric material, but it is challenging to be electrospun because of its low electrical conductivity. Using coaxial electrospinning, Teflon™ can be electrospun with the help of electrospinnable core, resulting in Teflon™-coated polymer micro/nanofibers, illustrated in Figure 31a. Because of

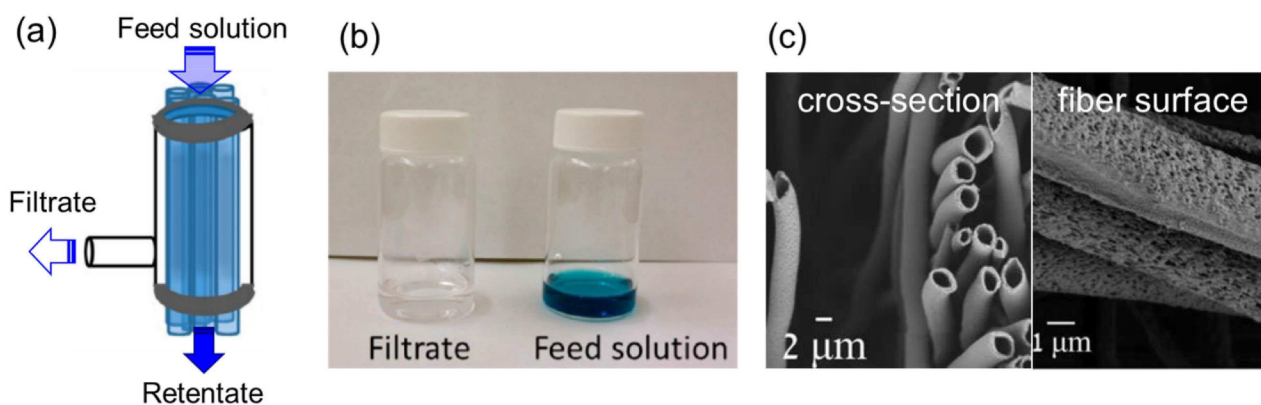


Figure 32. Water filtration: (a) filter module configuration; (b) color differences between filtrate and feed solution. Adapted with permission from Ref [125]. Copyright 2013 American Chemical Society.; (c) SEM images of PSU hollow fibers Reprinted with permission from Ref [126]. Copyright 2016 John Wiley and Sons.

the Teflon™ sheath layer, core-sheath fiber membranes exhibit the lowest surface tension and excellent chemical resistance, as well as properties (e.g. mechanical, electrical, magnetic, etc.) from the core material. The Teflon™ fiber coating, in combination with the inherent surface roughness of the nano/microporous membranes, resulted in superhydrophobicity with high contact angle $\sim 158^\circ$ (Figure 31b) and low water rolling-off angle $\sim 5^\circ$ (Figure 31c). Excellent water repellency in dynamic conditions, such as falling water drops and water jet dispensing, was also demonstrated.

While a membrane with a superhydrophobic fiber surface also exhibits self-cleaning behavior when shedding water drops, photocatalytic self-cleaning surface was also demonstrated^[121] by the same group. TiO₂ nanoparticles were incorporated into the fiber sheath. Self-cleaning activity was observed under indoor lighting conditions and outperforms fiber textiles conventionally-surface loaded with TiO₂ nanoparticles.

Another important aspect of advanced textiles is incorporation of protection from chemical warfare agents. Light-weight and strong textiles with the ability to react and respond to external threats are necessary. Using coaxial electrospinning, catalytic DFPase enzyme against organophosphate nerve agent (such as sarin and diisopropylfluorophosphate [DFP]), was incorporated into the sheath layer, providing excellent neutralization efficiency against DFP, compared to blended DFPase/polymer fibers^[122]

Significant improvement of mechanical properties of fiber membranes was demonstrated using triaxial electrospinning. Thermoplastic polyurethane (TPU) sandwiched between polystyrene layers enhanced mechanical properties dramatically, yielding $>270 \text{ J g}^{-1}$ toughness and 300% elongation without any cracking compared to single PS fiber that shows $<0.5 \text{ J g}^{-1}$ and $<5\%$ elongation. The triaxial PS-TPU-PS fibers were reported to have much higher toughness and elongation at break than coaxial PS-TPU fibers, 1376% and 628%, respectively.^[123]

In addition to protective clothing, coaxially electrospun fiber textiles have also been used for assorted other purposes, such as filters, water-harvesting, separators and self-healing surfaces.

Filtration is one of most readily implementable applications using electrospinning because of the wide variety of material selection (including carbon materials) and easy control of pore size and fiber morphologies. Electrospinning-related filtration activities have mostly used conventional single nozzle electrospinning.^[124] Although air filtration research using coaxial electrospinning is still immature, there is a good opportunity for the use of core-sheath fibers combining two different material properties. For example, a sheath layer of functional materials (filtering target friendly, chemically resistive, superhydrophobic, etc.) with a core layer of mechanically robust material can be easily combined using coaxial electrospinning.

For water treatment applications involving filtration and desalination processes, coaxially electrospun hollow PAN nanofibers (diameter $<1 \mu\text{m}$) were demonstrated. In the filter configuration shown in Figure 32a aligned PAN hollow fibers were placed inside a plastic tube and a vacuum pump with a cold trap is connected to the filtrate outlet. Coaxially electrospun hollow PAN fibers provided excellent filtration performance with 100% and 98% rejection for indigo carmine dye (Figure 32b) and sodium chloride salt.^[125] More recently, Halaui et al. demonstrated various polymeric hollow fibers for possible water treatment applications. The hollow fibers maintain a stable inner pore up to $\sim 4 \mu\text{m}$. Using PVP-K90 core solution in non-volatile DMSO solvent successfully inhibits the fiber buckling problem. Addition of PEG to the sheath solution could induce nanopores with $\sim 100\text{--}200 \text{ nm}$ diameter on the fiber surface, as shown in Figure 32c.^[126]

Another important environmental textile application is selective oil absorption from water/oil mixtures because of increasing oil spills in the oceans and their severe adverse effects on environment. Coaxial fiber with PU core and porous PS sheath was demonstrated for oil collection. Core-sheath PU/PS fiber sorbent exhibits 2–3 times higher capacity (motor oil $\sim 64.40 \text{ g/g}$ and sunflower seed oil $\sim 47.48 \text{ g/g}$) than widely used conventional polypropylene (PP) fibers with excellent reusability. The PU core provides good strength and elasticity, while the PS sheath provide the low surface energy to absorb the oil while excluding water.^[127]

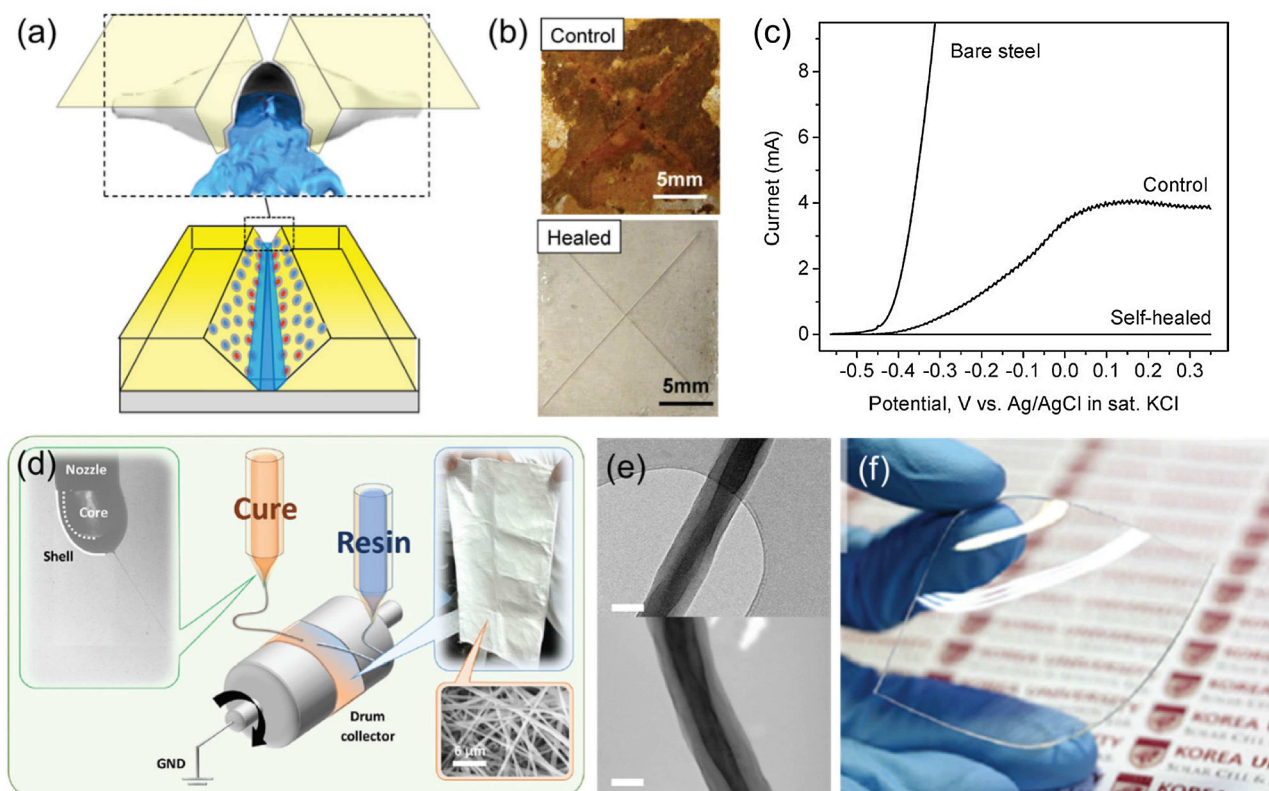


Figure 33. Self-healing coating using coaxial fibers: (a) illustration of healing agent release from mechanically broken capsules; (b) comparison between control and healed film coated steel sheets which were stored in ambient condition for 2 months after immersing into a salt water for 5 days; (c) evaluation of electrical insulation between the scribed surface (bare steel, control (unhealed), self-healed surfaces) and the liquid environment. Reprinted with permission from Ref [128]. Copyright 2010 Wiley-VCH. Highly transparent self-healing composite fibers: (d) simultaneous electrospinning from two coaxial nozzles – one with curing agent and the other with resin monomer; (e) TEM images of PAN core-sheath fibers encapsulating resin monomer (top) or curing agent (bottom), 200 nm scale bar; (f) photograph of highly flexible and transparent self-healing composite film. Reprinted with permission from Ref [129]. Copyright 2015 Royal Society of Chemistry.

Self-Healing Coaxial Fibers

Metallic structures have always struggled with corrosion issues, costing \$276 billion annually.^[130] One suggested solution is coating the metal with anti-corrosion organic material.^[131] However, it is not a long-term solution because the anti-corrosion coating can be hardly maintained without any crack or damage for longer time period. Thus, self-healing material is very attractive to address this issue. Using coaxially electrospun fibers, self-healing material mimicking the biological healing process in living organism was demonstrated by Park and Braun in 2010. Healing agent liquids, polysiloxane precursor Part A and B, were separately encapsulated within PVP sheath using coaxial electrospinning. After sequential coaxial electrospinning on the steel surface, polymer was spin cast on the coaxial fibers. The membrane was successfully embedded into the polymer film as a self-healing unit. After scribing the polymer film, embedded coaxial fibers were broken releasing curing agents that sealed the opening, as illustrated in Figure 33a. In Figure 33b photographs visually demonstrate the difference between the non-healed (control) surface and the self-healed surface. These samples were immersed into a salt water solution for 5 days after scribing and then stored at ambient for

2 months. While the control sample was badly rusted along the scribed area, the self-healed surface did not show any sign of rust. After scribing the surface, electrical evaluation (Figure 33c) shows that the self-healed film does not allow any current flow due to the sealing of the opened damage region, while other surfaces allow the electrical current flow.^[128]

Self-healing films that are optically transparent have potential utilization in optoelectronic devices, such as digital displays and solar cells. Highly transparent (~90%) self-healing composite film embedding coaxial fibers was reported. Two separate coaxial spinnerets were used for the resin monomer and for the curing agent in the inner nozzle and PAN in both outer nozzles, as illustrated in Figure 33d. Forming a membrane by simultaneously drawing coaxial fibers from both spinnerets resulted in very effective mixing of the resin and cure materials, which improved self-healing performance. While in previous reports of self-curing fibers, the curing agents were incorporated into the core as an emulsion, these continuous core-sheath fibers (Figure 33e) resulted in highly flexible and transparent self-healing composite film (Figure 33f). TEM images of resin monomer (top) or curing agent (bottom) encapsulated PAN fiber are shown in Figure 33e. In electric-insulation performance, the self-healing sample maintains its insulation

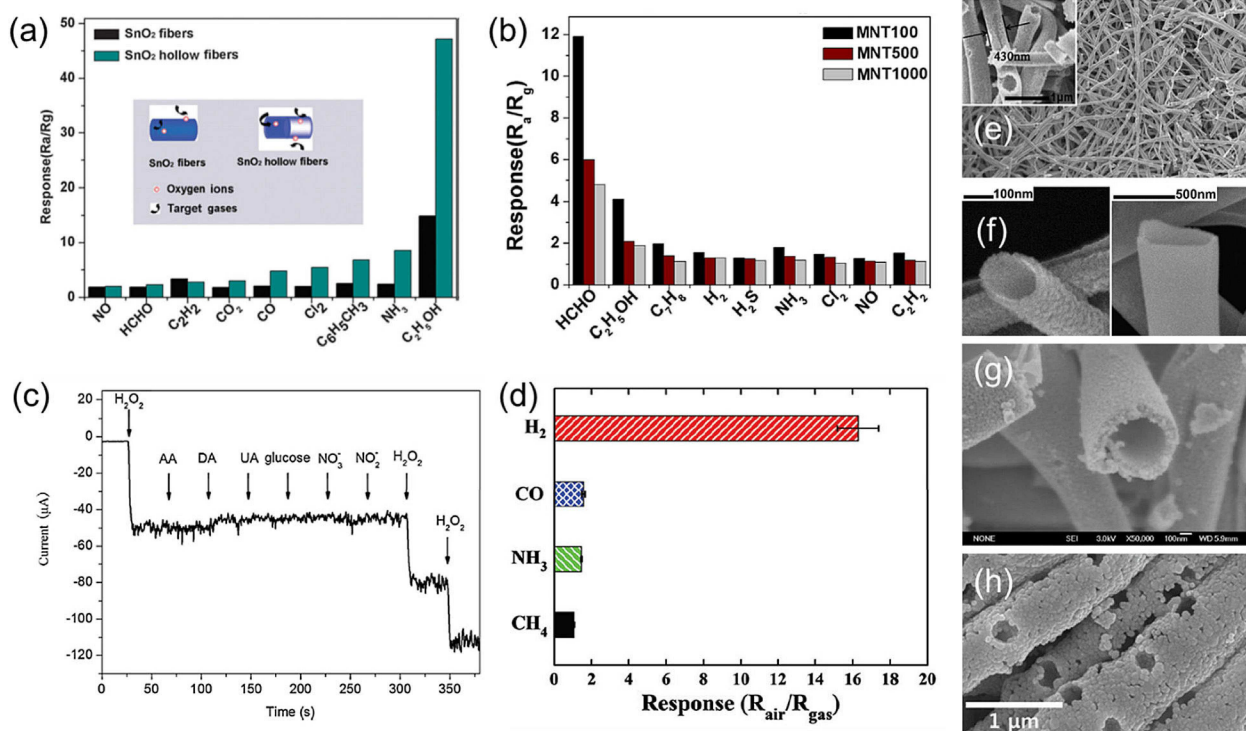


Figure 34. Gas sensing selectivity of hollow metal oxide fibers: (a) SnO₂ hollow fibers and SnO₂ solid fibers for ethanol detection. Reprinted with permission from Ref [132]. Copyright 2013 Royal Society of Chemistry.; (b) In₂O₃ hollow fibers in diameter of 120 nm (MNT100), 500 nm (MNT500) and 1100 nm (MNT1000) for formaldehyde detection. Reprinted with permission from Ref [133]. Copyright 2014 Elsevier.; (c) Au-loaded SnO₂ hollow fibers. Reprinted with permission from Ref [134]. Copyright 2014 Elsevier.; (d) Pd-loaded macro-porous WO₃ hollow fibers. Reprinted with permission from Ref [135]. Copyright 2016 Royal Society of Chemistry.. Corresponding SEM images are shown in (e), (f), (g), and (h), respectively.

with no current flow in acetic acid solution while the control shows the current flow of up to 25 mA.^[129] Very recently, many interesting state-of-art methods including electrospinning in the field of self-healing researches were thoroughly reviewed by Lee, Yoon and Yarin.^[136]

Sensor Applications

Semiconducting metal oxides have been widely utilized as electric gas sensor materials because of their high sensitivity, low cost, ease of integration, rapid response, good stability, and compatibility with silicon technologies. Very recently, electrospun metal oxide gas sensors were reviewed by Kim and Rothschild.^[137] To achieve ultra-sensitive sensors, the sensors need to have high surface area and high porosity in order to be permeable to the gas analyte. Therefore, electrospun membranes are very attractive to develop ultrasensitive sensors due to their remarkably high surface area and high porosity.

In addition, coaxial electrospinning can provide hollow structured fibers that can further increase the surface area for improved sensitivity. To produce hollow metal oxide fibers, a precursor for the targeted metal oxide is used for the fiber sheath while sacrificial solutions, such as paraffins and oils, are used for the core layer. After electrospinning, a calcination process at high temperature forms the metal oxide sheath layer while removing the sacrificial core material, resulting in hollow

structured metal oxide fibers. Cao et al. demonstrated SnO₂ hollow nanofibers for ethanol detection. Compared to SnO₂ solid fibers, SnO₂ hollow fibers (Figure 34e) provided ~3 times higher response to ethanol and exhibited excellent selectivity against other chemical gases, and a very fast response time within 1 s, as shown in Figure 34a.^[132] In₂O₃ hollow metal oxide fibers were formed by coaxial electrospinning using sacrificial paraffin core and PVP/indium nitrate sheath. Prepared hollow In₂O₃ fibers (Figure 34f) were used to detect a formaldehyde (HCHO) gas with rapid response of 10 s, recovery rates of 15 s, high sensitivity (a ratio of resistance in air to resistance in gas of R_{air}/R_{gas} ~11.9) and selectivity (Figure 34b). In Figure 34b, MNT100, MNT500, and MNT1000 samples have different diameters of 120 nm, 500 nm, and 1100 nm, respectively. Clearly, thinner fiber diameter provided higher sensitivity and better selectivity. Hollow In₂O₃ fibers < 100 nm diameter detected 1 ppm HCHO consistently.^[133] Catalytic nanoparticle (NP)-incorporated metal oxide fibers can be also used in aqueous environment. Hydrogen peroxide (H₂O₂) sensitive Au-loaded hollow SnO₂ fiber (Figure 34g) was demonstrated for non-enzymatic H₂O₂ detection. Au-salt (HAuCl₄) was added to the sheath solution forming Au-NPs on hollow wall after calcination. A linear detection range from 10 μM to 1 mM (r = 0.997) was reported with a detection limit of ~0.60 μM at a signal-to-noise ratio of 3, as well as the excellent selectivity for H₂O₂. Figure 34c shows the decrease in electrical current when H₂O₂ was added to the measuring solution.^[134]

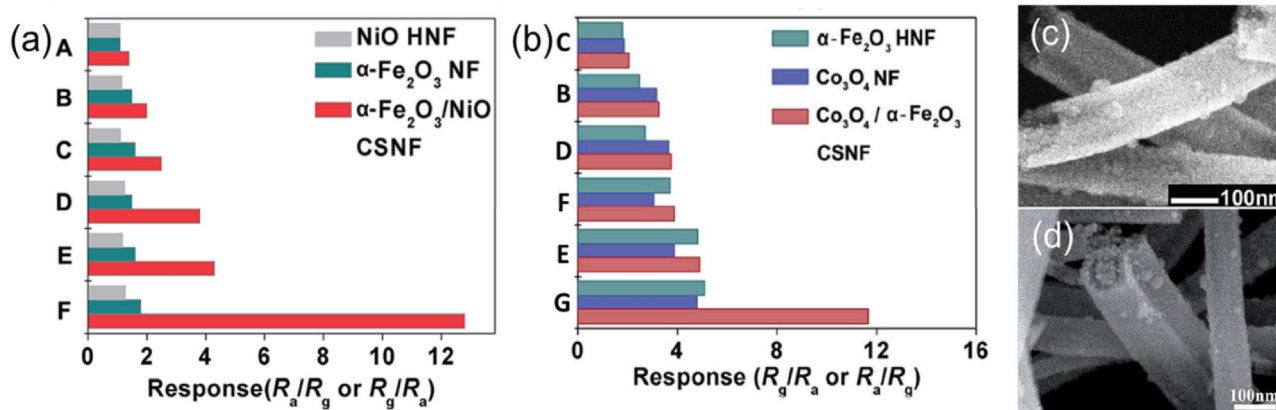


Figure 35. Core-sheath metal oxide fiber sensors: (a) gas selectivity comparison of α - Fe_2O_3 core and NiO sheath fibers (α - $\text{Fe}_2\text{O}_3/\text{NiO}$ CSNF), α - Fe_2O_3 solid fibers (α - Fe_2O_3 NF) and NiO hollow fibers (NiO HNF) to different gases (50 ppm). Adapted with permission from Ref [138]. Copyright 2015 Royal Society of Chemistry; (b) responses of $\text{Co}_3\text{O}_4/\alpha$ - Fe_2O_3 coaxial fiber (CSNF), Co_3O_4 solid fiber (NF) and α - Fe_2O_3 hollow fiber (HNF) sensors to various test gases (50 ppm) at 240 °C. Adapted with permission from Ref [139]. Copyright 2015 Royal Society of Chemistry. (A: ethyne, B: ammonia, C: trichloromethane, D: methylbenzene, E: ethanol, F: formaldehyde, G: acetone). Corresponding SEM images: (c) α - $\text{Fe}_2\text{O}_3/\text{NiO}$ CSNF; (d) $\text{Co}_3\text{O}_4/\alpha$ - Fe_2O_3 CSNF.

Similarly, macro-porous WO_3 hollow fibers with catalytic Pd nanoparticles (Figure 34h) were demonstrated for hydrogen sensors. In this case, catalytic Pd nanoparticles were synthesized by apoferritin protein cage, and then added to the sheath solution for coaxial electrospinning process. Adding colloidal polystyrene particles to the sheath precursor solution formed ~ 175 nm surface pores on the hollow wall surface after thermal calcination. Prepared membranes exhibited a very high response ($R_{\text{air}}/R_{\text{gas}} \sim 17.6$) against 500 ppm H_2 gas and very weak responses ($R_{\text{air}}/R_{\text{gas}} < 2$) to other gases such as CO, NH_3 , and CH_4 (Figure 34d). The limit of detection was ~ 10 ppm and a fast response time (~ 25 s) was reported.^[135]

In addition to producing hollow fibers, coaxial electrospinning also enables the combination of two different properties from core and sheath materials as mentioned earlier. This approach was also applied to metal oxide gas sensor developments. Cao et al. developed core-sheath fibers combining n-type α - Fe_2O_3 core and p-type NiO sheath for HCHO gas sensor. As shown in Figure 35a, the p-n junction core-sheath nanofibers (CSNF) presented 10 and 7 times higher sensitivity against HCHO than NiO hollow fibers and α - Fe_2O_3 solid nanofibers, respectively. It also showed very low limit of detection ~ 1 ppm, fast response (~ 2 s) and recovery time (~ 9 s) at the optimal working temperature of 240 °C. Synergy from the p-n heterojunction structure enhances the performance of the semi-conducting metal oxide gas sensors.^[138] The same group also reported core-sheath fibers for acetone gas sensors using p-type Co_3O_4 core and n-type α - Fe_2O_3 sheath. While no selectivity was shown in homogenous fiber with each material, the core-sheath fibers show much higher response to the acetone gas (Figure 35b).^[139] SEM images of these two cases are shown in Figure 35c and d, respectively.

Catalyst Applications

Catalytic enzymes are very versatile natural biocatalysts for inducing various chemical reactions in many applications, such as sensors and bio-fuels.^[142] However, because of the lack of reusability and stability in the form of additive powders, significant research to immobilize catalytic enzymes without losing their activity has been pursued.^[143] Among other methods, electrospinning is a versatile immobilization method of enzymes on nanofiber membranes.^[144] In particular, multi-enzyme and coenzyme confined biomimetic cells can mimic the multi-stage biosynthesis of biological cells, providing a promising solution as a biocatalyst.

Using coaxial electrospinning, multiple enzymes 3 α -hydroxysteroid dehydrogenase (HSD) and/or diaphorase (DP) were successfully immobilized into hollow nanofibers, as illustrated in Figure 36a. The core solution is a mixture of glycerol and water containing the dissolved multi-enzyme system for the bile acid and polyurethane solution for the sheath. It presents a combined activity recovery of 75% compared to the solution-based multi-enzyme system, while most reported immobilized coenzyme systems produce a reactivity of $\sim 1\%$ of their solution counterpart.^[145] Furthermore, enzymes encapsulated in hollow fibers have exceptional stability, more than a 170-fold increase in half-life at 25 °C. Multi-enzyme reactions involving coenzyme regeneration have been demonstrated.^[140] Subsequently, this approach was used as a regenerative energy tool to enzymatically convert CO_2 to methanol (Figure 36b,c). Related enzymes and cofactors were immobilized inside the fiber using cationic polyelectrolyte. It provides the highest methanol yield of 103.2% and 80% productivity was retained even after 10 reuse cycles, generating a cumulative methanol yield of 940.5% with hollow fiber system.^[141]

Hierarchically macro-meso-microporous zeolite (ZSM-5) electrospun fibers with tunable macro-porosity were demonstrated and applied for catalytic reactions. ZSM-5 nanocrystal suspension in PVP for sheath and paraffin oil for core were used

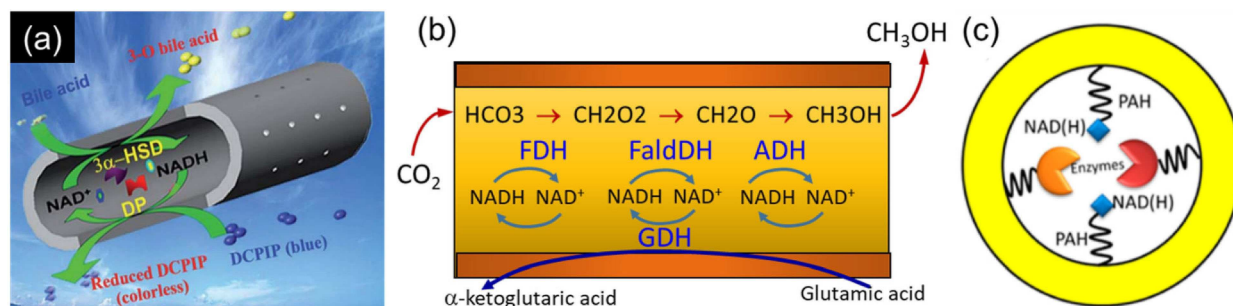


Figure 36. Schematic illustrations for hollow nanofibers containing enzymes: (a) multi-enzyme artificial cells involving 3 α -HSD, DP and NAD(H) for the bile acid assay. Reprinted with permission from Ref [140]. Copyright 2014 Royal Society of Chemistry.; (b) hollow nanofiber multienzyme system for methanol synthesis from CO₂ with *in situ* regeneration of NADH; (c) fiber configuration of nanostructured enzyme-cofactor enzyme catalyst. Reprinted with permission from Ref [141]. Copyright 2015 American Chemical Society.

for the coaxial electrospinning process. Catalytic activities against isobutane (~99.8%) were slightly higher than that of solid meso-microporous zeolite fibers (~99.0%) and higher than conventional ZSM-5 powder (~93.9%), because hierarchical pores provide enhanced diffusion and accessibility to sites. ZSM-5 fibers also exhibit high yield (~41.2%) of propylene (intermediate product in the cracking of isobutane) vs. conventional ZSM-5 (~37.7%), as well as good anti-coking stability in the cracking reaction of isobutane.^[146]

Gold nanoparticles (AuNPs) has been a popular catalyst. However, nanoparticle aggregation has to be prevented to preserve catalytic properties. Schöbel et al. recently immobilized AuNPs on the surface of core-sheath fibers consisting of PS and patchy worm-like crystalline core micelles (wCCM) sheath.^[147] By simply immersing into preformed citrate-stabilized AuNP solution, AuNPs are evenly and strongly attached to patches on core-sheath fiber surface. Prepared catalytic membranes show significantly faster conversion of dimethylphenylsilane (~7 h) with 70 \times times less amount of AuNPs compared to teabag-like catalyst system (26 h), consisting of AuNPs immobilized in poly (para-xylylene) tubes.^[148]

Energy Applications

Electrospinning of fiber materials has been extensively investigated in the development of novel methods for energy generation.

Li-ion Battery Anodes

The lithium ion battery (LIB) is a ubiquitous component of portable electronic devices. Emerging interest on replacing fossil fuels with electricity for high power applications such as hybrid/electric vehicles, renewable energy storage systems, requires both high energy and power densities. Also, to fully utilize renewable energy applications, such as solar and wind, stable high energy storage system has to be employed. Although metallic lithium has a very high energy density ~3860 mA-h/g, it cannot be used directly as an anode material due to

severe safety concerns caused by the low melting point, dendrite growth of lithium, and high reactivity against electrolytes.^[149] Therefore, more stable lithium loaded compounds have been used for LIB. Since the first commercialization by Sony in 1991, carbon-based graphite is the major material used for LIB anode because of its good capacity, long lifespan, low cost, eco-friendliness, and low electrochemical potential against lithium metal.^[150] However, the current LIB is not suitable for applications requiring much higher capacity because the intrinsic capacity of graphite is only ~372 mA-h/g. Also, the formation of dendritic lithium metal growth around the anode (so-called lithium plating), is still unavoidable especially during high current operation that is critical for high power applications, resulting in safety hazards (such as fires and explosion), as well as poor cycling efficiency.^[151] Low specific capacity due to the bulky graphite structure and the limitation of diffusion rate within the bulk electrode material are additional disadvantages. To resolve these issues, two main approaches have been pursued: (1) developing nano-/micro-porous anode material; (2) utilizing composite materials that have better electrochemical properties, such as intrinsic capacity and conductivity. Combining these two approaches has brought significant improvement of LIB performance, positively impacting the commercialization of high power/energy products, such as electric cars.

In regard to the material selection, various materials which have much higher intrinsic capacity have been evaluated as LIB anodes. In particular, metal oxides such as ZnO (978), TiO₂ (335), SnO₂ (782), GeOx (2152 mA-h/g) have been intensively investigated because they have high theoretical capacity and stability, but suffer from both poor electrical conductivity and huge volume expansion (up to 400% during charge/discharge cycles). Their significant volume expansion and contraction, leading to material pulverization, electrical contact loss, internal resistance increase by forming a solid electrolyte interphase (SEI), have to be addressed for the practical use. Composite carbon/metal oxide materials are one of most effective approaches to address these issues. They can not only improve the electrochemical properties, but also relieve the volume expansion aspect. Synergistic effect from metal oxides and carbon nanocomposites lead to enhanced capacity and me-

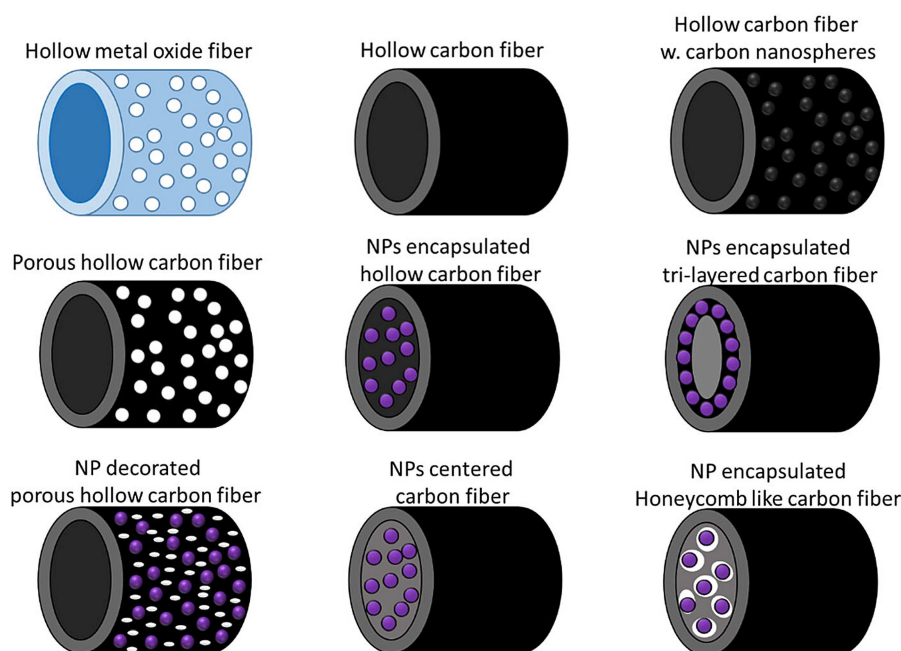


Figure 37. Summary of coaxial fibers potentially useful for energy applications.

chanical integrity. Recent progress in metal oxide anodes for LIB was carefully reviewed recently by Cao *et al.*^[152] Other potential electrode materials, such as Si, Sn, Ge and S, have been investigated due to their extremely high intrinsic (theoretical) capacities of 4212, 990, 1640, and 1672 mA-h/g, respectively. Si has received the most attention due to its high specific capacity and low working potential.^[153] However, similar to metal oxides, these materials have also suffered from significant volume expansion and low conductivity.

In addition to material selection, novel structural aspects have been investigated. The porous structured anode provides both much higher surface area for lithium ion storage and buffering capacity for the severe volume expansion of anode materials. It also enhances the electron and ion transfer rates by shortening the diffusion length down to the nanoscale. Among various nanomaterials, electrospun one-dimensional nanofiber membranes have attracted strong interest because of their excellent flexibility in dimensions and structures, wide material selection, as well as physical stability. Moreover, coaxial electrospinning is the most versatile method to combine carbon with other high capacity materials, providing additional benefits of (a) core-sheath or hollow structured nanofiber and (b) multi-layered structure to incorporate nanoparticles. Efficient incorporation of targeted nanoparticles into carbon nanofibers is the key aspect in order to engage all nanoparticles into the electrochemical reaction. For this purpose, various nanostructures have been developed using coaxial electrospinning. Several examples are shown in Figure 37, and selected research results are described below.

Another pathway to improve the LIB performance is developing a binder-free LIB device. In conventional LIB electrodes, electro-active materials are fixed on the electrode using

polymeric binders that are non-conductive and not electro-active. Therefore, addition of conductive additives is needed to improve the conductivity. Since the portion of binder and conductive additives is relatively large (up to 30%), the LIB performance is significantly hindered by limiting the possible amount of electro-active materials within the device. However, because electrospinning produces a free-standing electro-active electrode, it is a very attractive method to develop binder- and additive-free LIB that can maximize electrochemical performance.

Yuan *et al.* developed an LIB anode using Ag nanoparticle (AgNP) embedded into TiO₂ hollow nanofibers, without using binder and conductive additives to the current collector. The approach is illustrated in the schematic of Figure 38a. AgNPs were uniformly distributed within the mesoporous TiO₂ hollow fibers, improving the poor conductivity of TiO₂ hollow nanofibers. Silver paste modification on the copper foil increased the surface roughness of current collector, leading to significantly increased electrode performance with the second discharge capacity reaching 130 mA-hr/g at 1 C charge/discharge rate (1 A for 1 hr). TiO₂ or TiO₂/Ag hollow fibers also provide much better reversible capacity and cycling stability (after 50 cycles at 1 C rate) than binder-added TiO₂ powder electrode (Figure 38b).^[154]

Anatase TiO₂ provides promising characteristics, such as minimal volume change (~3.7%), relatively low cost, wide availability, and minimal toxicity. First demonstration of TiO₂ nanofiber anode in full-cell configuration was reported by Zhang *et al.* The full-cell configuration using commercial LiFePO₄ cathode and TiO₂ hollow nanofiber anode delivered a reversible capacity of 103 mA-h/g at a current density of 100 mA/g with an operating potential of ~1.4 V. The full-cell retained a reversible capacity after 300 cycles of ~88%.^[159]

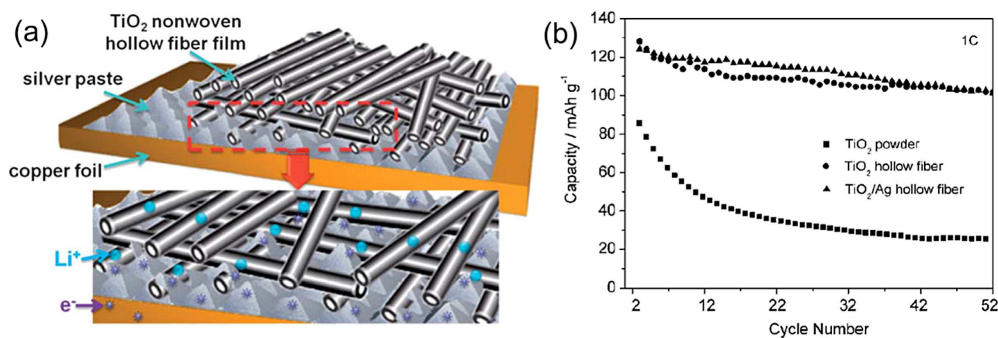


Figure 38. TiO₂ nonwoven hollow fibers on the silver paste modified copper foil: (a) schematic drawing; (b) cycling performance comparison. Reprinted with permission from Ref [154]. Copyright 2011 Royal Society of Chemistry.

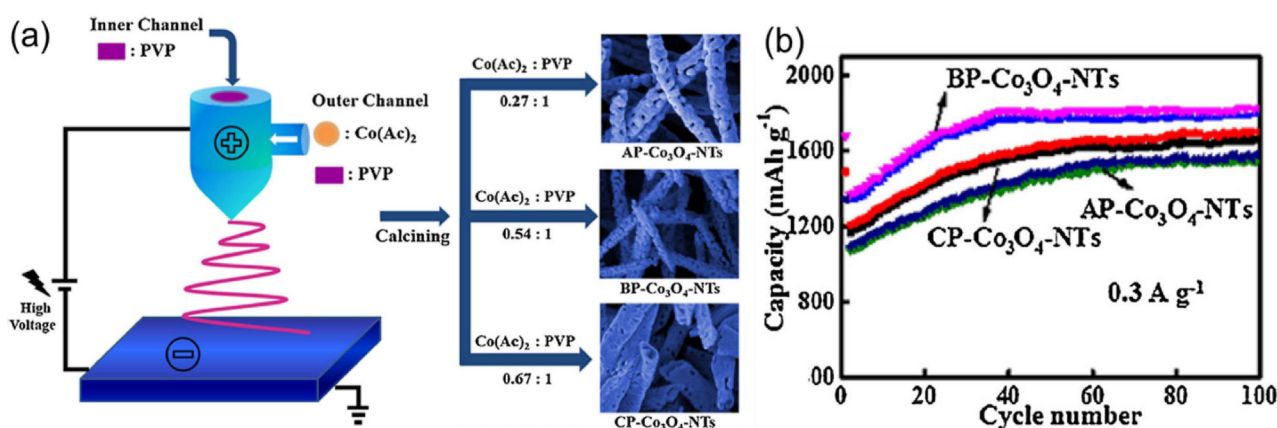


Figure 39. Porous hollow cobalt nanofibers: (a) schematic illustration for the electrospinning synthesis and photos showing morphology dependence on mass ratios between cobalt precursor and PVP; (b) electrochemical performance of three samples at 0.3 A/g current density. Reprinted with permission from Ref [155]. Copyright 2015 Elsevier.

The p-type semiconducting cobalt oxide, Co₃O₄, has a high theoretical capacity of 890 mA-h/g and high rate performance because 8 lithium ions can be stored per molecule unit.^[160] Porous hollow Co₃O₄ nanofibers were coaxially produced using PVP sacrificial core and cobaltous acetate/PVP sheath followed by the calcination process shown in Figure 39a. Due to its porous sheath and hollow structure, high reversible specific capacity of 1826.2 mA/g at the current density of 0.3 A/g after 100 cycles were reported. Interestingly, the mass ratio between cobalt precursor and PVP material strongly affects the porous fiber morphology (Figure 39a) as well as the electrochemical performance, as shown in Figure 39b.^[155]

When coaxial electrospinning is utilized for LIB anode, the starting step is most commonly hollow carbon fibers, which can serve as a substrate for non-conductive materials having very high intrinsic capacity. Anodic properties of hollow carbon nanofibers have been evaluated^[156] by Lee *et al.* Styrene-co-acrylonitrile (SAN) core and PAN sheath solutions were coaxially electrospun into fibers that subsequently experienced carbonization processes at different high temperatures. During carbonization, the SAN core decomposed while the PAN sheath was carbonized. Due to the immiscibility of SAN and PAN, excellent hollow carbon fiber structure was obtained, as shown in Figure 40a. Interestingly, as carbonization temperature was

increased, the reversible capacity of the hollow carbon fibers decreased from 477 mA-h/g (800 °C) to 142 mA-h/g (1600 °C). This is because the larger graphitic area is available at lower carbonization temperature, where the reversible intercalation of Li ions occurs.^[156] Porous hollow carbon nanofiber was also demonstrated using sacrificial core solution and emulsified shell solution, shown in Figure 40b. As the pores are introduced (Figure 40c), the initial capacity and reversible capacity rates are increased significantly to 1003 mA-h/g and 61.8%, respectively, compared to 653 mA-h/g and 53.9% of nonporous hollow carbon fibers.^[157] Carbon nanotube decorated with graphitic carbon nanosphere was produced using triple-coaxial (*aka* triaxial) electrospinning, as shown in Figure 40d. Mineral oil core was removed during the stabilization process and decomposition of nickel acetate Ni(Ac)₂ formed Ni nanoparticles (NiNP) on carbon fiber surface. During carbonization, graphitic carbon layer formed on NiNPs. After immersing into HCl solution, the Ni core was dissolved away, resulting in hollow graphitic carbon nanospheres. NiNP-decorated fibers are observed in Figure 40e. The hollow structures of carbon fibers and nanospheres are seen in a TEM image (Figure 40f). These carbon fiber anodes produced very high specific capacity of ~970 mA-h/g at a current density of 50 mA/g, which is ~2.6 times higher than the theoretical capacity of graphite. The

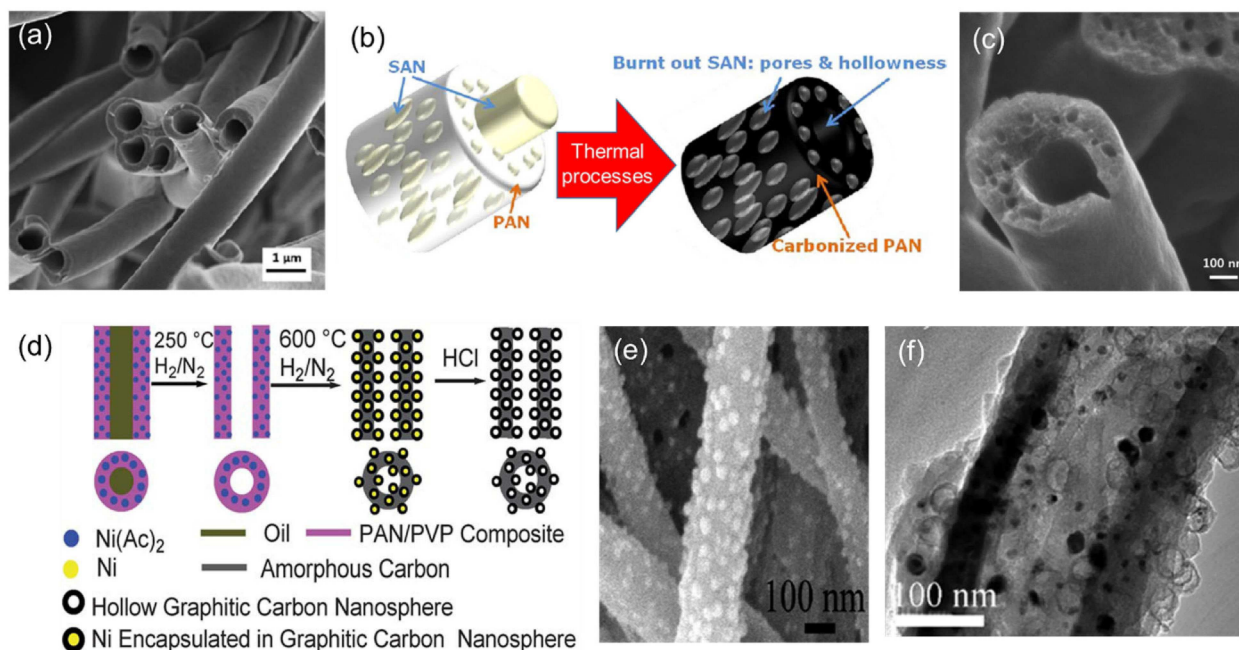


Figure 40. Carbon fibers: (a) SEM image of hollow fibers. Reprinted with permission from Ref [156]. Copyright 2012 Elsevier.; Porous hollow carbon nanofibers: (b) synthesis process and (c) SEM observation. Reprinted with permission from Ref [157]. Copyright 2012 American Chemical Society. Hollow carbon fibers decorated with hollow graphitic carbon nanospheres: (d) synthesis process, (e) SEM, and (f) TEM observations. Reprinted with permission from Ref [158]. Copyright 2012 Royal Society of Chemistry.

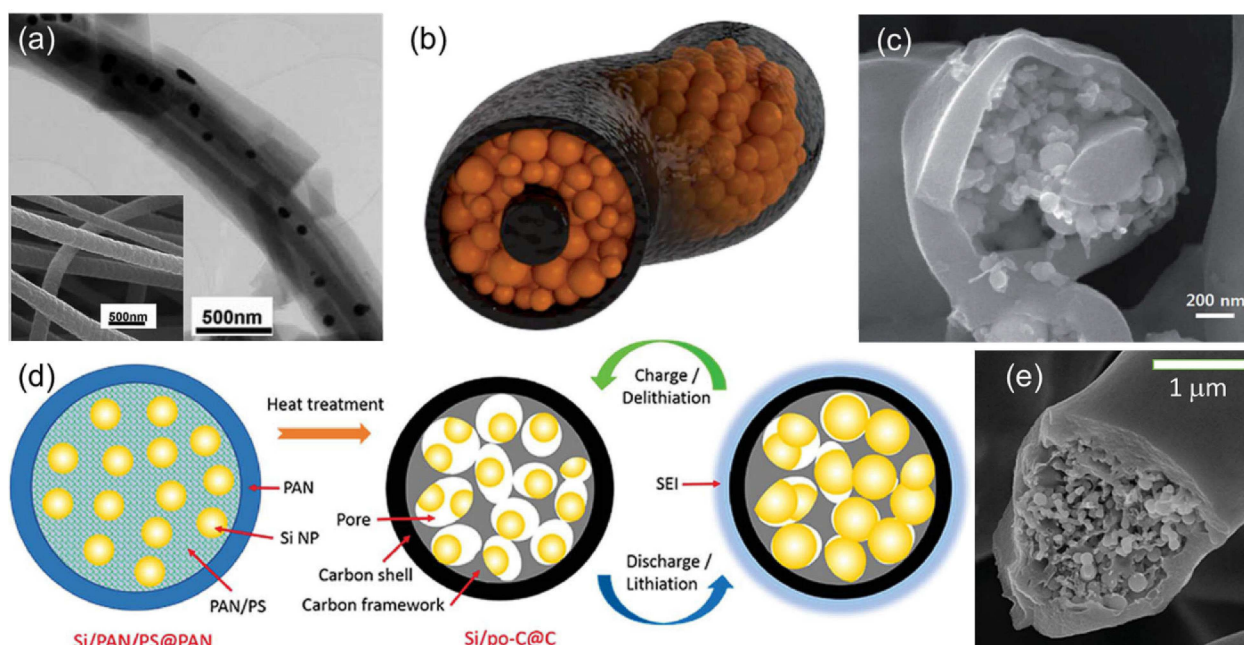


Figure 41. Si nanoparticle incorporated carbon fibers: (a) TEM image of SiNP-encapsulated hollow carbon fibers (inset: SEM image). Reprinted with permission from Ref [161]. Copyright 2013 Royal Society of Chemistry. Tri-layered C-core/Si-intermediate/C-shell nanofiber: (b) schematic diagram; (c) highly magnified cross-sectional FE-SEM image. Reprinted with permission from Ref [162]. Copyright 2014 Royal Society of Chemistry. Honeycomb-like Si/porous carbon core and carbon sheath composite fiber: (d) structural formation and change of coaxial fibers during cycling process; (e) cross-sectional SEM image. Reprinted with permission from Ref [163]. Copyright 2015 Royal Society of Chemistry.

electrodes also displayed a high volumetric capacity of ~ 1.42 A-h/cm³ and good cycling stability.^[158]

Highly reversible Li-ion energy storage using hollow carbon nanofibers encapsulated with Si nanoparticle (SiNP) was

demonstrated. SiNP-dispersed mineral oil and PAN solution were used for core and sheath layers. Encapsulated SiNPs in hollow carbon fibers are observed in TEM images (Figure 41a). After carbonizing the prepared core-sheath fibers, high rever-

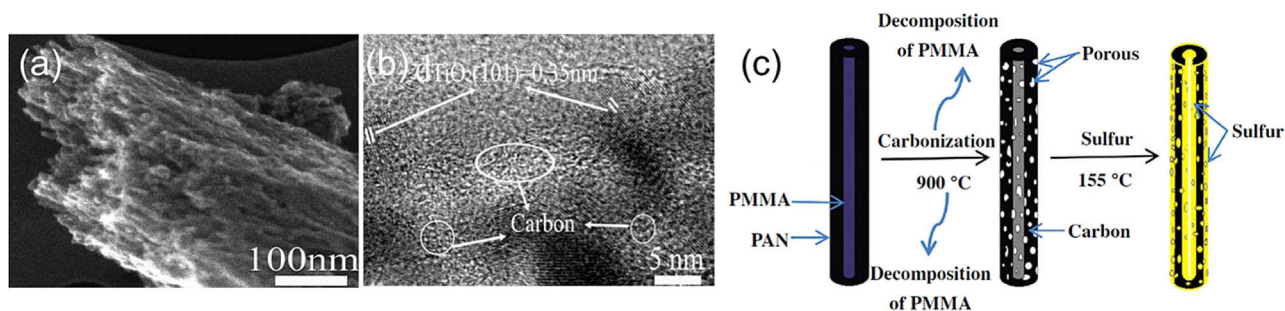


Figure 42. Porous TiO₂-carbon nanofiber morphologies: (a) FE-TEM; (b) TEM observations. Reprinted with permission from Ref [165]. Copyright 2014 Royal Society of Chemistry. (c) Synthesis process for the sulfur loaded mesohollow and microporous carbon fibers developed as cathode in lithium-sulfur battery. Reprinted with permission from Ref [166]. Copyright 2014 Elsevier.

sible capacity of 1300 mA-h/g was displayed even after 80 cycles at 0.5 C rate and a high reversible discharge capacity of ~700 mA-h/g when cycled at 3 C. This high capacity was attributed to the extremely high theoretical specific capacity of Si of ~4200 mA-h/g. Carbon acts as a structural buffer for silicon volume expansion and as a conductive medium to transport electrons.^[161] Furthermore, tri-layered C/Si/C composite coaxial fibers provide significantly improved electrochemical properties by physically sandwiching SiNPs within carbon fiber layers as illustrated in Figure 41b. Cross-sectional SEM image (Figure 41c) shows the concentric tri-layered structure. The carbon core also provides enhanced conductive pathway for Li-ions. The fiber membrane electrode produces a total specific capacity of 2045.4 mA-h/g and reversible capacity of 1210.7 mA-h/g. Excluding the carbon layers, the reversible specific capacity of SiNPs is calculated to be 3627 mA-h/g, which is close to the theoretical maximum value of Si at room temperature. Capacity retentions were 91.48% and 74.68% after 30 cycles and 100 cycles, respectively. Interestingly, the specific capacity at a high current rate of 12 000 mA/g (10 C) still maintained above 820 mA-h/g due to the continuous carbon core assisting Li-ion insertion/extraction.^[162]

A similar approach utilizes SiNPs incorporated into honeycomb-like carbon nanofibers with porous carbon core, illustrated in Figure 41d. These fibers provide strong electrochemical performance of reversible capacity of 997 mA-h/g and a capacity retention of 71% after 150 cycles with a current density of 0.2 A/g. SiNPs encapsulated into a porous carbon core were obtained from PS/PAN/Si nanoparticle mixture due to the different carbon yield of PS and PAN after heat treatments. Figure 41e shows the nanoparticles contained within the porous core and wrapped with a uniform sheath layer. Because most SiNPs are in close contact with the carbon core, an efficient interaction between SiNPs and carbon substrate can be obtained. At the same time the porous core provides a buffering capacity to the volume expansion of SiNPs.^[163] Follow-up work from the same group also demonstrated a cobweb-like interconnected carbon shell network using multi wall carbon nanotubes (MWCNT) incorporated into a PVP sheath and a PMMA/PAN/SiNP core. The PVP sheath melts earlier during the carbonization process and results in an interconnected carbon nanofiber network, which can reduce the contact resistance

between fibers. This strategy provided promising reversible capacity of 903 mA-h/g and better capacity retention of 89% after 100 cycles with a current density of 0.2 A/g.^[164]

Highly porous TiO₂-carbon nanofibers were demonstrated. Core-sheath fibers were produced with PMMA core and PS/Ti(OiPr)₄ sheath. Unlike other cases that used heavy mineral oil,^[156] PEO^[159] and SAN^[157] for the sacrificial core component, PMMA was selected as the sacrificial component to produce surface pores in addition to hollow structure, while Ti(OiPr)₄ and PS were used for TiO₂ precursor and carbon source. After calcination treatments at 400 °C for 3 hr, highly porous TiO₂-carbon nanofibers were prepared, as shown in Figure 42a. The presence of TiO₂ and carbon components was confirmed using high resolution TEM observation (Figure 42b). Due to the high density of pores, Li ions can be easily transported from the ambient membrane space into the inner space of the fibers, which acts as a storage area. This brought remarkable specific reversible capacity of ~806 mA-h/g and a high volumetric capacity of ~1.2 A-h/cm³. The device maintained a capacity of ~680 mA-h/g after 250 cycles at a current density of 100 mA/g and exhibit an exceptional discharge rate capability of 5 A/g while retaining a capacity of ~260 mA-h/g after 1600 cycles.^[165]

Carbon nanofibers with a mesohollow and microporous structure have also been used for cathodes in lithium-sulfur batteries. Such fibers were produced by forming a PMMA core and a PAN sheath, followed by a high temperature carbonization process. Volatile decomposition of PMMA core during carbonization produced a mesohollow core and induced micropores in the carbonized PAN sheath layer as illustrated in Figure 42c. Subsequently, it was heat-treated with sublimed sulfur to form a S/carbon fiber composite cathode. Sulfur is impregnated into micropores preventing the dissolution of polysulfides, while mesohollow channels provide a capillary path for molten sulfur enabling high loading of sulfur inside conductive carbon fibers. Maximum capacity of 815 mA-h/g at 0.1 C after several activation cycles as a cathode material for Li-S batteries was obtained along with a capacity retention of 88% after 70 cycles.^[166]

Similarly to Si NPs, germanium (Ge) and its oxide (GeOx) have also elicited significant interest as promising materials due to high theoretical capacity of ~1640 and ~2152 mA-h-g⁻¹, respectively. Li et al. demonstrated highly stable GeOx NPs

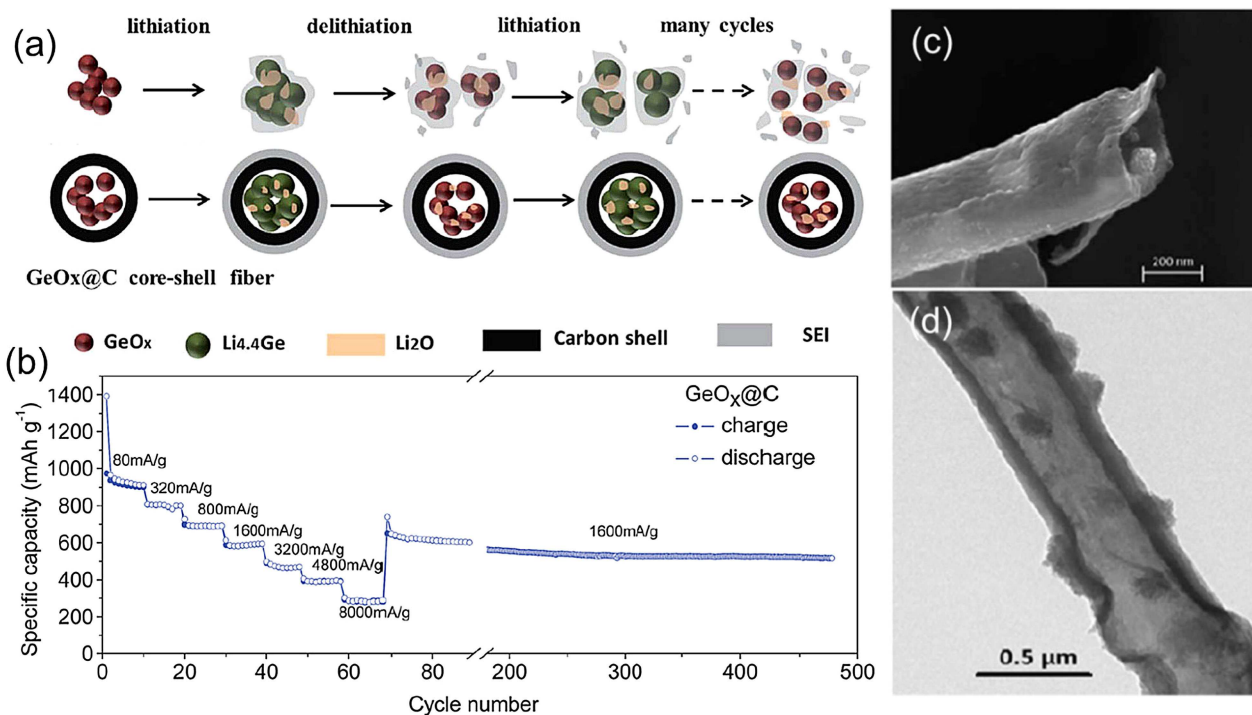


Figure 43. Ge nanoparticle encapsulated hollow nanofibers: (a) schematic of the lithium reaction mechanisms of bare GeO_x NPs and GeO_x NPs encapsulated carbon fibers (GeO_x@C). The carbon shell acts as buffer layer to suppress the fracture of GeO_x NPs during repeated cycling and also forms a stable SEI layer to provide enhanced electrical pathway for the electrochemical reaction between Li and GeO_x. Reprinted with permission from Ref [167]. Copyright 2015 Royal Society of Chemistry.; (b) rate capability of GeO_x@C electrode; (c) SEM and (d) TEM images of ZnO nanoparticles encapsulated in hollow fibers made of carbon/reduced graphene oxide sheath. Reprinted with permission from Ref [168]. Copyright 2015 Royal Society of Chemistry.

encapsulated in hollow carbon nanofibers showing excellent cycling ability. Figure 43a illustrates the different outcomes of cycling between the NPs-only and the NP-encapsulated hollow fibers. As the lithiation/delithiation processes are repeated, NPs experience large volume changes leading to pulverization. Also, the unstable solid electrolyte interface (SEI) surrounding the NP clusters decreases the lithium diffusion rate between Ge and the electrolyte. However, NP-encapsulated fibers show good volume buffering capacity and stable SEI formation, facilitating improved electrochemical properties. As a result this approach produces a reversible specific capacity of 875 mA-h/g at 160 mA/g⁻ after 400 cycles along with an improved rate capacity of 513 mA-h/g even at a high current density of 1600 mA/g upon 500 cycles, as shown in Figure 43b. Ge has lower capacity and higher cost than Si, but 400× higher lithium ion diffusion coefficient and 10,000× higher electrical conductivity.^[167]

Because tin and tin-based materials are also attractive for LIB anode due to high capacity and low cost, core-sheath fibers with Sn-embedded carbon core and carbon sheath were also investigated. These core-sheath fibers provided higher reversible specific capacity of 626 mA-h/g and better cycling performance (73% capacity retention after 50 cycles) than either pure carbon nanofibers (CNFs) or Sn nanofibers. Pure Sn nanofiber shows very high specific capacity, but its cycling performance was very low (46% after 50 cycles), while CNF shows low capacity with good stability. The flow rate ratio between core and sheath plays an important role to optimize the embedded

Sn amount and the carbon wall thickness. Although a thinner carbon wall (i.e. relatively more Sn) provides higher capacity, a stable conformal carbon sheath around the tin-carbon core cannot be maintained during cycles when the carbon wall thickness is too thin, which leads to poor electrical connection and cycling performance.^[169] Hollow carbon fibers encapsulating SnO₂ NPs provide a reversible capacity of 1002 mA-h/g (for the initial cycle at 100 mA/g), excellent rate capability, and a highly stable cycling performance with a discharge capacity of 833 mA-h/g after 500 cycles at 600 mA/g. The void volume offers sufficient space for alleviating the volume changes of SnO₂ NPs.^[170] ZnO NP encapsulated carbon-reduced graphene oxide hollow fibers (Figure 43c, d) have been reported to result in a high capacity of 815 mA-h/g at a current density of 50 mA/g with capacity retention of ~80% after 100 cycles. The ZnO NPs were synthesized from Zn(OAc)₂ precursor (mixed into the core solution) during calcination at 400 °C. Reduced graphene oxide (rGO) in the carbon sheath contributes to the capacity, conductivity, and mechanical stability during volume changes of the resulting fibers.^[168]

Selected summary of materials, fiber compositions, and key properties are listed in Table 3.

Li-ion Battery Separator

While the majority of coaxial electrospinning research on LIB is developing novel anodes and cathodes, many novel studies on

Table 3. Summary of coaxial fibers for lithium-ion battery applications.

Materials for electrospinning	Fiber compositions	Key Findings	Ref
Li-ion Battery			
Core – mineral oil + Ag NPs	Core – form hollow structure & incorporating Ag NPs.	130 mA-h/g at 1 C discharge rate	[154]
Sheath – PVP + Ti(OiPr) ₄	Sheath – form TiO ₂ sheath after calcination	77% after 50 cycles	'11
Core – styrene-co-acrylonitrile (SAN)	Core – sacrificial layer	518 mA-h/g at 50 mA/g	[156]
Sheath – PAN	Sheath – form carbon after carbonization	75% after 10 cycles	'12
Core – mineral oil	Core – sacrificial layer	969 mA-h/g at 50 mA/g	[158]
Middle – PAN	Middle – converted to carbon sheath	volumetric capacity of ~1.42 Ah cm ⁻³	'12
Sheath – PVP/nickel acetate Ni (Ac) ₂	Sheath – graphitic C nanosphere after Ni removal	965 mA h g ⁻¹ after 100 cycles	
Core – SAN	Core – sacrificial layer	620 (pore) vs. 352 (no pore) mA-h/g at 50 mA/g.	[157]
Sheath – SAN-island PAN emulsion	Sheath – porous carbon wall	81% after 10 cycles	'12
Core – PEO	Core – sacrificial layer	First demo in full-cell configuration.	[159]
Sheath – PVP/Titanium tetra-sopropoxide	Sheath – TiO ₂ sheath layer	103 mA-h/g at 100 mA/g	'13
Core – Si NPs + mineral oil	Core – Si	88% after 300 cycles	
Sheath – PAN	Sheath – Carbon sheath layer	1300 mA-h/g (95%) after 80 cycles at 0.5 C.	[161]
Core – PAN	Core – carbon core enhancing electrical properties	1013 mA h g ⁻¹ at 2 C.	'13
Middle – SAN + Si NPs	Core – SAN for sacrificial layer, Si NPs enhancing capacity	1210.7 mA-h/g at 50 mA/g	[162]
Sheath – PAN	Sheath – carbon sheath encapsulating Si NPs	75% after 100 cycles	'14
Core – PMMA	Core – sacrificial layer	~800 mA-h/g at 100 mA/g	[165]
Sheath – PS + Ti(OiPr) ₄	Sheath – Carbon + TiO ₂	85% after 250 cycles	'14
Core – PMMA	Core – sacrificial layer for mesohollow fiber. Also making micropores on carbon sheath.	Designed for Cathode material	[166]
Sheath – PAN	Sheath – sublimed sulfur incorporated microporous carbon	815 mA-h/g @ 0.1 C	'14
Core – SnCl ₄ + PAN (1:1 or 1:2 wt ratio)	Core – tin incorporated carbon composite core	88% after 70 cycles	
Sheath – PAN	Sheath – carbon wall	626 mA-h/g at 50 mA/g	[169]
Core – SnO ₂ NPs + PMMA	Core – SnO ₂ nanoparticles & Hollow core.	73% after 50 cycles	'14
Sheath – PAN	Sheath – carbon wall	1002 mA-h/g for initial cycle at 100 mA/g	[170]
Core – Zn(OAc) ₂ + PMMA solution	Core – ZnO NPs	833 mA-h/g after 500 cycles at 600 mA/g	'15
Sheath – graphene oxide (GO) + PAN	Sheath – rGO incorporated glassy carbon	815 mA-h/g at 50 mA/g	[168]
Core – PAN/PS + Si NPs	Core – Si NPs in porous carbon	80% after 100 cycles	'15
Sheath – PAN	Sheath – carbon sheath	997 mA-h/g at 200 mA/g	[163]
	* Honeycomb-like structure	71% after 150 cycles	'15
Core – PAN/PMMA + Si NPs	Core – Si NPs in porous carbon	603 mA-h/g after 300 cycles at 500 mA/g	
Sheath – PVP + MWCNTs	Sheath – carbon with MWCNTs (added conductive pathway)	903 mA-h/g at 0.2 A/g	[164]
	* Honeycomb-cobweb structure	89% after 100 cycles at 200 mA/g	'16
Core – PMMA + GeOx NPs	Core – GeOx NPs	875 mA-h/g at 160 mA/g after 400 cycles	[167]
Sheath – PAN	Sheath – carbon sheath.	513 mA-h/g at 1600 mA/g upon 500 cycles	'15
Core – PVP	Core – hollow	1826.2 mA-h/g at 300 mA/g after 100 cycles	[155]
Sheath – PVP + Co(Ac) ₂	Sheath – Porous tubular cobalt oxide		'15
LIB separator			
Core – polysulfonamide (PSA)	Higher porosity, better electrolyte wettability and superior thermal stability than commercial PP separator. As a cell, PSA@PVDF-HFP membrane showed superior rate capability and better retention rate.		[171]
Sheath – PVDF-HFP			'13
Core – Cellulose acetate (CA)	Good tensile strength, high porosity, excellent thermal stability, and super electrolyte compatibility. Compared to commercial separator, it shows lower interfacial resistance ~98.5 Ω and higher ionic conductivity ~6.16 mS/m as well as superior rate capability ~138 mA-h/g and cycling performance ~75.4% after 100 cycles.		[172]
Sheath – PVDF-HFP			'15

the separator membrane between anode and cathode have been carried out. Commercial separators made of polyolefin-based materials, such as polyethylene (PE) or polypropylene (PP), provide good electrochemical stability, thermal shut-down property, and good mechanical properties. However, the poor wettability to the electrolyte is limiting the rate capability and cycling stability of LIB. Severe thermal shrinkage causes serious safety hazards by forming electrical short-circuits.

Zhou et al. developed high power Li-ion battery separator using core-sheath fiber membranes made of polysulfonamide (PSA) core and polyvinylidene fluoride-co-hexafluoropropene (PVDF-HFP) sheath. While the PSA core provides excellent mechanical properties and thermal resistance, the PVDF-HFP

sheath provides anodic stability and good wettability to the liquid electrolyte. Compared to the commercial PP separator, superior rate capability was observed. At 8 C rate, the PSA core/PVDF-HFP sheath fiber (PSA@PVDF-HFP) separator provided higher capacity of 85 mA-h/g than the commercial PP separator of 54 mA-h/g. Cycling performance was also improved using PSA@PVDF-HFP separator. It retained 82% of capability after 100 cycles at 0.5 C rate, while commercial PP separators only retained ~69% capacity. The PSA@PVDF-HFP separator also provided lower cell impedance (~23 Ω) than that using commercial PP (47 Ω), implying better interface stability and electrolyte wettability.^[171]

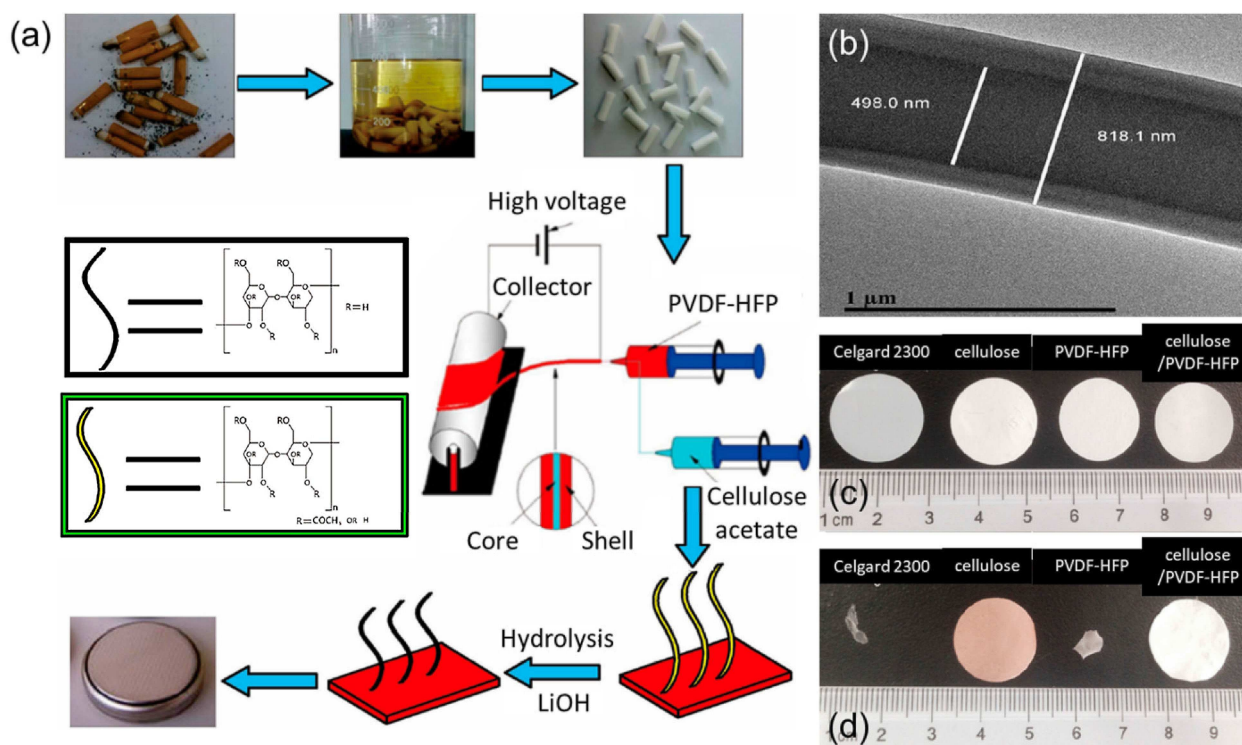


Figure 44. Core (cellulose) – sheath (PVDF-HFP) nanofiber separators: (a) preparation process from cigarette filter to nanofibers; (b) TEM observation of prepared core-sheath fibers; (c) as-prepared separators (Celgard 2300 commercial separator, cellulose fiber separator, PVDF-HFP fiber separator, and cellulose core & PVDF-HFP sheath fiber separator); (d) corresponding separator conditions after heat treatment in at 200 °C for 1 hr. Reprinted with permission from Ref [172]. Copyright 2015 American Chemical Society.

An interesting eco-friendly cellulose-based membrane separator for high-performance lithium-ion batteries was developed using waste cigarette filters. Cellulose has some attractive properties as a LIB separator, including thermal stability and hydrophilicity. Due to its excellent thermal stability, cellulose acetate is being used for cigarette filters. Recycled cigarette filter was dissolved in core solution, while PVDF-HFP polymer solution used as a sheath, as shown in Fig 44a. Cellulose core and PVDF-HFP sheath structure was very well formed as observed by TEM (Figure 44b) and exhibited good tensile strength ~ 34.1 MPa, high porosity $\sim 66\%$, excellent thermal stability, and electrolyte compatibility. The thermal stability is demonstrated by observing before (Figure 44c) and after (Figure 44d) heat treatment. Commercial separator and PVDF-HFP fiber are severely shrunk while the core-sheath separator remains intact. Compared to commercial separator, it also shows lower interfacial resistance $\sim 98.5 \Omega$, higher ionic conductivity ~ 6.16 mS/m, superior rate capability ~ 138 mA-h/g and cycling performance $\sim 75.4\%$ after 100 cycles.^[172]

In recent years, the increasing popularity of electric cars has created a huge demand for highly packed large-scale energy storage devices. Because of Li-ion battery limitations, such as fire safety hazard, limited abundance, and poor recyclability, other alternative batteries are being investigated. Zinc battery is a possible alternative because zinc has very high theoretical capacity (1086 Wh/kg) and is a very abundant material, which can be much safer and highly recyclable compared to Li-ion

batteries. Very recently, Wang et al. demonstrated^[173] Zn air battery using CuCo₂O₄ nanoparticle incorporated mesoporous hollow carbon fibers. While CuCo₂O₄ nanoparticles provided high catalytic activity with fine tuning capability of the performance, the hollow carbon fibers provided good conductivity for good cycling stability. Surface pores on hollow fibers provide more pathways for oxygens and hydroxyls for catalytic reactions. Obviously, there are still huge opportunities to develop other types of batteries as well as Li-ion batteries using coaxial electrospinning.

Supercapacitors

Compared to rechargeable batteries, supercapacitors have certain advantages, such as simple construction, environmental safety, fast rate capability, high power density, safety and long cycle life. Same benefits from (coaxially) electrospun nanofibers that applied to battery operation also apply to supercapacitor functions. Supercapacitors made of coaxial fibers with titanium nitride (TiN) core and vanadium nitride (VN) sheath have been demonstrated. The core-sheath structure is shown in Figure 45a and b. The fibers have a very porous structure that is beneficial for increased capacity. The TiN core exhibits a better electronic conductivity with low capacity, while the vanadium nitride (VN) sheath possesses a higher capacity with poor electronic conductivity. Combining better rate capability of TiN and higher

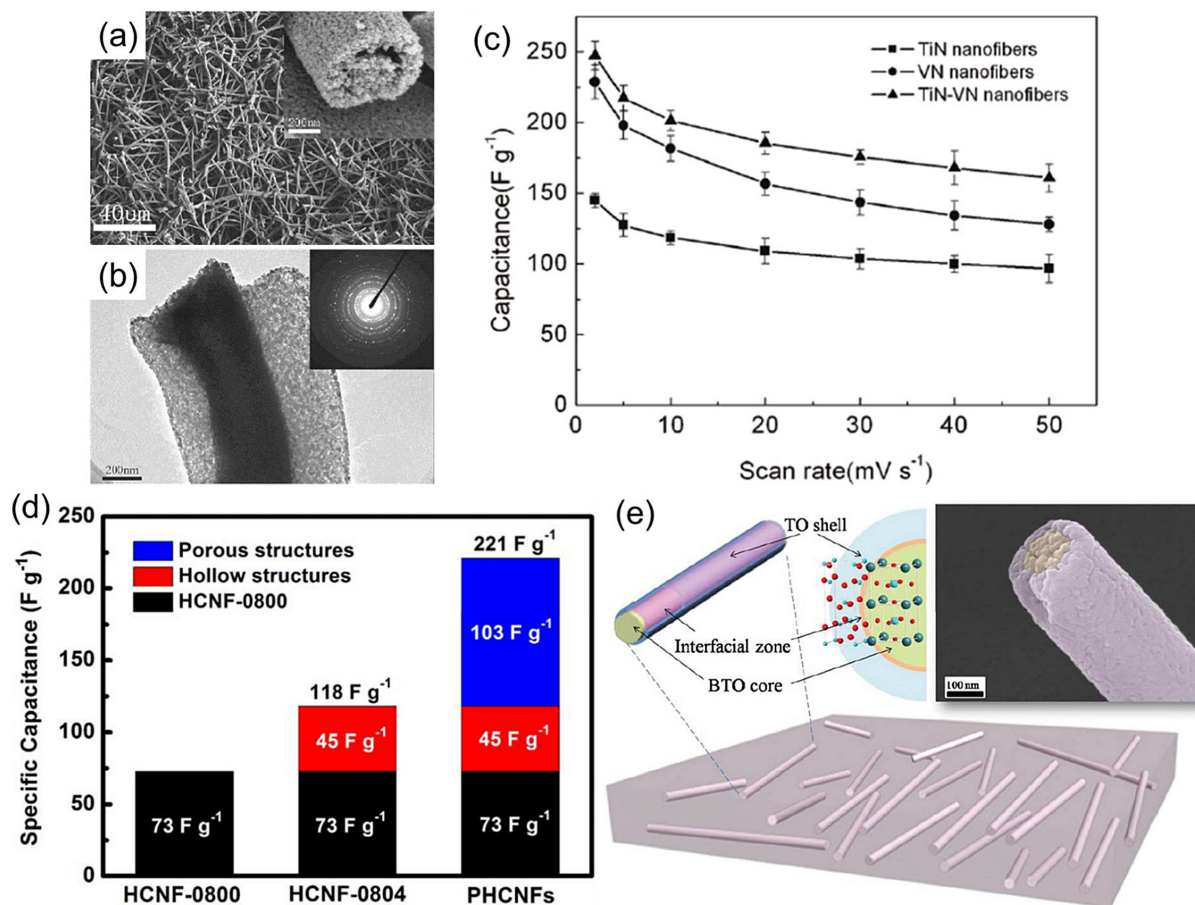


Figure 45. Morphology observations of core-sheath TiN-VN fibers using (a) SEM and (b) TEM. (c) Specific capacitances of electrodes with TiN, VN, and TiN-VN fibers for scan rates from 2 to 50 mV/s. Reprinted with permission from Ref [174]. Copyright 2011 American Chemical Society. Porous carbon nanofibers: (d) specific capacitance comparison based on porous structures. Reprinted with permission from Ref [175]. Copyright 2015 John Wiley and Sons. BaTiO₃ core and TiO₂ sheath fiber embedded PVDF film capacitor: (e) Illustration of the composite PVDF film with BaTiO₃-TiO₂ core-sheath nanofibers showing lattice structures in different parts of the nanofiber. Inset: false color SEM image of the fractured BaTiO₃ core-TiO₂ sheath fiber. Reprinted with permission from Ref [176]. Copyright 2016 Royal Society of Chemistry.

specific capacitance of VN into core-sheath fibers, the coaxial fiber can provide a specific capacitance of 247.5 F/g at the scan rate of 2 mV/s and a better rate capability of 160.8 F/g at the higher scan rate of 50 mV/s, as shown in Figure 45c.^[174]

Porous hollow carbon nanofibers made by carbonizing SAN core and polyacrylic acid (PAA)/PVP sheath also provided very high specific capacitance of 221 F/g with superior capacitance retention of 95% after 5000 cycles at a scan rate of 0.1 V/s. PVP in the sheath was used as a pore inducer. Hollow core and porous sheath enhanced the capacitance ~20% and 47%, respectively (Figure 45d).^[175]

Although dielectric capacitors have very attractive features such as fast charging–discharging speeds and high-power density, achieving high energy density is needed in order to be used for many applications. Lin et al. achieved high energy density in film capacitor by incorporating BaTiO₃-TiO₂ core-sheath fibers into PVDF film as shown in Figure 47e. Charge shifting between core and sheath induces additional interfacial polarization and increases electric displacement in the film, while the breakdown strength is maintained because the charge shifting is limited to the local interfacial zone. This

nanocomposite film with 3% volume fraction of core-sheath fibers provided a large energy density ~10.94 J/cm³ at a field of 360 kV/mm, which is more than 2 and 4 times higher than PVDF and commercial BOPP (biaxially oriented polypropylene) films, respectively.^[176] Recently, coaxially electrospun BaTiO₃ nanotubes coated with a dense dopamine layer were incorporated into PVDF films to improve dielectric properties and energy density of the polymer composite material. Dopamine coating enables uniform distribution of nanotubes within the polymer film without having any aggregation and also confines the charge carrier movements in the interface between nanotubes and polymer host, resulting in enhanced dielectric properties of the composite film. Composite films (10.8 vol.% BaTiO₃ nanotubes) provided 5.7× dielectric constant (47.5) than the pristine PVDF of 8.26. Also, the energy density of 7.03 J/cm³ at relatively lower field of 330 MV/m is 6.25× higher than 1.2 J/cm³ at 640 MV/m of the commercial biaxially oriented polypropylene (BOPP).^[177]

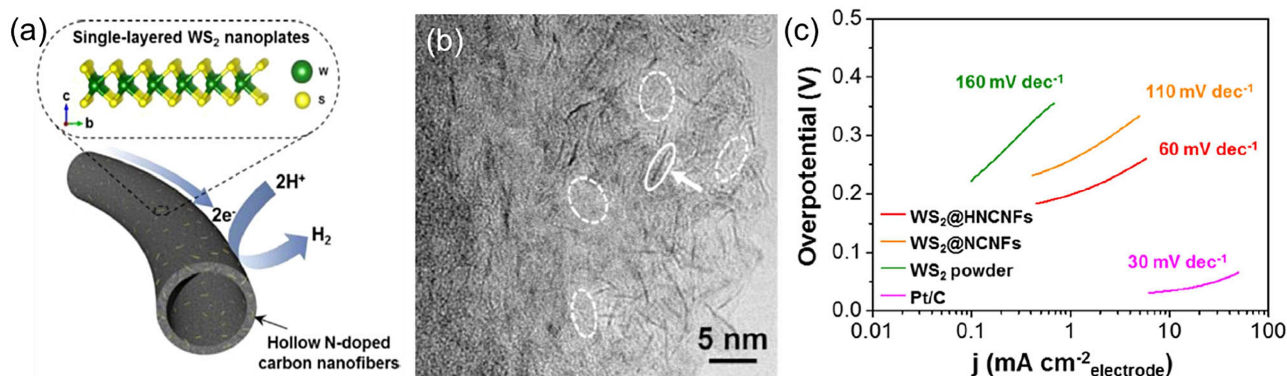


Figure 46. WS₂ single layer anchored hollow carbon nanofibers: (a) illustration of prepared fiber and (b) TEM image of WS₂ single layer anchored on carbon wall; (c) Tafel plots for the WS₂-based electrocatalysts and a commercial Pt/C electrocatalyst. Reprinted with permission from Ref [178]. Copyright 2015 American Chemical Society.

Solar Cells

In dye synthesized solar cells (DSSCs), the solar cell efficiency is closely related to the surface area of photovoltaic layer because more dye molecules can be anchored on photovoltaic materials efficiently, resulting in higher absorption of solar energy per unit area.^[179] Electrospun photovoltaic nanofiber membranes are one of most promising nanomaterial for this purpose. TiO₂ is known as an excellent photocatalytic material in DSSCs because of its UV absorption range, excellent electrochemical stability and the overall abundance. The Ramakrishna group evaluated hollow mesoporous TiO₂ nanofibers as a photoelectrode in DSSCs. Coaxially electrospun PEO core and PVP/titanium tetraisopropoxide (TTIP) sheath were prepared using coaxial electrospinning, followed by annealing at 450 °C. Hollow mesoporous TiO₂ nanofiber photoelectrode provided the solar-to-current power conversion efficiency (PCE) ~5.6% and short circuit current ~10.38 mA/cm², which are ~33% higher than that of equivalent conventional TiO₂ nanofibers (4.2% and 8.99 mA·cm⁻², respectively) prepared by single nozzle electrospinning. Core-sheath nanofiber membrane also shows faster electron diffusion and longer electron recombination time than conventional TiO₂ nanofibers, as well as commercial P25 TiO₂ nanoparticles.^[180]

Intense interests on organic photovoltaic devices has been raised in recent decade due to the potential of flexible, low cost and scalable solar cells.^[181] It mainly consists of one bulk heterojunction layer that combines electron donor and electron acceptor materials, such as poly(3-hexylthiophene) and phenyl-C₆₁-butyric acid methyl ester (P3HT:PCBM). Conventional electrospinning of P3HT:PCBM solutions does not yield suitable fibers. However, using coaxial electrospinning with a suitable sheath material (PCL) it has resulted in pure P3HT:PCBM nanofibers by post-formation selective PCL sheath removal with cyclopentanone solvent. P3HT:PCBM fibers incorporated into the active layer of a bulk heterojunction organic photovoltaic (BHJ-OPV) device produced the improved PCE of 4.0% compared to equivalent thin-film devices of ~3.2% PCE.^[182]

Hydrogen

Hydrogen is regarded as the ideal clean energy source due to the largest energy density and absence of CO₂ emission. Most hydrogen in use is produced by fossil fuels (typically natural gas – CH₄) in a process that releases a significant level of carbon dioxide byproduct.^[183] An alternative promising method is the environmentally friendly electrochemical water splitting. The hydrogen evolution reaction (HER, 2 H⁺ + 2 e⁻ → H₂) is the cathodic half reaction of electrochemical water splitting. For high energetic efficiency in water splitting, an electrocatalyst is required to minimize the overpotential and initiate the electrochemical reaction. Pt is the most efficient electrocatalyst but is hardly cost-effective.^[184] Hollow nitrogen-doped carbon nanofibers anchored with single-layered tungsten disulfide (WS₂) nanoplates was developed as a low cost and efficient electrocatalyst for enhanced HER. In coaxial electrospinning, SAN core provided robust support for the sheath structure due to immiscibility with WS₂ precursor dispersed PAN sheath solutions. In two step thermal treatments, single layer WS₂ nanoplates were formed at 400 °C and hollow carbon fibers were finalized at 700 °C (illustrated in Figure 46a). Nanopores from 2 to 50 nm in diameter were also formed on hollow carbon wall by generated sulfur gases and decomposed SAN core vapor during thermal treatments. Formation of WS₂ single layer nanoplates ~5 nm in length were confirmed in TEM observation (Figure 46b). Compared to the WS₂ single layer nanoplates anchored solid carbon nanofibers (WS₂@NCNFs) and WS₂ powders, WS₂ single layer nanoplates anchored hollow carbon nanofibers (WS₂@HNCNFs) provides lower overpotential of 280 mV to reach -10 mA/cm² with lower charge transfer resistance of 24 Ω, a small Tafel slope of 60 mV/dec (Figure 46c), and excellent durability, which are beneficial for enhancing HER performance.^[178]

Electronics Applications Conductive Fibers

Most conductive nanofibers consist of non-polymeric materials obtained through a high temperature process. Conductive

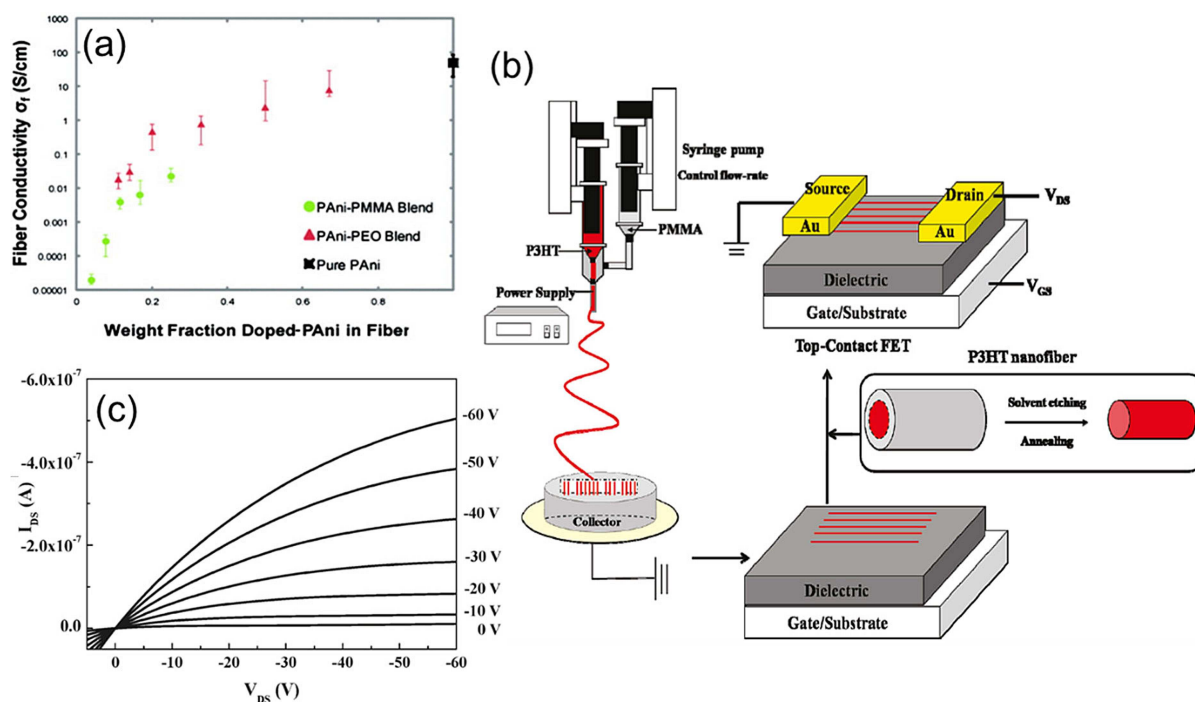


Figure 47. Electronic applications of nanofibers and their characteristics: (a) fiber conductivity (log scale) vs. weight fraction of PANi in electrospun fibers. Reprinted with permission from Ref [185]. Copyright 2012 American Chemical Society. (b) Process to fabricate aligned P3HT nanofiber FET and (c) FET output characteristics. Reprinted with permission from Ref [186]. Copyright 2011 American Chemical Society.

polymers such as polyaniline (PANI), polypyrrole (PPy), poly(3,4-ethylenedioxythiophene) (PEDOT) are not electrospinnable due to their low molecular weight and non-elasticity of their polymer chain. Therefore, they have been frequently blended with non-conducting electrospinnable polymers to produce the conductive nanofibers, although their conductivity was dramatically reduced. Coaxial electrospinning can be utilized to form a pure conductive fiber without a host polymer. Zhang and Rutledge demonstrated^[185] pure PANi nanofibers formed by coaxial electrospinning after selective removal of PMMA sheath used for fiber formation. As shown in Figure 47a, pure PANi fiber shows excellent fiber conductivity of 50 ± 30 S/cm. Interestingly, added polymers also affected the blended fiber conductivity due to the difference of their intrinsic conductivities and PANi compatibility. PEO blended PANi showed higher conductivity and better fiber formation than that of PMMA. Further aligning PANi molecules to the axis of current flow by simple mechanical stretching enhanced the conductivity up to 130 ± 40 S/cm.

Field-Effect Transistors (FETs)

One-dimensional nanofiber would significantly improve the charge mobility by enabling anisotropic charge transport and better molecular arrangement. P3HT has been popularly used as a semiconducting material for organic field effect transistor (OFET) due to superior carrier mobilities up to $0.1 \text{ cm}^2/(\text{V}\cdot\text{s})$.^[187] However, due to the difficulty of electrospinning P3HT, conventional single nozzle electrospinning could not produce nano-

fibers with consistent diameter without bead formation.^[188] Lee et al. successfully demonstrated^[189] continuous P3HT fibers using coaxial electrospinning. A P3HT chloroform solution was used for the core and chloroform solvent was also used for the sheath to prevent early P3HT precipitation at the nozzle. Field effect transistors fabricated with pure P3HT fibers resulted in good charge mobility of $0.017 \text{ cm}^2/(\text{V}\cdot\text{s})$, which is $\sim 10\times$ higher than P3HT:PCL (8:2 wt. ratio) blended fibers of $\sim 0.0012 \text{ cm}^2/(\text{V}\cdot\text{s})$. This approach would be also useful for other materials in highly volatile solvents. Chen et al. also demonstrated^[186] organic FET (OFET) using core-sheath fibers with P3HT core and PMMA sacrificial sheath. As shown in Figure 47b, core-sheath fibers were uniaxially deposited and then transferred to a 200 nm-thick SiO_2 coated heavily n-doped silicon substrate. After PMMA sheath removal using selective solvent and thermal annealing, 350 nm-thick source and drain gold electrodes were deposited on top of fibers, providing a good contact between fibers and electrodes. Lower flow rate of PMMA sheath solution induced enhanced π - π stacking and crystallinity of P3HT, which dramatically improved the charge mobility of fibers to $0.19 \text{ cm}^2/(\text{V}\cdot\text{s})$. Optimizing thermal annealing temperature is also important to prevent the relaxation of P3HT molecular orientation.

Light-Emitting Devices

Light-emitting nanofibers can be useful for integration of optoelectronic devices into smart textiles. Previously, single nozzle electrospun light-emitting fibers embedded with ruthe-

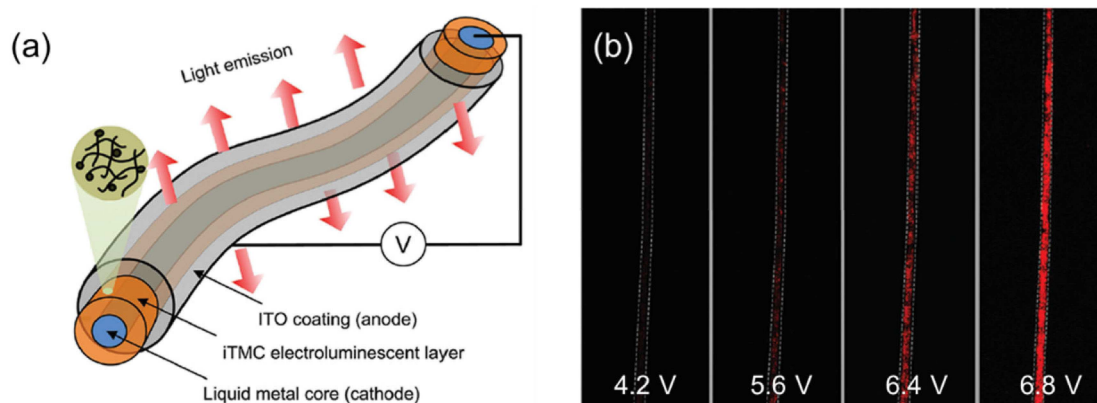


Figure 48. Light emitting coaxial fibers: (a) structural and operational schematic; (b) luminescence response based on device applied voltage in N_2 environment. Reprinted with permission from Ref [190]. Copyright 2012 American Chemical Society.

nium-based ionic transition-metal complex (ITMC) were demonstrated.^[191] Electrospun fibers deposited between two electrodes produced luminescence upon applying bias. Using coaxial electrospinning, Yang et al. successfully integrated^[190] two electrodes into coaxial structure, as illustrated in Figure 48a. Highly conductive Galinstan (containing Ga, In and Sn) liquid metal was used for the core (cathode) and the mixture of ruthenium(II) tris(bipyridine) and PEO was used for the electroluminescent sheath. A transparent and conducting ITO thin layer (anode) was evaporated on the core-sheath fibers. While single electroluminescent fibers only produced light within the narrow gap between two electrodes, core-sheath fibers can produce electroluminescence over the entire fiber length. Higher applied bias can produce stronger luminescence, as demonstrated in Figure 48b. These self-supporting fibers provide one-dimensional flexible, lightweight, and conformable light sources that have potential applications in optoelectronic textiles, bioimaging, flexible display, etc.

Magnetoelectric Coupling

Stronger coupling between electric and magnetic fields in multiferroic materials is potentially useful for multiple-state memory devices (electric writing/magnetic reading), *electrically controlled* microwave phase shifters or ferromagnetic resonance devices, *magnetically controlled* electro-optic or piezoelectric devices, and broadband magnetic field sensors. Nanostructure is useful for magnetoelectric (ME) coupling due to the stronger effect with better flexibility in terms of the size, interface, and epitaxial strain. Multiferroic nanofibers made of $CoFe_2O_4$ magnetic core and $Pb(Zr_{0.52}Ti_{0.48})O_3$ piezoelectric sheath were successfully demonstrated, providing two orders of magnitude higher lateral magnetoelectric coefficient [$\sim 2.95 \times 10^4$ mV/(cm-Oe)] than multiferroic thin film with similar composition [220 mV/(cm-Oe) @ 1 kHz] produced by sol-gel process.^{[192][193]}

Applied Coaxial Electrospinning

Going beyond the two layer core-sheath structure of coaxially electrospun fibers, modified or applied coaxial electrospinning can provide additional combinations and functions, including the tri-layered core-intermediate-sheath fiber structure, multi-core or multi-channel (hollow) fibers, position control of fiber deposition combining with near-field electrospinning, and mass production of core-sheath fibers.

Triaxial Electrospinning

Tri-layered coaxial (core-intermediate-sheath) fibers produced by electrospinning using a spinneret with three coaxially aligned inlets (*aka* "triaxial electrospinning") have emerged recently due to their novel and unique benefits: (a) combination of three different sets of material properties; (b) enhanced separation between core and sheath layers; (c) stronger binding between two materials from the sandwich configuration; (d) controlled release of encapsulated materials regardless of sheath surface properties. The basic fiber formation mechanisms are the same as with coaxial electrospinning, although additional parameters related with interactions between solutions need to be considered. A third syringe pump set is required to feed the triaxial nozzle, as illustrated in Figure 49a.

Although this variation of fiber electrospinning is a nascent field, the flexibility and versatility that triaxial electrospinning offers makes it very likely that it will develop rapidly in the near future. Selected examples of fiber formation and related applications using triaxial electrospinning are summarized in Table 4. Chen et al. successfully demonstrated the unique nanowire-in-tube structure shown in Figure 49b and c.^[194] TiO_2 precursor was used for core and sheath, while a paraffin emulsion solution was used for the sacrificial intermediate layer.

Electrosprayed tri-layered microparticles were demonstrated by Kim and Kim.^[195] For triaxial electrospinning, PLGA solution was fed into both core and sheath nozzle outlets, while PDLLA solution was fed into the intermediate outlet. Very uniform

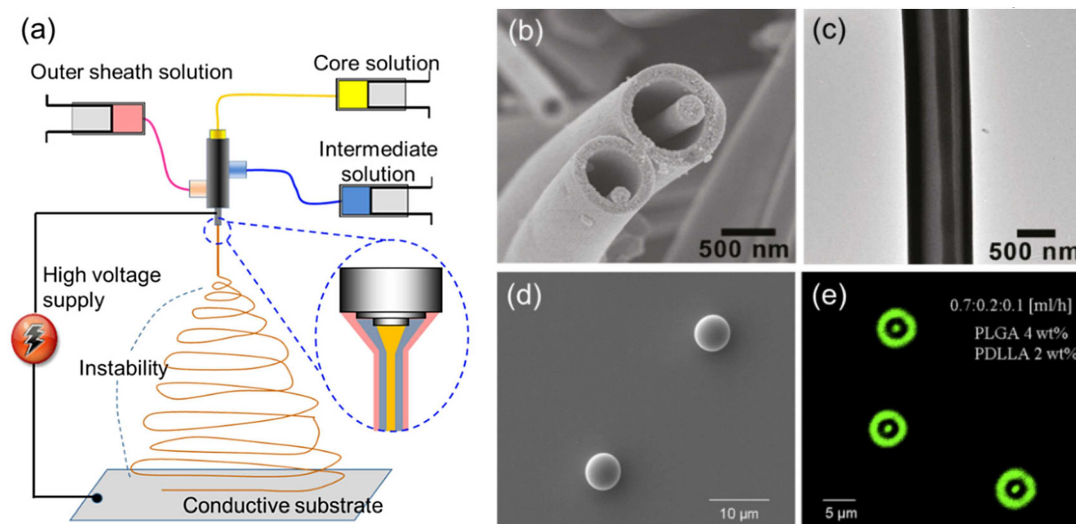


Figure 49. Triaxial electrospinning: (a) experimental configuration. Reprinted with permission from Ref [107]. Copyright 2013 American Chemical Society. Fiber-in-tube structures: (b) SEM photo; (c) TEM photo. Reprinted with permission from Ref [194]. Copyright 2010 American Chemical Society. Triaxially electrospayed microcapsules: (d) SEM morphology; (e) laser confocal image. Reprinted with permission from Ref [195]. Copyright 2011 Elsevier.

Table 4. Summary of triaxial electrospinning approaches.					
Core	Intermediate (middle)	Sheath	Purpose/Features	Ref (year)	
Glycerin	Lignin	Ethanol	Produce hollow carbon nanofibers. Ethanol sheath prevents the Taylor cone solidification while glycerin core acts as a template for hollow structure.	[196] (2007)	
Silica	poly(styrene- <i>b</i> -isoprene)	Silica	To investigate effect of interfacial interaction when self-assembly material is sandwiched by silica layers.	[197] (2009)	
TiO ₂	paraffin oil emulsion	TiO ₂	Nanowire-in-nanotube structured fiber. Even miscible core and sheath solution can have sharp interface with no diffusion.	[194] (2010)	
PLGA/coumarin-6	PDLLA	PLGA/coumarin-6	Uniform tri-layered capsules containing anti-tumor agents produced in single step.	[195] (2011)	
gelatin	PCL	gelatin	Demonstrate biodegradable tri-layered fibers.	[198] (2013)	
PVP/KAB dye	PCL	PCL/KAU dye	Demonstrate dual delivery with different release kinetics: quick release from sheath and controlled release from core.	[107] (2013)	
PS	PU	PS	Although PS is brittle, these PS fibers are highly flexible and strong. Triaxial structure provides a good interface between incompatible PS and TPU.	[123] (2014)	
Ethyl cellulose/highest KET concentration	Ethyl cellulose/moderate KET concentration	Ethyl cellulose/lowest KET concentration	Linear release of ketoprofen (KET) over 20 hr.	[120] (2015)	
Nisin/PVP	PCL	Cellulose acetate	Long term delivery of natural antimicrobial bacteriocins: excellent biocidal activities for up to 5 days and then biostatic activity for 2 or more days.	[199] (2017)	
PAN or mineral oil	TPU	air blowing	Produce core-sheath fibers or hollow fibers with much higher production rate using air-blowing assist.	[200] (2019)	

monodisperse-sized microcapsules were obtained (Figure 49d) and their concentric tri-layered structure was observed using laser confocal microscopy (Figure 49e). The capsule size and shell thickness can be easily manipulated by adjusting flow rates and polymer concentrations.

A slightly modified version of multiple input electrospinning was reported by Zhao et al.,^[201] as shown in Figure 50a. Fibers with multiple parallel hollow channels were formed using multiple inner fluids fed in parallel rather than coaxially. This interesting internal structure is displayed in the SEM photographs of Figure 50b. By varying the number of input solutions, hollow fibers with 2, 3, 4, and 5 parallel hollow channels were demonstrated. These unique structures including fiber-in-tube

structure (Figure 49b) are potentially very useful for various applications, such as energy, electronics, thermal barriers, etc.

Mass-Production Considerations

As mentioned earlier in Introduction (Figure 9), mass production of single electrospun nanofibers has been well developed in last decade. However, mass production of core-sheath fibers via coaxial electrospinning is more challenging because of the complexity of dealing with two different solutions in separate layers. In addition to clogging issues and the repulsive interaction between adjacent liquid jets, sufficiently high

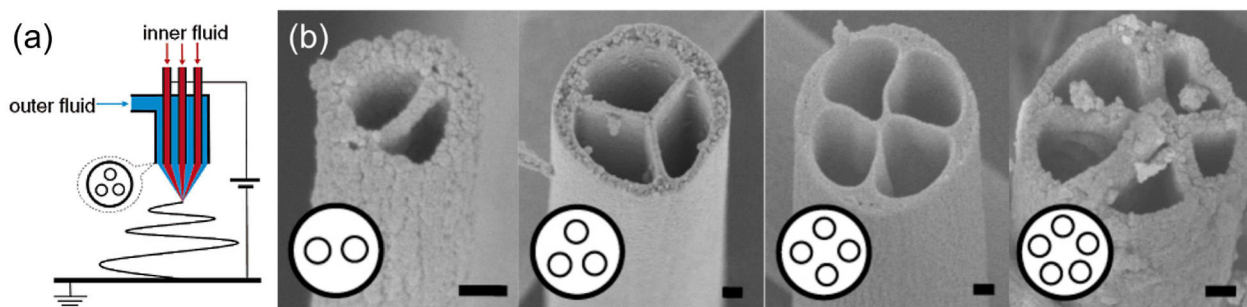


Figure 50. Multi-channel hollow microtubes by multiple input electrospinning: (a) experimental configuration; (b) cross-sectional SEM photographs of fibers with different numbers of inner fluid channels. Reprinted with permission from Ref [201]. Copyright 2007 American Chemical Society.

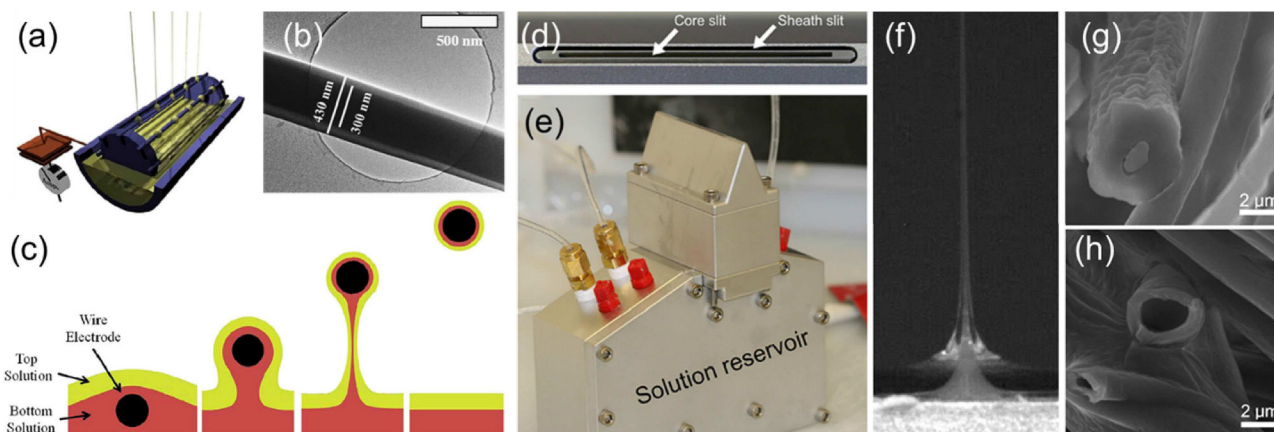


Figure 51. Free surface electrospinning using wire electrodes: (a) wire electrode/bath configuration; (b) TEM photograph of resultant fibers with PEO/PEG core and PS sheath; (c) evolution of surface profiles of two immiscible liquids as wire (viewed end-on) travels through liquid interfaces. Reprinted with permission from Ref [202]. Copyright 2013 Elsevier. Slit-surface electrospinning: (d) slit configuration (top view); (e) slit unit; (f) compound coaxial jet ejection (side view); (g) resultant core-sheath fiber; (h) resultant hollow fiber. Reprinted with permission from Ref [204]. Copyright 2015 Public Library of Science.

production rate for commercial needs cannot be achieved by integrating several nozzles. Nozzleless electrospinning, which can generate hundreds to thousands liquid jets without mechanical complications is more suitable for large-scale mass production of fiber mats than conventional nozzle-based electrospinning. Innovative techniques are being explored for adapting nozzleless electrospinning to the formation of core-sheath fibers. Forward et al. developed^[202] a nozzleless coaxial electrospinning approach using wire electrodes (Figure 51a). As illustrated in Figure 51c, a wire electrode is drawn through a liquid bath with two layered immiscible liquids. As the wire sweeps through the bath, it is first coated with the bottom liquid and then with the top liquid, forming a compound liquid layer which then breaks into compound droplets on the wire, producing core-sheath fibers (Figure 51b). Another approach for nozzleless coaxial electrospinning was proposed using a weir spinneret^[203] and a slit spinneret (Figure 51d–e).^[204] For the slit coaxial electrospinning, solutions are fed into the core and sheath slits separately and form multiple compound coaxial liquid jets, as shown in Figure 51f. Core-sheath fibers (Figure 51g) and hollow fibers (Figure 51h) were successfully obtained using this method. However, although the potential for scale up of electrospun core/shell fiber production is greatly enhanced, there currently still exist some limitations, such as

solvent immiscibility, vapor pressure differences, formation of defect-free sheath layers, that need to be solved. Recently, air-blowing assisted coaxial electrospinning using a triaxial nozzle was demonstrated to provide higher production rate of core-sheath/hollow nanofibers by Duan and Greiner.^[200] Air-blowing enables much higher flow rate of fed solutions, providing the total flow rate of 5.8–12 mL/hr and the productivity up to 3.6 g/hr, which is much higher than conventional coaxial electrospinning.^[200]

Near-Field Coaxial Electrospinning

While mass production capability is paramount for commercial development, precision deposition of core-sheath nanofibers on a desired location or specific pattern is very important in expanding the versatility and applications of electrospinning. The Lin group demonstrated the concept of near-field electrospinning in 2006.^[205] Dramatically reducing the gap between the solution dipped needle and the substrate prevents the instability of the liquid jet and confined the area of fiber deposition. Using a motor-controlled collector, position-controlled deposition of individual or patterned fiber deposition was realized. The speed of the motorized collector is an

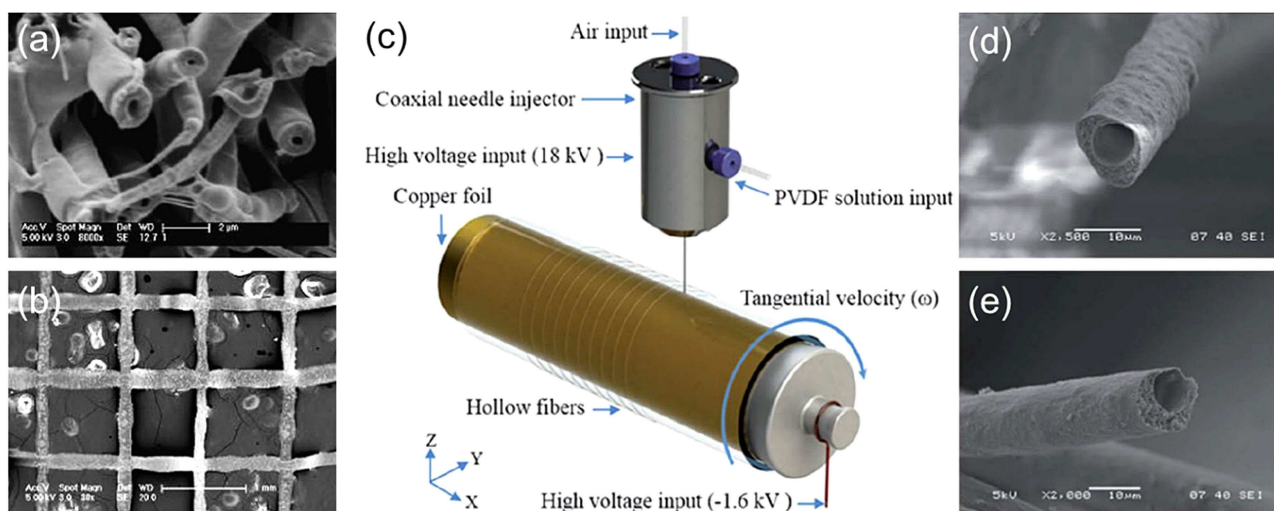


Figure 52. Near-field coaxial electrospinning: (a) hollow PCL fibers (core: sugar); (b) patterned grid of sugar-PCL core-sheath fibers. Reprinted with permission from Ref [209]. Copyright 2011 Elsevier.; (c) illustration of near-field coaxial electrospinning on a rotating collector. Resultant hollow PVDF fibers produced with air flow rate of (d) 12 mL/hr; (e) 15 mL/hr. Reprinted with permission from Ref [210]. Copyright 2015 RSC Publishing.

important consideration to produce straight, waved, or coiled fibers along the moving axis. Since the first demonstration of the near-field electrospinning, many related results have been reported to accomplish improved control of the near-field electrospinning process^[206] and to utilize it in a variety of applications such as mechanical energy harvesting^[207] and tissue engineering.^[208]

A comprehensive review of near-field electrospinning was recently reported by the Long group.^[211] Near-field electrospinning was also applied to coaxial electrospinning and produced aligned and patterned sugar-PCL core-sheath fibers, as shown in Figure 52a and b.^[209] While the motorized x-y stage has been mostly used for moving the collector, Pan et al. utilized the rotating collector fixed on x-y stage as shown in Figure 52c, which can provide relatively fast lateral speed and

conveniently collect many aligned fibers. The gap between aligned fibers is controlled by an X–Y stage under the rotating collector. With air being pumped through the core of the nozzle, hollow piezoelectric PVDF fibers were formed (Figure 52d and e), which can be challenging in conventional coaxial electrospinning. Hollow piezoelectric PVDF fibers provided $\sim 2.5\times$ higher power generation than the solid piezoelectric PVDF fibers.^[210]

Summary and Future Perspective

The characteristic features of coaxial electrospinning in the formation of fibers with unique and versatile properties, such as multifunctional materials properties, in/organic and biological material encapsulation, complex multilayered (solid or hollow) structure and geometry, has enabled the field to grow at a rapidly increasing pace, expanding and bearing fruit in various areas, as illustrated in Figure 53. Moreover, the recent addition of mass production capability is accelerating the commercialization of novel core-sheath nanofiber products.

Some applications of coaxial electrospinning, primarily in the biomedical and energy fields, have been and continue to be vigorously investigated, resulting in many advances and novel approaches that can lead to industrial commercialization in the near future. For biomedical applications, the simple but powerful combination of two different functional materials into the core and sheath of a single fiber is now evolving into “smart function” membranes that are designed to respond in a specific fashion to a given condition or environment. Future research in this field will likely converge into two directions: (1) on the technical front – controlled “on-demand” release of encapsulated functional molecules; (2) on the medical front – treatment of various diseases and healthcare applications, increasing *in-vivo* evaluation and clinical trials. Related to these directions,

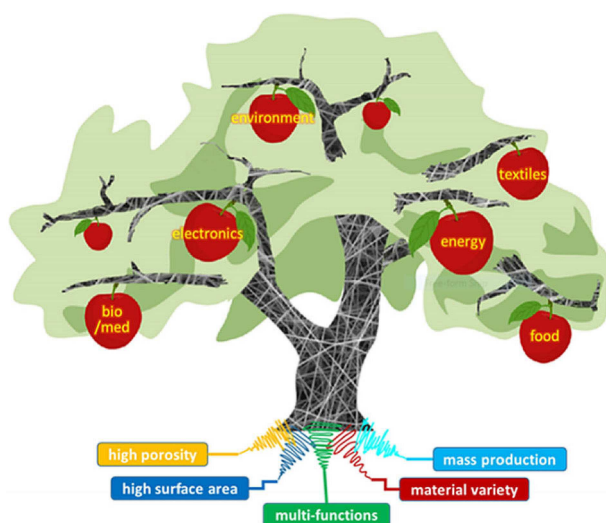


Figure 53. Application tree for fiber membranes formed by electrospinning.

current schemes for “on-demand” release of drugs and/or other functional molecules from electrospun fiber membranes need to be evaluated under *in vivo* conditions to consider not only the beneficial aspects of released molecules, but also to evaluate cytotoxicity aspects of stimuli-responsive materials. *In vivo* evaluation of biocompatible membranes with on-demand release capability is anticipated in the near future.

Another major area of coaxial electrospinning research is centered on the energy area. Among many energy-related applications, the development of advanced electrodes for the rechargeable Li-ion battery has been a major interest given their high demand. The ability of coaxial electrospinning to create and customize hollow and porous fiber membranes made of various metal oxide and carbon materials has led to growing research on this topic in academia and industry. Two critical considerations are: (1) buffering capacity for volume expansion during lithium insertion/desertion processes; (2) efficient electrochemical and physical incorporation of highly electro-active materials within the conductive carbon hollow or solid nanofiber substrate. For these considerations, coaxial or multi-axial electrospinning is the most effective method of fabricating porous hollow nanofibers that can provide improved physical and chemical incorporation of electrochemically functional materials.

In addition to the biomedical and energy areas, some “eye-catching” results using core-sheath fibers have been developed for other application areas, such as textiles and electronics. While the number of coaxial electrospinning advances and publications in these other fields does not match those in the biomedical and energy areas, it is apparent that many possibilities exist for fundamental advances and commercial opportunities in these areas. For example, although nanofiber membranes have been considered as very promising materials for air filtration, core-sheath fibers have not been developed for this application possibly due to previous lack of mass production capability. Because surface properties are the key parameter for improved filtration efficiency, coaxial electrospinning can be utilized for the formation of fibers combining the sheath material that provides the desired surface properties with a mechanically stable core material. Also, coaxially made hierarchical structures, such as wrinkled and/or porous structures, can be beneficial for filtering much smaller particles.

Although many conventionally electrospun fiber commercial products are indicated in Table 1, no core-sheath fiber products are commercialized to date. Recent on-going efforts on the mass production of core-sheath fiber will very likely lead to successful commercialization activities in the near future.

List of Abbreviations

AuNP	gold nanoparticle
BFGF	basic fibroblast growth factor
BHJ-OPV	bulk heterojunction organic photovoltaic
BMP-2	bone morphogenetic protein-2
BMSC	bone marrow derived stem cell
BOPP	biaxially oriented polypropylene

BSA	bovine serum albumin
CAP	cellulose acetate phthalate
CLSD	CO ₂ laser supersonic drawing
CNF	carbon nanofiber
CS	chitosan
DEX	dexamethasone
DFP	diisopropylfluorophosphate
DFPase	diisopropylfluorophosphatase
DMSO	dimethyl sulfoxide
DOX	doxorubicin
DP	diaphorase
DSSC	dye synthesized solar cell
EC	endothelial cell
ECM	extracellular matrix
EGCG	epigallocatechin-3-O-gallate
GTP	guanosine-5'-triphosphate
GTR	guided tissue regeneration
HA	hydroxyapatite
HA	hyaluronic acid
HDF	human dermal fibroblasts
HER	hydrogen evolution reaction
hMSC	human-bone-marrow-derived MSC
hPDLSC	human periodontal ligament stem cell
HSD	hydroxysteroid dehydrogenase
HSP	Hansen solubility parameter
IMPDH	inosine monophosphate dehydrogenase
iTMC	ionic transition-metal complex
ITO	indium tin oxide
KAB	keyacid blue
KAU	keyacid uranine
KET	ketoprofen
KCZ	ketoconazole
LED	light-emitting diode
LIB	Li-ion battery
MNA	metronidazole
MPA	mycophenolic acid
MSC	mesenchymal stem cells
MWCNT	multi wall carbon nanotubes
NGF	nerve growth factor
nHAP	nanohydroxyapatite
NiNP	Ni nanoparticle
NIPS	nonsolvent induced phase separation
NP	nanoparticle
OFET	organic field effect transistor
P3HT	poly(3-hexylthiophene)
PAA	polyacrylic acid
PAN	polyacrylonitrile
PANi or PANi	polyaniline
PAN-co-PS	poly(acrylonitrile-co-styrene)
PBS	phosphate-buffered saline
PCBM	phenyl-C ₆₁ -butyric acid methyl ester
PCE	power conversion efficiency
PCL	poly(ϵ -caprolactone)
PCM	phase change material
PDMS	polydimethylsiloxane
PDT	poly(dodecylthiophene)
PE	polyethylene

PEDOT	poly(3,4-ethylenedioxythiophene)
PEG	polyethylene glycol
PEI	polyethylenimine
PEO	poly(ethylene oxide)
PGS	poly(glycerol sebacate)
PLA	poly(L-lactide)
PLCL	poly(L-lactic acid)-co-poly(ϵ -caprolactone)
PLGA	poly(lactic-co-glycolic acid)
PLLA	poly(L-lactic acid)
P(LLA-CL)	poly(L-lactic acid-co- ϵ -caprolactone)
PLLCL	poly(L-lactic acid)-co-Poly(ϵ -caprolactone)
PDLLA	poly(DL-lactic acid)
PMMA	poly(methyl methacrylate)
P(MMA-ran-MAA)	poly(methylmethacrylate-co-methacrylic acid) random copolymer
PP	polypropylene
PPy	polypyrrole
PS	polystyrene
PSA	Polysulfonamide
PSU	polysulfone
PU	polyurethane
PVA	polyvinyl alcohol
PVDF	poly(vinylidene fluoride)
PVDF-HFP	polyvinylidene fluoride-co-hexafluoropropene
PVOH	poly(vinyl alcohol)
PVP	polyvinylpyrrolidone
SAN	styrene-co-acrylonitrile
SC	Schwann cell
SEI	solid electrolyte interphase
SF	silk fibroin
SiNP	Si nanoparticle
SIP	self-immolative polymer
TFA	trifluoroacetic acid
TPU	thermoplastic polyurethane
TCH	tetracycline hydrochloride
TIPS	thermally induced phase separation
TUFT	tubes by fiber templates
VEGF	vascular endothelial growth factor
VIPS	vapor induced phase separation
wCCM	worm-like crystalline core micelles

Conflict of Interest

The authors declare no conflict of interest.

Keywords: biomaterials · coaxial electrospinning · core–sheath fibers · energy · nanofibers · drug delivery

- [1] a) T. Ondarçuhu, C. Joachim, *Europhys. Lett.* **1998**, *42*, 215; b) J. Ma, Q. Zhang, Y. Zhang, L. Zhou, J. Yang, Z. Ni, *Appl. Phys. Lett.* **2016**, *109*, 033101.
- [2] a) S. Zhang, *Nat. Biotechnol.* **2003**, *21*, 1171; b) H.-S. Liao, J. Lin, Y. Liu, P. Huang, A. Jin, X. Chen, *Nanoscale* **2016**, *8*, 14814–14820.
- [3] a) C. R. Martin, *Chem. Mater.* **1996**, *8*, 1739–1746; b) J. Martín, J. Maiz, J. Sacristan, C. Mijangos, *Polymer* **2012**, *53*, 1149–1166.
- [4] a) R. L. Shambaugh, *Ind. Eng. Chem. Res.* **1988**, *27*, 2363–2372; b) C. J. Ellison, A. Phatak, D. W. Giles, C. W. Macosko, F. S. Bates, *Polymer* **2007**, *48*, 3306–3316.
- [5] A. M. Behrens, B. J. Casey, M. J. Sikorski, K. L. Wu, W. Tutak, A. D. Sandler, P. Kofinas, *ACS Macro Lett.* **2014**, *3*, 249–254.
- [6] a) A. Suzuki, K. Aoki, *Eur. Polym. J.* **2008**, *44*, 2499–2505; b) A. Suzuki, T. Mikuni, T. Hasegawa, *J. Appl. Polym. Sci.* **2014**, *131*, n/a–n/a.
- [7] a) L. Ren, R. Ozisik, S. P. Kotha, P. T. Underhill, *Macromolecules* **2015**, *48*, 2593–2602; b) M. R. Badrossamay, H. A. McIlwee, J. A. Goss, K. K. Parker, *Nano Lett.* **2010**, *10*, 2257–2261.
- [8] H. Xu, B. W. Zeiger, K. S. Suslick, *Chem. Soc. Rev.* **2013**, *42*, 2555–2567.
- [9] X. Hu, X. Zhang, X. Shen, H. Li, O. Takai, N. Saito, *Plasma Chem. Plasma Process.* **2014**, *34*, 1129–1139.
- [10] A. Formhals, *Vol. U. S. Patent 1,975,504, 1934.*
- [11] G. Taylor, *Proc. R. Soc. London A Math. Phys. Sci.* **1964**, *280*, 383.
- [12] G. Taylor, *Proc. R. Soc. London Ser. A Math. Phys. Sci.* **1969**, *313*, 453–475.
- [13] J. Doshi, D. H. Reneker, *J. Electrostat.* **1995**, *35*, 151–160.
- [14] M. Bognitzki, H. Hou, M. Ishaque, T. Frese, M. Hellwig, C. Schwarte, A. Schaper, J. H. Wendorff, A. Greiner, *Adv. Mater.* **2000**, *12*, 637–640.
- [15] G. Liu, L. Qiao, A. Guo, *Macromolecules* **1996**, *29*, 5508–5510.
- [16] J. Jang, B. Lim, J. Lee, T. Hyeon, *Chem. Commun.* **2001**, *1*, 83–84.
- [17] A. K. Moghe, B. S. Gupta, *Polym. Rev.* **2008**, *48*, 353–377.
- [18] a) J. Yoon, H.-S. Yang, B.-S. Lee, W.-R. Yu, *Adv. Mater.* **2018**, *30*, 1704765; b) M. Naeimirad, A. Zadhoush, R. Kotek, R. Esmaeely Neisiany, S. Nouri Khorasani, S. Ramakrishna, *J. Appl. Polym. Sci.* **2018**, *135*, 46265.
- [19] a) A. Khalif, S. V. Madihally, *Eur. J. Pharm. Biopharm.* **2017**, *112*, 1–17; b) Y. Lu, J. Huang, G. Yu, R. Cardenas, S. Wei, E. K. Wujcik, Z. Guo, *Wiley Interdiscip. Rev. Nanomed. Nanobiotechnol.* **2016**, *8*, 654–677; c) H. Qu, S. Wei, Z. Guo, *J. Mater. Chem. A* **2013**, *1*, 11513–11528.
- [20] D. H. Reneker, A. L. Yarin, H. Fong, S. Koombhongse, *J. Appl. Phys.* **2000**, *87*, 4531–4547.
- [21] a) S. De Vrieze, T. Van Camp, A. Nelvig, B. Hagström, P. Westbroek, K. De Clerck, *J. Mater. Sci.* **2009**, *44*, 1357–1362; b) G.-Z. Yang, H.-P. Li, J.-H. Yang, J. Wan, D.-G. Yu, *Nanoscale Res. Lett.* **2017**, *12*, 55.
- [22] J. Pelipenko, J. Kristl, B. Janković, S. Baumgartner, P. Kocbek, *Int. J. Pharm.* **2013**, *456*, 125–134.
- [23] S. L. Shenoy, W. D. Bates, H. L. Frisch, G. E. Wnek, *Polymer* **2005**, *46*, 3372–3384.
- [24] D. Papanagopoulos, A. Dondos, *Polymer* **1995**, *36*, 369–372.
- [25] Z. Kurban, A. Lovell, S. M. Bennington, D. W. K. Jenkins, K. R. Ryan, M. O. Jones, N. T. Skipper, W. I. F. David, *J. Phys. Chem. C* **2010**, *114*, 21201–21213.
- [26] D. Han, A. J. Steckl, *Langmuir* **2009**, *25*, 9454–9462.
- [27] a) J. S. Choi, S. H. Choi, H. S. Yoo, *J. Mater. Chem.* **2011**, *21*, 5258–5267; b) L. Tian, M. P. Prabhakaran, X. Ding, D. Kai, S. Ramakrishna, *J. Mater. Sci.* **2012**, *47*, 3272–3281.
- [28] Y. Dror, W. Salalha, R. Avrahami, E. Zussman, A. L. Yarin, R. Dersch, A. Greiner, J. H. Wendorff, *Small* **2007**, *3*, 1064–1073.
- [29] S. Megelski, J. S. Stephens, D. B. Chase, J. F. Rabolt, *Macromolecules* **2002**, *35*, 8456–8466.
- [30] a) C.-L. Pai, M. C. Boyce, G. C. Rutledge, *Macromolecules* **2009**, *42*, 2102–2114; b) R. M. Nezarati, M. B. Eifert, E. Cosgriff-Hernandez, *Tissue Eng., Part C* **2013**, *19*, 810–819.
- [31] T. Hai, X. Wan, D.-G. Yu, K. Wang, Y. Yang, Z.-P. Liu, *Mater. Des.* **2019**, *162*, 70–79.
- [32] B. S. Lee, S. Y. Jeon, H. Park, G. Lee, H. S. Yang, W. R. Yu, *Sci. Rep.* **2014**, *4*.
- [33] S. N. Reznik, A. L. Yarin, E. Zussman, L. Bercovici, *Phys. Fluids* **2006**, *18*, 062101.
- [34] S. Petrik, M. Maly, *Mater. Res. Soc. Symp. Proc.* **2011**, *1240*, 1240-WW1203-1207.
- [35] Elmarco, NS Production Line NS 8S1600U, can be found under <http://www.elmarco.com/nanofiber-equipment/nanofiber-production-lines-ns8s1600u/>.
- [36] Revolution Fibres LLC, can be found under <https://www.revolutionfibres.com/>, **2019**.
- [37] ElectrospinTech, Electrospun Applied Products, can be found under <http://electrospintech.com/products.html#XHBl4hkjBY>.
- [38] a) J. E. Díaz Gómez, Á. G. Marín, M. Marquez, A. Barrero, I. G. Loscertales, *Biotechnol. J.* **2006**, *1*, 963–968; b) I. G. Loscertales, A. Barrero, I. Guerrero, R. Cortijo, M. Marquez, A. M. Gañán-Calvo, *Science* **2002**, *295*, 1695–1698; c) Á. G. Marín, I. G. Loscertales, M. Márquez, A. Barrero, *Phys. Rev. Lett.* **2007**, *98*, 014502.

- [39] Y. Liu, J. H. He, *Int. J. Nonlinear Sci. Numer. Simul.* **2007**, *8*, 393.
- [40] B. Farkas, A. Balogh, R. Cselkó, K. Molnár, A. Farkas, E. Borbás, G. Marosi, Z. K. Nagy, *Int. J. Pharm.* **2019**, *561*, 219–227.
- [41] M. Yu, R.-H. Dong, X. Yan, G.-F. Yu, M.-H. You, X. Ning, Y.-Z. Long, *Macromol. Mater. Eng.* **2017**, *302*, 1700002–n/a.
- [42] Z. C. Sun, E. Zussman, A. L. Yarin, J. H. Wendorff, A. Greiner, *Adv. Mater.* **2003**, *15*, 1929–1932.
- [43] H. J. Yu, S. V. Fridrikh, G. C. Rutledge, *Adv. Mater.* **2004**, *16*, 1562–1566.
- [44] D. Li, Y. Xia, *Nano Lett.* **2004**, *4*, 933–938.
- [45] G. Larsen, R. Spretz, R. Velarde-Ortiz, *Adv. Mater.* **2004**, *16*, 166–169.
- [46] I. C. Um, D. Fang, B. S. Hsiao, A. Okamoto, B. Chu, *Biomacromolecules* **2004**, *5*, 1428–1436.
- [47] Y. Z. Zhang, J. Venugopal, Z. M. Huang, C. T. Lim, S. Ramakrishna, *Biomacromolecules* **2005**, *6*, 2583–2589.
- [48] a) D. Han, S. T. Boyce, A. J. Steckl, *Mater. Res. Soc. Symp. Proc.* **2008**, *1094*, 1094-DD1006-1002; b) P. Zhao, H. Jiang, H. Pan, K. Zhu, W. Chen, *J. Biomed. Mater. Res. Part A* **2007**, *83 A*, 372–382.
- [49] H. Jiang, Y. Hu, Y. Li, P. Zhao, K. Zhu, W. Chen, *J. Controlled Release* **2005**, *108*, 237–243.
- [50] J. T. McCann, M. Marquez, Y. Xia, *Nano Lett.* **2006**, *6*, 2868–2872.
- [51] T. D. Brown, P. D. Dalton, D. W. Huttmacher, *Adv. Mater.* **2011**, *23*, 5651–5657.
- [52] S. J. Kim, D. H. Jang, W. H. Park, B.-M. Min, *Polymer* **2010**, *51*, 1320–1327.
- [53] P. D. Dalton, D. Grafahrend, K. Klinkhammer, D. Klee, M. Möller, *Polymer* **2007**, *48*, 6823–6833.
- [54] T. D. Brown, P. D. Dalton, D. W. Huttmacher, *Prog. Polym. Sci.* **2016**, *56*, 116–166.
- [55] Z. K. Nagy, A. Balogh, G. Drávavölgyi, J. Ferguson, H. Pataki, B. Vajna, G. Marosi, *J. Pharm. Sci.* **2013**, *102*, 508–517.
- [56] A. Townsend-Nicholson, S. N. Jayasinghe, *Biomacromolecules* **2006**, *7*, 3364–3369.
- [57] M. Ma, V. Krikorian, J. H. Yu, E. L. Thomas, G. C. Rutledge, *Nano Lett.* **2006**, *6*, 2969–2972.
- [58] V. Kalra, S. Mendez, J. H. Lee, H. Nguyen, M. Marquez, Y. L. Joo, *Adv. Mater.* **2006**, *18*, 3299–3303.
- [59] a) E. Luong-Van, L. Grøndahl, K. N. Chua, K. W. Leong, V. Nurcombe, S. M. Cool, *Biomaterials* **2006**, *27*, 2042–2050; b) A. Cipitria, A. Skelton, T. R. Dargaville, P. D. Dalton, D. W. Huttmacher, *J. Mater. Chem.* **2011**, *21*, 9419–9453.
- [60] a) F. Yang, R. Murugan, S. Wang, S. Ramakrishna, *Biomaterials* **2005**, *26*, 2603–2610; b) C. L. He, Z. M. Huang, X. J. Han, L. Liu, H. S. Zhang, L. S. Chen, *J. Macromol. Sci., Part B* **2006**, *45*, 515–524.
- [61] a) K. Kim, Y. K. Luu, C. Chang, D. Fang, B. S. Hsiao, B. Chu, M. Hadjiargyrou, *J. Controlled Release* **2004**, *98*, 47–56; b) H. Nie, C.-H. Wang, *J. Controlled Release* **2007**, *120*, 111–121.
- [62] a) B. Ding, H.-Y. Kim, S.-C. Lee, C.-L. Shao, D.-R. Lee, S.-J. Park, G.-B. Kwag, K.-J. Choi, *J. Polym. Sci. Part B: Polym. Phys.* **2002**, *40*, 1261–1268; b) L. Yao, T. W. Haas, A. Guiseppi-Elie, G. L. Bowlin, D. G. Simpson, G. E. Wnek, *Chem. Mater.* **2003**, *15*, 1860–1864.
- [63] a) X. He, Q. Xiao, C. Lu, Y. Wang, X. Zhang, J. Zhao, W. Zhang, X. Zhang, Y. Deng, *Biomacromolecules* **2014**, *15*, 618–627; b) A. Frenot, M. W. Henrikssohn, P. Walkenström, *J. Appl. Polym. Sci.* **2007**, *103*, 1473–1482.
- [64] a) M. Pakravan, M. C. Heuzey, A. Ajji, *Biomacromolecules* **2012**, *13*, 412–421; b) T. T. T. Nguyen, O. H. Chung, J. S. Park, *Carbohydr. Polym.* **2011**, *86*, 1799–1806.
- [65] a) B. Dong, O. Arnoult, M. E. Smith, G. E. Wnek, *Macromol. Rapid Commun.* **2009**, *30*, 539–542; b) B. S. Jha, C. E. Ayres, J. R. Bowman, T. A. Telemeco, S. A. Sell, G. L. Bowlin, D. G. Simpson, *J. Nanomater.* **2011**, *2011*, 15.
- [66] Z.-M. Huang, Y. Z. Zhang, S. Ramakrishna, C. T. Lim, *Polymer* **2004**, *45*, 5361–5368.
- [67] H. Jiang, P. Zhao, K. Zhu, *Macromol. Biosci.* **2007**, *7*, 517–525.
- [68] X. Xu, X. Chen, P. Ma, X. Wang, X. Jing, *Eur. J. Pharm. Biopharm.* **2008**, *70*, 165–170.
- [69] a) X.-J. Han, Z.-M. Huang, C.-L. He, L. Liu, Q.-S. Wu, *Polym. Compos.* **2008**, *29*, 579–584; b) R. Ravichandran, J. R. Venugopal, S. Sundarajan, S. Mukherjee, R. Sridhar, S. Ramakrishna, *Int. J. Cardiol.* **2013**, *167*, 1461–1468; c) R. Chen, C. Huang, Q. Ke, C. He, H. Wang, X. Mo, *Colloids Surf. B* **2010**, *79*, 315–325; d) X. Ji, W. Yang, T. Wang, C. Mao, L. Guo, J. Xiao, N. He, *J. Biomed. Nanotechnol.* **2013**, *9*, 1672–1678.
- [70] F. Wang, L. Zhang, X. Bai, X. Cao, X. Jiao, Y. Huang, Y. Li, Y. Qin, Y. Wen, *ACS Appl. Mater. Interfaces* **2018**, *10*, 22767–22775.
- [71] K. Jalaja, D. Naskar, S. C. Kundu, N. R. James, *Carbohydr. Polym.* **2016**, *136*, 1098–1107.
- [72] Y. Su, Q. Su, W. Liu, M. Lim, J. R. Venugopal, X. Mo, S. Ramakrishna, S. S. Al-Deyab, M. El-Newehy, *Acta Biomater.* **2012**, *8*, 763–771.
- [73] K. D. McKeon-Fischer, D. H. Flagg, J. W. Freeman, *J. Biomed. Mater. Res. Part B* **2011**, *99 A*, 493–499.
- [74] G. Jin, M. P. Prabhakaran, D. Kai, S. Ramakrishna, *Eur. J. Pharm. Biopharm.* **2013**, *85*, 689–698.
- [75] R. Rajeswari, V. Jayarama Reddy, S. Subramanian, M. Shayanti, S. Radhakrishnan, R. Seeram, *Nanotechnology* **2012**, *23*, 385102.
- [76] a) X. Jia, C. Zhao, P. Li, H. Zhang, Y. Huang, H. Li, J. Fan, W. Feng, X. Yuan, Y. Fan, *J. Biomater. Sci. Polym. Ed.* **2011**, *22*, 1811–1827; b) T. Wang, X. Ji, L. Jin, Z. Feng, J. Wu, J. Zheng, H. Wang, Z.-W. Xu, L. Guo, N. He, *ACS Appl. Mater. Interfaces* **2013**, *5*, 3757–3763.
- [77] a) J. J. Liu, C. Y. Wang, J. G. Wang, H. J. Ruan, C. Y. Fan, *J. Biomed. Mater. Res. Part A* **2011**, *96 A*, 13–20; b) C.-Y. Wang, J.-J. Liu, C.-Y. Fan, X.-M. Mo, H.-J. Ruan, F.-F. Li, *J. Biomater. Sci. Polym. Ed.* **2012**, *23*, 167–184.
- [78] S. Sahoo, L. T. Ang, J. C. H. Goh, S. L. Toh, *J. Biomed. Mater. Res. Part A* **2010**, *93*, 1539–1550.
- [79] a) C. L. He, Z. M. Huang, X. J. Han, *J. Biomed. Mater. Res. Part A* **2009**, *89*, 80–95; b) W. Hu, Z. M. Huang, X. Y. Liu, *Nanotechnology* **2010**, *21*.
- [80] I. C. Liao, S. Chen, J. B. Liu, K. W. Leong, *J. Controlled Release* **2009**, *139*, 48–55.
- [81] A. Saraf, L. S. Baggett, R. M. Raphael, F. K. Kasper, A. G. Mikos, *J. Controlled Release* **2010**, *143*, 95–103.
- [82] A. López-Rubio, E. Sanchez, Y. Sanz, J. M. Lagaron, *Biomacromolecules* **2009**, *10*, 2823–2829.
- [83] S. Klein, J. Kuhn, R. Avrahami, S. Tarre, M. Beliaevski, M. Green, E. Zussman, *Biomacromolecules* **2009**, *10*, 1751–1756.
- [84] A. Mickova, M. Buzgo, O. Benada, M. Rampichova, Z. Fisar, E. Filova, M. Tesarova, D. Lukas, E. Amler, *Biomacromolecules* **2012**, *13*, 952–962.
- [85] R. Korehei, J. F. Kadla, *Carbohydr. Polym.* **2014**, *100*, 150–157.
- [86] C. E. Schmidt, J. B. Leach, *Annu. Rev. Biomed. Eng.* **2003**, *5*, 293–347.
- [87] E. Kijeńska, M. P. Prabhakaran, W. Swieszkowski, K. J. Kurzydowski, S. Ramakrishna, *Eur. Polym. J.* **2014**, *50*, 30–38.
- [88] L. Tian, M. P. Prabhakaran, J. Hu, M. Chen, F. Besenbacher, S. Ramakrishna, *RSC Adv.* **2015**, *5*, 49838–49848.
- [89] K. T. Shalumon, G.-J. Lai, C.-H. Chen, J.-P. Chen, *ACS Appl. Mater. Interfaces* **2015**, *7*, 21170–21181.
- [90] W. Shao, J. He, F. Sang, B. Ding, L. Chen, S. Cui, K. Li, Q. Han, W. Tan, *Mater. Sci. Eng. C* **2016**, *58*, 342–351.
- [91] Y. Tang, L. Chen, K. Zhao, Z. Wu, Y. Wang, Q. Tan, *Compos. Sci. Technol.* **2016**, *125*, 100–107.
- [92] M. Ranjbar-Mohammadi, M. Zamani, M. P. Prabhakaran, S. H. Bahrami, S. Ramakrishna, *Mater. Sci. Eng. C* **2016**, *58*, 521–531.
- [93] Q. Xie, L.-n. Jia, H.-y. Xu, X.-g. Hu, W. Wang, J. Jia, *Stem Cells Int.* **2016**, *2016*, 11.
- [94] Š. Zupančič, S. Sinha-Ray, S. Sinha-Ray, J. Kristl, A. L. Yarin, *Mol. Pharm.* **2016**, *13*, 1393–1404.
- [95] S. Wang, X. M. Mo, B. J. Jiang, C. J. Gao, H. S. Wang, Y. G. Zhuang, L. J. Qiu, *Int. J. Nanomed.* **2013**, *8*, 2131–2139.
- [96] G. Yang, J. Wang, Y. Wang, L. Li, X. Guo, S. Zhou, *ACS Nano* **2015**, *9*, 1161–1174.
- [97] D. Han, M. Sasaki, H. Yoshino, S. Kofuji, A. T. Sasaki, A. J. Steckl, *J. Drug Delivery Sci. Technol.* **2017**, *40*, 45–50.
- [98] M. He, H. Jiang, R. Wang, Y. Xie, C. Zhao, *J. Colloid Interface Sci.* **2017**, *490*, 270–278.
- [99] a) T. Sun, Y. S. Zhang, B. Pang, D. C. Hyun, M. Yang, Y. Xia, *Angew. Chem. Int. Ed.* **2014**, *53*, 12320–12364; *Angew. Chem.* **2014**, *126*, 12520–12568; b) I. Brigger, C. Dubernet, P. Couvreur, *Adv. Drug Delivery Rev.* **2002**, *54*, 631–651.
- [100] K. T. Nguyen, *J. Nanomed. Nanotechnol.* **2011**, *2*, 1000103e.
- [101] E. Yan, Y. Fan, Z. Sun, J. Gao, X. Hao, S. Pei, C. Wang, L. Sun, D. Zhang, *Mater. Sci. Eng. C* **2014**, *41*, 217–223.
- [102] S. B. Qasim, M. S. Zafar, S. Najeib, Z. Khurshid, A. H. Shah, S. Husain, I. U. Rehman, *Int. J. Mol. Sci.* **2018**, *19*, 407.
- [103] A. Sohrali, P. M. Shaibani, H. Etayash, K. Kaur, T. Thundath, *Polymer* **2013**, *54*, 2699–2705.
- [104] Y. C. Shin, D. M. Shin, E. J. Lee, J. H. Lee, J. E. Kim, S. H. Song, D. Y. Hwang, J. J. Lee, B. Kim, D. Lim, S. H. Hyon, Y. J. Lim, D. W. Han, *Adv. Healthcare Mater.* **2016**, *5*, 3035–3045.
- [105] Q. Wei, F. Xu, X. Xu, X. Geng, L. Ye, A. Zhang, Z. Feng, *Front. Mater. Sci.* **2016**, *10*, 113–121.
- [106] Y. Su, Q. Su, W. Liu, G. Jin, X. Mo, S. Ramakrishna, *J. Biomater. Sci. Polym. Ed.* **2012**, *23*, 861–871.
- [107] D. Han, A. J. Steckl, *ACS Appl. Mater. Interfaces* **2013**, *5*, 8241–8245.

- [108] J. Zhang, K. Qiu, B. Sun, J. Fang, K. Zhang, H. Ei-Hamshary, S. S. Al-Deyab, X. Mo, *J. Mater. Chem. B* **2014**, *2*, 7945–7954.
- [109] B. Wang, H. Zheng, M.-W. Chang, Z. Ahmad, J.-S. Li, *Colloids Surf. B* **2016**, *145*, 757–767.
- [110] Z. Man, L. Yin, Z. Shao, X. Zhang, X. Hu, J. Zhu, L. Dai, H. Huang, L. Yuan, C. Zhou, H. Chen, Y. Ao, *Biomaterials* **2014**, *35*, 5250–5260.
- [111] M. S. Birajdar, J. Lee, *Chem. Eng. J.* **2016**, *288*, 1–8.
- [112] D. Hua, Z. Liu, F. Wang, B. Gao, F. Chen, Q. Zhang, R. Xiong, J. Han, S. K. Samal, S. C. De Smedt, C. Huang, *Carbohydr. Polym.* **2016**, *151*, 1240–1244.
- [113] D. Han, A. J. Steckl, *ACS Appl. Mater. Interfaces* **2017**, *9*, 42653–42660.
- [114] C. Yang, D.-G. Yu, D. Pan, X.-K. Liu, X. Wang, S. W. A. Bligh, G. R. Williams, *Acta Biomater.* **2016**, *35*, 77–86.
- [115] D. Han, X. Yu, N. Ayres, A. J. Steckl, *ACS Appl. Mater. Interfaces* **2016**, *9*, 11858–11865.
- [116] B. Fan, J. F. Trant, A. D. Wong, E. R. Gillies, *J. Am. Chem. Soc.* **2014**, *136*, 10116–10123.
- [117] R. Weinstein, P. S. Baran, D. Shabat, *Bioconjugate Chem.* **2009**, *20*, 1783–1791.
- [118] A. M. DiLauro, A. Abbaspourrad, D. A. Weitz, S. T. Phillips, *Macromolecules* **2013**, *46*, 3309–3313.
- [119] L. Viry, S. E. Moulton, T. Romeo, C. Suhr, D. Mawad, M. Cook, G. G. Wallace, *J. Mater. Chem.* **2012**, *22*, 11347–11353.
- [120] D. G. Yu, X. Y. Li, X. Wang, J. H. Yang, S. W. A. Bligh, G. R. Williams, *ACS Appl. Mater. Interfaces* **2015**, *7*, 18891–18897.
- [121] N. M. Bedford, A. J. Steckl, *ACS Appl. Mater. Interfaces* **2010**, *2*, 2448–2455.
- [122] D. Han, S. Filocamo, R. Kirby, A. J. Steckl, *ACS Appl. Mater. Interfaces* **2011**, *3*, 4633–4639.
- [123] S. Jiang, G. Duan, E. Zussman, A. Greiner, S. Agarwal, *ACS Appl. Mater. Interfaces* **2014**, *6*, 5918–5923.
- [124] M. Zhu, J. Han, F. Wang, W. Shao, R. Xiong, Q. Zhang, H. Pan, Y. Yang, S. K. Samal, F. Zhang, C. Huang, *Macromol. Mater. Eng.* **2017**, *302*, 1600353.
- [125] F. H. Anka, K. J. Balkus, *Ind. Eng. Chem. Res.* **2013**, *52*, 3473–3480.
- [126] R. Haloui, E. Zussman, R. Khalfin, R. Semiat, Y. Cohen, *Polym. Adv. Technol.* **2017**, *28*, 570–582.
- [127] J. Lin, F. Tian, Y. Shang, F. Wang, B. Ding, J. Yu, Z. Guo, *Nanoscale* **2013**, *5*, 2745–2755.
- [128] J.-H. Park, P. V. Braun, *Adv. Mater.* **2010**, *22*, 496–499.
- [129] S. An, M. Liou, K. Y. Song, H. S. Jo, M. W. Lee, S. S. Al-Deyab, A. L. Yarin, S. S. Yoon, *Nanoscale* **2015**, *7*, 17778–17785.
- [130] G. H. Koch, M. P. Brongers, N. G. Thompson, Y. P. Virmani, J. H. Payer, NACE International, **2002**.
- [131] E. W. Brooman, *Met. Finish.* **2002**, *100*, 48–53.
- [132] J. Cao, T. Zhang, F. Li, H. Yang, S. Liu, *New J. Chem.* **2013**, *37*, 2031–2036.
- [133] J. Cao, H. Dou, H. Zhang, H. Mei, S. Liu, T. Fei, R. Wang, L. Wang, T. Zhang, *Sens. Actuators B* **2014**, *198*, 180–187.
- [134] S. Liu, B. Yu, F. Li, Y. Ji, T. Zhang, *Electrochim. Acta* **2014**, *141*, 161–166.
- [135] S.-J. Choi, S. Chattopadhyay, J. J. Kim, S.-J. Kim, H. L. Tuller, G. C. Rutledge, I.-D. Kim, *Nanoscale* **2016**, *8*, 9159–9166.
- [136] M. W. Lee, S. An, S. S. Yoon, A. L. Yarin, *Adv. Colloid Interface Sci.* **2018**, *252*, 21–37.
- [137] I. D. Kim, A. Rothschild, *Polym. Adv. Technol.* **2011**, *22*, 318–325.
- [138] J. Cao, Z. Wang, R. Wang, S. Liu, T. Fei, L. Wang, T. Zhang, *J. Mater. Chem. A* **2015**, *3*, 5635–5641.
- [139] J. Cao, Z. Wang, R. Wang, S. Liu, T. Fei, L. Wang, T. Zhang, *RSC Adv.* **2015**, *5*, 36340–36346.
- [140] X. Ji, P. Wang, Z. Su, G. Ma, S. Zhang, *J. Mater. Chem. B* **2014**, *2*, 181–190.
- [141] X. Ji, Z. Su, P. Wang, G. Ma, S. Zhang, *ACS Nano* **2015**, *9*, 4600–4610.
- [142] a) A. Zebda, C. Gondran, A. Le Goff, M. Holzinger, P. Cinquin, S. Cosnier, *Nat. Commun.* **2011**, *2*, 370; b) N. K. Navani, Y. Li, *Curr. Opin. Chem. Biol.* **2006**, *10*, 272–281.
- [143] R. A. Sheldon, *Adv. Synth. Catal.* **2007**, *349*, 1289–1307.
- [144] Z.-G. Wang, L.-S. Wan, Z.-M. Liu, X.-J. Huang, Z.-K. Xu, *J. Mol. Catal. B: Enzym.* **2009**, *56*, 189–195.
- [145] B. El-Zahab, D. Donnelly, P. Wang, *Biotechnol. Bioeng.* **2008**, *99*, 508–514.
- [146] J. Liu, G. Jiang, Y. Liu, J. Di, Y. Wang, Z. Zhao, Q. Sun, C. Xu, J. Gao, A. Duan, J. Liu, Y. Wei, Y. Zhao, L. Jiang, *Sci. Rep.* **2014**, *4*, 7276.
- [147] J. Schöbel, M. Burgard, C. Hils, R. Dersch, M. Dulle, K. Volk, M. Karg, A. Greiner, H. Schmalz, *Angew. Chem. Int. Ed.* **2017**, *56*, 405–408; *Angew. Chem.* **2017**, *129*, 416–419.
- [148] F. Mitschang, H. Schmalz, S. Agarwal, A. Greiner, *Angew. Chem. Int. Ed.* **2014**, *53*, 4972–4975; *Angew. Chem.* **2014**, *126*, 5073–5076.
- [149] M.-K. Song, S. Park, F. M. Alamgir, J. Cho, M. Liu, *Mater. Sci. Eng. R* **2011**, *72*, 203–252.
- [150] R. M. Dell, *Solid State Ionics* **2000**, *134*, 139–158.
- [151] J. M. Tarascon, M. Armand, *Nature* **2001**, *414*, 359.
- [152] K. Cao, T. Jin, L. Yang, L. Jiao, *Mater. Chem. Front.* **2017**, *1*, 2213–2242.
- [153] L. Xue, K. Fu, Y. Li, G. Xu, Y. Lu, S. Zhang, O. Toprakci, X. Zhang, *Nano Energy* **2013**, *2*, 361–367.
- [154] T. Yuan, B. Zhao, R. Cai, Y. Zhou, Z. Shao, *J. Mater. Chem.* **2011**, *21*, 15041–15048.
- [155] Z. Cui, S. Wang, Y. Zhang, M. Cao, *Electrochim. Acta* **2015**, *182*, 507–515.
- [156] B. S. Lee, S. B. Son, K. M. Park, W. R. Yu, K. H. Oh, S. H. Lee, *J. Power Sources* **2012**, *199*, 53–60.
- [157] B. S. Lee, S. B. Son, K. M. Park, G. Lee, K. H. Oh, S. H. Lee, W. R. Yu, *ACS Appl. Mater. Interfaces* **2012**, *4*, 6702–6710.
- [158] Y. Chen, Z. Lu, L. Zhou, Y. W. Mai, H. Huang, *Energy Environ. Sci.* **2012**, *5*, 7898–7902.
- [159] X. Zhang, V. Aravindan, P. S. Kumar, H. Liu, J. Sundaramurthy, S. Ramakrishna, S. Madhavi, *Nanoscale* **2013**, *5*, 5973–5980.
- [160] Y. Shi, X. Pan, B. Li, M. Zhao, H. Pang, *Chem. Eng. J.* **2018**, *343*, 427–446.
- [161] J. Wang, Y. Yu, L. Gu, C. Wang, K. Tang, J. Maier, *Nanoscale* **2013**, *5*, 2647–2650.
- [162] B.-S. Lee, H.-S. Yang, H. Jung, S.-Y. Jeon, C. Jung, S.-W. Kim, J. Bae, C.-L. Cheong, J. Im, U. I. Chung, J.-J. Park, W.-R. Yu, *Nanoscale* **2014**, *6*, 5989–5998.
- [163] H. Zhang, X. Qin, J. Wu, Y.-B. He, H. Du, B. Li, F. Kang, *J. Mater. Chem. A* **2015**, *3*, 7112–7120.
- [164] J. Wu, X. Qin, C. Miao, Y. B. He, G. Liang, D. Zhou, M. Liu, C. Han, B. Li, F. Kang, *Carbon* **2016**, *98*, 582–591.
- [165] X. Li, Y. Chen, L. Zhou, Y.-W. Mai, H. Huang, *J. Mater. Chem. A* **2014**, *2*, 3875–3880.
- [166] Y. Wu, M. Gao, X. Li, Y. Liu, H. Pan, *J. Alloys Compd.* **2014**, *608*, 220–228.
- [167] M. Li, D. Zhou, W.-L. Song, X. Li, L.-Z. Fan, *J. Mater. Chem. A* **2015**, *3*, 19907–19912.
- [168] Shilpa, B. M. Basavaraja, S. B. Majumder, A. Sharma, *J. Mater. Chem. A* **2015**, *3*, 5344–5351.
- [169] X. Xia, X. Wang, H. Zhou, X. Niu, L. Xue, X. Zhang, Q. Wei, *Electrochim. Acta* **2014**, *121*, 345–351.
- [170] D. Zhou, W.-L. Song, L.-Z. Fan, *ACS Appl. Mater. Interfaces* **2015**, *7*, 21472–21478.
- [171] X. Zhou, L. Yue, J. Zhang, Q. Kong, Z. Liu, J. Yao, G. Cui, *J. Electrochem. Soc.* **2013**, *160*, A1341–A1347.
- [172] F. Huang, Y. Xu, B. Peng, Y. Su, F. Jiang, Y.-L. Hsieh, Q. Wei, *ACS Sustainable Chem. Eng.* **2015**, *3*, 932–940.
- [173] X. Wang, Y. Li, T. Jin, J. Meng, L. Jiao, M. Zhu, J. Chen, *Nano Lett.* **2017**, *17*, 7989–7994.
- [174] X. Zhou, C. Shang, L. Gu, S. Dong, X. Chen, P. Han, L. Li, J. Yao, Z. Liu, H. Xu, Y. Zhu, G. Cui, *ACS Appl. Mater. Interfaces* **2011**, *3*, 3058–3063.
- [175] T. H. Le, Y. Yang, L. Yu, T. Gao, Z. Huang, F. Kang, *J. Appl. Polym. Sci.* **2016**, *133*, n/a–n/a.
- [176] X. Lin, P. Hu, Z. Jia, S. Gao, *J. Mater. Chem. A* **2016**, *4*, 2314–2320.
- [177] Z. Pan, L. Yao, J. Zhai, B. Shen, H. Wang, *Compos. Sci. Technol.* **2017**, *147*, 30–38.
- [178] S. Yu, J. Kim, K. R. Yoon, J.-W. Jung, J. Oh, I.-D. Kim, *ACS Appl. Mater. Interfaces* **2015**, *7*, 28116–28121.
- [179] A. Hagfeldt, G. Boschloo, L. Sun, L. Kloo, H. Pettersson, *Chem. Rev.* **2010**, *110*, 6595–6663.
- [180] X. Zhang, V. Thavasi, S. G. Mhaisalkar, S. Ramakrishna, *Nanoscale* **2012**, *4*, 1707–1716.
- [181] G. J. Hedley, A. Ruseckas, I. D. W. Samuel, *Chem. Rev.* **2017**, *117*, 796–837.
- [182] N. M. Bedford, M. B. Dickerson, L. F. Drummy, H. Koerner, K. M. Singh, M. C. Vasudev, M. F. Durstock, R. R. Naik, A. J. Steckl, *Adv. Energy Mater.* **2012**, *2*, 1136–1144.
- [183] M. Balat, M. Balat, *Int. J. Hydrogen Energy* **2009**, *34*, 3589–3603.
- [184] K. Ojha, S. Saha, P. Dagar, A. K. Ganguli, *Phys. Chem. Chem. Phys.* **2018**, *20*, 6777–6799.
- [185] Y. Zhang, G. C. Rutledge, *Macromolecules* **2012**, *45*, 4238–4246.
- [186] J. Y. Chen, C. C. Kuo, C. S. Lai, W. C. Chen, H. L. Chen, *Macromolecules* **2011**, *44*, 2883–2892.
- [187] H. Sirringhaus, P. J. Brown, R. H. Friend, M. M. Nielsen, K. Bechgaard, B. M. W. Langeveld-Voss, A. J. H. Spiering, R. A. J. Janssen, E. W. Meijer, *Synth. Met.* **2000**, *111–112*, 129–132.

- [188] H. Liu, C. H. Reccius, H. G. Craighead, *Appl. Phys. Lett.* **2005**, *87*, 253106.
- [189] S. Lee, G. D. Moon, U. Jeong, *J. Mater. Chem.* **2009**, *19*, 743–748.
- [190] H. Yang, C. R. Lightner, L. Dong, *ACS Nano* **2012**, *6*, 622–628.
- [191] J. M. Moran-Mirabal, J. D. Slinker, J. A. DeFranco, S. S. Verbridge, R. Ilic, S. Flores-Torres, H. Abruña, G. G. Malliaras, H. G. Craighead, *Nano Lett.* **2007**, *7*, 458–463.
- [192] J. G. Wan, X. W. Wang, Y. J. Wu, M. Zeng, Y. Wang, H. Jiang, W. Q. Zhou, G. H. Wang, J.-M. Liu, *Appl. Phys. Lett.* **2005**, *86*, 122501.
- [193] S. Xie, F. Ma, Y. Liu, J. Li, *Nanoscale* **2011**, *3*, 3152–3158.
- [194] H. Chen, N. Wang, J. Di, Y. Zhao, Y. Song, L. Jiang, *Langmuir* **2010**, *26*, 11291–11296.
- [195] W. Kim, S. S. Kim, *Polymer* **2011**, *52*, 3325–3336.
- [196] M. Lallave, J. Bedia, R. Ruiz-Rosas, J. Rodríguez-Mirasol, T. Cordero, J. C. Otero, M. Marquez, A. Barrero, I. G. Loscertales, *Adv. Mater.* **2007**, *19*, 4292–4296.
- [197] V. Kalra, J. H. Lee, J. H. Park, M. Marquez, Y. L. Joo, *Small* **2009**, *5*, 2323–2332.
- [198] W. Liu, C. Ni, D. B. Chase, J. F. Rabolt, *ACS Macro Lett.* **2013**, *2*, 466–468.
- [199] D. Han, S. Sherman, S. Filocamo, A. J. Steckl, *Acta Biomater.* **2017**, *53*, 242–249.
- [200] G. Duan, A. Greiner, *Macromol. Mater. Eng.* **2019**, *0*, 1800669.
- [201] Y. Zhao, X. Cao, L. Jiang, *J. Am. Chem. Soc.* **2007**, *129*, 764–765.
- [202] K. M. Forward, A. Flores, G. C. Rutledge, *Chem. Eng. Sci.* **2013**, *104*, 250–259.
- [203] L. Vysloužilová, M. Buzgo, P. Pokorný, J. Chvojka, A. Míčková, M. Rampichová, J. Kula, K. Pejchar, M. Bílek, D. Lukáš, E. Amler, *Int. J. Pharm.* **2017**, *516*, 293–300.
- [204] X. Yan, J. Marini, R. Mulligan, A. Deleault, U. Sharma, M. P. Brenner, G. C. Rutledge, T. Freyman, Q. P. Pham, *PLoS One* **2015**, *10*, e0125407.
- [205] D. Sun, C. Chang, S. Li, L. Lin, *Nano Lett.* **2006**, *6*, 839–842.
- [206] a) Z. Gaofeng, L. Wenwang, W. Xiang, W. Dezhi, S. Daoheng, L. Liwei, *J. Phys. D* **2010**, *43*, 415501; b) D. Parajuli, P. Koomsap, A. A. Parkhi, P. Supaphol, *Virtual Phys. Prototyp.* **2016**, *11*, 193–207.
- [207] C. Chang, V. H. Tran, J. Wang, Y.-K. Fuh, L. Lin, *Nano Lett.* **2010**, *10*, 726–731.
- [208] Y.-K. Fuh, Y.-C. Wu, Z.-Y. He, Z.-M. Huang, W.-W. Hu, *Mater. Sci. Eng. C* **2016**, *62*, 879–887.
- [209] F. L. Zhou, P. L. Hubbard, S. J. Eichhorn, G. J. M. Parker, *Polymer* **2011**, *52*, 3603–3610.
- [210] C. T. Pan, C. K. Yen, S. Y. Wang, Y. C. Lai, L. Lin, J. C. Huang, S. W. Kuo, *RSC Adv.* **2015**, *5*, 85073–85081.
- [211] X.-X. He, J. Zheng, G.-F. Yu, M.-H. You, M. Yu, X. Ning, Y.-Z. Long, *J. Phys. Chem. C* **2017**, *121*, 8663–8678.

Manuscript received: May 1, 2019

Revised manuscript received: June 27, 2019

Accepted manuscript online: June 28, 2019